Magnus Glosli Jacobsen

Identifying active constraint regions for optimal operation of process plants

With application to LNG and distillation processes

Doctoral thesis
for the degree of philosophiae doctor

Trondheim, October 2011

Norwegian University of Science and Technology
The Faculty of Natural Sciences and Technology
Department of Chemical Engineering

NTNU

Norwegian University of Science and Technology

Doctoral thesis
for the degree of philosophiae doctor

The Faculty of Natural Sciences and Technology
Department of Chemical Engineering

ISBN 978-82-471-3138-1 (printed version)
ISBN 978-82-471-3139-8 (electronic version)
ISSN 1503-8181

Doctoral theses at NTNU, 2011:284

Printed by NTNU-trykk

Abstract

Optimal operation and control of chemical processes depends on external conditions or *disturbances*. In order to achieve optimal or near-optimal control, one wants to control the active constraints, and the active constraints will frequently change with disturbances.

Any remaining degrees of freedom can be used to control variables whose optimal values are relatively insensitive to disturbances, these are called *self-optimizing variables*. However, when disturbances cause the active constraints to change, the best choice of self-optimizing variables will change as well. Thus it is important to have knowledge of how the set of active constraints changes with disturbances. This is particularly important when designing the *control structure* for a process.

The first chapter of the thesis deals with identifying active constraint regions, and describes a simple method for doing this in the case of two disturbances. This method is then later in the thesis applied on distillation case studies, and on a natural gas liquefaction process.

The second half of the thesis focuses on optimization and optimal operation of natural gas liquefaction plants. Liquefied natural gas (LNG) has been an important product in the gas industry since the 1960s, but optimal operation of liquefaction plants has not gained much attention in the open literature until the last decade. The thesis aims to give an overview over earlier work in this area. It is found that most attempts at optimization of such processes involves use of gradient-free optimization methods. A chapter of the thesis is dedicated to studying challenges in optimization, and serves to partly explain why this is the case. In particular, this chapter discusses the effect of model formulation on optimization performance.

Finally, the findings of the previous chapters are used to identify active constraint regions for the PRICO liquefaction process, which is much used in earlier academic case studies because of its simplicity. In this chapter, a control structure for the PRICO process is also suggested.

Acknowledgements

Day after day, day after day,
We stuck, nor breath nor
motion;
As idle as a painted ship,
Upon a painted ocean

S. T. Coleridge, *Rime of the Ancient Mariner*

The above quote describes what being a PhD student has been like at times. Periods of hard work has been followed by periods where I have felt completely out of ideas and stuck in the middle of the ocean. Fortunately, there have been people around me to give me wind in the sails again, until I finally have arrived at the harbor which is the completion of the thesis.

First and foremost I would like to thank my main supervisor, professor Sigurd Skogestad, who has always been there to discuss with and to provide direction to my work when I have found none myself. Without his valuable input I would not have been able to complete this work.

During these four years I have had the privilege to work with people from nearly all corners of the world. To all my colleagues in the Process Systems Engineering group, thank you for enriching my life. Special thanks goes to Johannes Jäschke, who has proofread parts of this thesis for me.

In addition, I have had the pleasure to be co-supervisor of several master students. Discussions with them have many times helped me to come to new realizations in my own work, and they have also been great guys to work with.

I also owe thanks to my friends outside the Department of Chemical Engineering. In times when I have been stuck and felt lost, you have helped me keep my head up and look at the positive side of things.

Naturally, I wish to thank my family at home in Torsnes for taking good care of me when I have needed a break, and for believing in me even when

I have doubted myself.

Finally, I would also like to thank the Gas Technology Centre NTNU-SINTEF for founding my PhD work.

Contents

Chapter 1

Introduction

1.1 Motivation

Optimal operation of process plants is a wide field, and within our research group the later years have seen contributions both related to general theory and to specific applications. This thesis aims to contribute in both categories.

The project which has led to this thesis, started from the thesis by Jørgen Jensen (Jensen, 2008), which dealt with optimal operation of cooling cycles (in particular natural gas liquefaction plants). It soon became clear that optimal operation of such plants was a field where not much has been done in the open literature. Therefore, one part of the thesis focuses on optimization and optimal operation of natural gas liquefaction processes.

An important focus within our group is the idea of *self-optimizing control* (Skogestad, 2000). When seeking to find a self-optimizing control structure, one must first take care of the active constraints. However, not much effort has been put into actually identifying how the set of active constraints vary when the process is exposed to disturbances. The disturbance space can be divided into regions where different constraints are active. This thesis addresses how to identify these regions in a two-dimensional disturbance space. Since this issue has hardly been addressed in the open literature, this thesis should provide a good starting point for discussion.

1.2 Overview of the thesis

- Chapter 2 introduces a simple method for finding active constraint regions in a two-dimensional disturbance space. The method is then applied on a toy example, namely a reactor-separator-recycle process

where unreacted reactant is separated from the product and recycled to the reactor. This chapter also briefly discusses the applicability of the method.

- In Chapter 3, the method introduced in Chapter 2 is applied to more realistic case studies on distillation columns. In addition, the so-called "avoid product giveaway rule" is discussed in relation to the active constraint regions.
- Chapter 4 provides a literature review of the work that has been done on simulation and optimization of natural gas liquefaction processes.
- Chapter 5 addresses challenges in optimization of natural gas liquefaction processes. This chapter includes a comparison of the solution reliability of various formulations of the steady state-model of the propane precooled mixed-refrigerant (C3-MR) process (Newton et al., 1986).
- Chapter 6 applies the method from Chapters 2-3, to work out active constraint regions for a simple liquefaction process (the PRICO process, Price and Mortko (1996)).
- Chapter 7 summarizes the main conclusions of the thesis, and suggests future work based on what is presented here.

1.3 Main contributions of the thesis

The aim of the thesis is to contribute to two separate problems within the broader scope of optimal operation and control:

- The first main contribution is the method for finding active constraint regions in the disturbance space. This is a little researched problem, and in the opinion of the author, Chapter 2 opens up for wider discussion of the problem.
- The main contribution of Chapter 3 is to provide new insight into optimal operation of distillation columns.
- Few have looked into the challenges that exist in optimization of liquefaction processes. Instead, most have found a solution to fit their problem. Chapter 5 contributes to the understanding of which challenges actually exist, and should be of interest for all those who try to use different software for simulation and optimization.

- To the knowledge of the author, no earlier work exists that addresses active constraint regions for liquefaction processes. Thus, Chapter 6 should be a worthwhile contribution to the LNG field.

1.4 Publications

1.4.1 Included in the thesis

Several chapters in the thesis are based on papers that have been submitted to scientific journals:

- Chapter 2: Submitted to *Industrial & Engineering Chemistry Research* as: **Magnus G. Jacobsen and Sigurd Skogestad: "Active constraint regions for optimal operation of chemical processes"**. This paper has been accepted and is currently in press.
- Chapter 3: Submitted to *Industrial & Engineering Chemistry Research* as: **Magnus G. Jacobsen and Sigurd Skogestad: "Active constraint regions for optimal operation of distillation columns"**.
- Chapter 5: This chapter is based on the following publication: **Magnus G. Jacobsen and Sigurd Skogestad: "Optimization of LNG plants - Challenges and strategies", proceedings of the 21st European Symposium on Computer-Aided Process Engineering (ESCAPE-21), Porto Carras, Chalkidiki, Greece, May 29-31, 2011. pp. 1854-1858**.
- Chapter 5 has also been submitted for a special issue of *Computers & Chemical Engineering*, which is to be published in 2012.
- Chapter 6: Submitted to *Journal of Natural Gas Science and Engineering* as: **Magnus G. Jacobsen and Sigurd Skogestad: "Active constraint regions for a natural gas liquefaction process"**. An abstract has also been submitted to the 2nd Trondheim Gas Technology Conference, to be held on 2-3 November, 2011 in Trondheim, Norway.

1.4.2 Other

During my PhD studies I have given the following conference presentations, that have not been included in the thesis:
2010

- Magnus G. Jacobsen: "Challenges in optimization of LNG plants", 16th Nordic Process Control Workshop 2010, Lund, Sweden, August 25-27.

- Magnus G. Jacobsen: "Optimal selection of controlled variables for the C3-MR process for liquefaction of natural gas", 1st Trondheim Gas Technology Conference, Trondheim, Norway, October 21-22.

2009

- Magnus G. Jacobsen, Sigurd Skogestad: "Control of maldistribution of flow in parallell heat exchangers", 15th Nordic Process Control Workshop, Porsgrunn, Norway, January 29-31

References

Jensen, J., 2008. Optimal operation of cyclic processes - Application to LNG processes. Ph.D. thesis, NTNU.

Newton, C., Kinard, G., Liu, Y., 1986. C3-MR processes for liquefaction of natural gas. In: 8th International Conference & Exhibition on Liquefied Natural Gas, Los Angeles, USA, June 15-19.

Price, B., Mortko, R., 1996. PRICO - a simple, flexible proven approach to natural gas liquefaction. In: GASTECH, LNG, Natural Gas, LPG international conference, Vienna.

Skogestad, S., 2000. Plantwide control: The search for the self-optimizing control structure. Journal of process control 10 (5), 487.

Chapter 2

Active constraint regions for optimal operation of chemical processes

Accepted by *Industrial & Engineering Chemistry Research* - in press

When designing the control structure of a chemical plant, with optimal operation and control in mind, it is important to know how the active set of constraints changes with disturbances.The generation of optimal active constraints regions using optimization is generally very time consuming, and this paper discusses how to use process knowledge to minimize the need for numerical calculations that is, minimize the number of optimization problems that need to be solved. We consider the case of two disturbances, as this can be nicely represented graphically.

In this chapter, we study economically optimal operation of a reactor-separator-recycle process, and show how the set of active constraints changes with feed flow rate and energy cost as disturbances. We also identify the economical and physical bottleneck of the process. For this case study process, we find five distinct regions with different active sets. This illustrates that, even for simple cases, the map of active constraint regions can be quite complex.

2.1 Introduction

2.1.1 Motivation

In optimization and control of chemical processes, active constraints play an important role. The set of active constraints influence both on plant economy and plant control. If one does not control the active constraints, one will have to accept economical loss (Aske, 2009). Also, knowing which variables are optimally at their constraint value is crucial for control structure design. If a manipulated variable which is optimally at a constraint, is used to control another variable, we can not keep it at its optimal value at all times. Thus it is necessary to know how the active constraints vary with disturbances. It is also useful to know which active constraints are important for plant economy and which are not. Say, for example, that a variable is optimally unconstrained in a particular region, and we decide to use this variable for control. Now if this variable is constrained in a neighboring region, we may have to replace it in our control scheme. However, if backing off from the constraint gives a *small* loss, it might be acceptable to keep the same control structure.

Reactor-separator-recycle systems have been researched actively over the years and is a widely used example in control literature (Gilliland et al., 1964; Wua et al., 2001; Wu and Yu, 1996; Luyben and Fluodas, 1994; Luyben, 1993). These articles mainly focus on basic regulatory control. Kiss et al. (2004) study state multiplicity, which may complicate optimization of such plants severely. Little work has gone into identifying economically optimal operating conditions for such systems, though. Larsson et al. (2003) focuses on choosing *self-optimizing variables* (Skogestad, 2000) among the unconstrained variables. Maarleveld and Rijnsdorp (1970) offer a study of constraint control on distillation columns, and discusses how constraints change with different process variables. Except for Maarleveld and Rijnsdorp (1970) and the recent work by Jagtap et al. (2010), there is little emphasis on active constraints in the literature.

2.1.2 Contribution and organization of this chapter

When one seeks to find the (approximate) regions in which each constraint is active, one will usually have to carry out at least a few optimizations. In multi-parametric programming one will typically carry out *many* optimizations, and if the optimization problem itself is difficult, this may be a time-consuming process. In this chapter, we address how one can use knowledge about the optimization problem and process model to simplify

this work, and obtain approximate active constraint regions using few optimizations. Part of the purpose is to explain what we can find out just using process knowledge, and what we must solve for numerically. We suggest a step-by-step method for sketching the active constraint regions for a two-dimensional disturbance space, and use this method on a reactor-separator-recycle process. The chapter is structured as follows:

- In Section 2.2 we briefly discuss optimal operation in general and discuss the link between the input space and the disturbance space.
- In Section 2.3 some general points about optimization are included to provide background for the rest of the chapter (and subsequent chapters).
- In Section 2.4, a method for finding approximate active constraint regions is outlined.
- In Section 2.5 we describe the process we have used for the case study
- In Section 2.6 we define optimal operation of the process and give a degree-of-freedom analysis
- In Section 2.7, the results are shown
- In Section 2.8 the results and the efficiency of the method are discussed, and we compare our results to those from Jagtap et al. (2010).
- Finally the conclusions are summarized.

2.2 Optimal operation and constraint regions

When optimizing operation of chemical processes, we start with formulating a cost function J which is to be minimized, and identifying the degrees of freedom u that can be adjusted to minimize J. Since we consider steady-state optimization, causality is not an issue - thus it does not matter which variables we select as our degrees of freedom, as long as the remaining variables of the model form an independent set. For example, when optimizing a distillation column, the degrees of freedom could be flows (e.g. reflux L and vapor boilup V, so $u = [L\,V]$) or compositions ($u = [x_B\,x_D]$). Finally, we need to identify the constraints c on operation (for example $L, V > 0$, $V \leq V_{max}$), and the most important disturbances d.

The optimal solution will often be at the intersection of constraints. In Figure 2.1, we illustrate how constraints and objectives may change when disturbances change, for a simple example with the constraints

$$\begin{aligned} c_1 &\geq c_{1,min} \\ c_1 &\leq c_{1,max} \\ c_2 &\geq c_{2,min} \\ c_2 &\leq c_{1,max} \end{aligned} \tag{2.1}$$

and two degrees of freedom u_1 and u_2. The constraints define a two-dimensional region in the input space, and the optimal solution may lay in the interior of this region (Figure 2.1(a)), on one of its edges (Figure 2.1(b)) or at one of its corners (Figure 2.1(c)). Operation outside this region is infeasible. In this example the feasible set of u is shown as being unchanged as d changes. This will typically be the case if the disturbance which changes is a price. If it is a process disturbance, the constraint lines are likely to change as well.

In this chapter, we focus on how the set of active constraints depends on the *disturbances*. The different points indicated in Figures 2.1(a) - 2.1(c) would belong in different *constraint regions* in the disturbance space. In the case of one disturbance, each region corresponds to a line segment, as shown in Figure 2.2. It is worth noticing that "region III" in Figures 2.1(a) - 2.1(c) refers to just one point, whereas in the disturbance space, "Region III" includes all d which makes that particular point optimal.

In the case of *two* disturbances, each region is a subset of the now two-dimensional disturbance space. Later in this chapter (Section 2.4), we use a two-dimensional example to illustrate the suggested method for identifying the active constraint regions. Figure 2.4(a) is thus a two-dimensional equivalent to Figure 2.2.

2.3 Optimization theory

2.3.1 General form of the optimization problem

Optimization of chemical processes is typically a nonlinear problem on the form

$$\begin{aligned} \min_{u} \quad & J(x,u,d) \\ \text{subject to} \quad & f(x,u,d) = 0 \\ & c(x,u,d) \leq 0 \end{aligned} \tag{2.2}$$

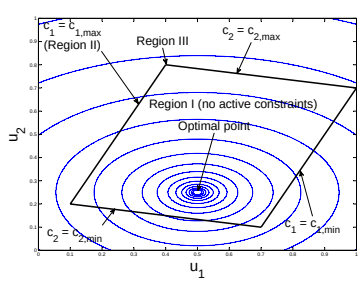

(a) Optimum in unconstrained region

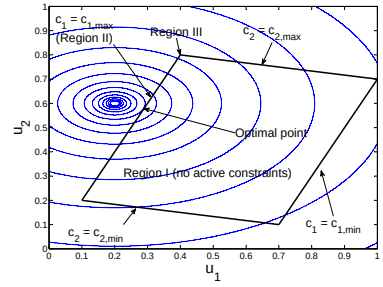

(b) Optimum at $c_1 = c_{1,max}$ (region II)

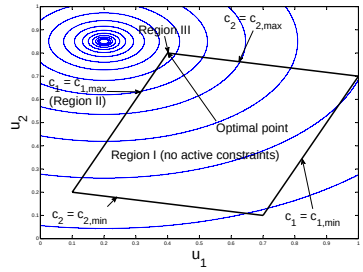

(c) Optimum at $c_1 = c_{1,max}$, $c_2 = c_{2,max}$ (region III)

Figure 2.1: Constraint lines and objective function as functions of degrees of freedom u

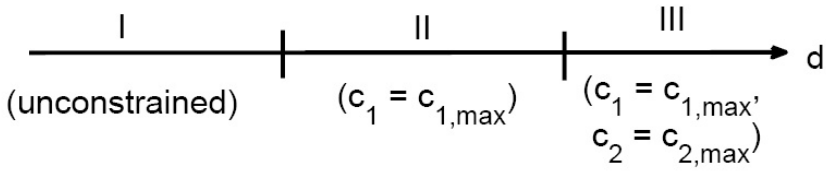

Figure 2.2: Constraint regions in one-dimensional disturbance space (one disturbance)

where J is the economical objective, $f(x, u, d)$ the process model equations and $c(x, u, d)$ the process constraints. The process model equations may be included in the optimization problem, or solved separately. The latter gives rise to different (and more complex) shapes of J and c, but eliminates x from the equations. Which approach to use depends on which is more robust - i.e. which approach is most certain to return a result. Especially in cases where recycles are involved, it may be beneficial (or even necessary) to let the optimization solver solve the flowsheet model as well (for a discussion, see Biegler (2010)).

A solution of such a nonlinear optimization problem is characterized by the *Karusch-Kuhn-Tucker conditions* (Nocedal and Wright, 1999)). These are as follows (with X including both x and u, but not the disturbance d):

$$\begin{aligned}
&\nabla_X \mathcal{L}(X^\star, \lambda^\star) = 0 \\
&c_i(X^\star) = 0 && \text{for } i \in \mathcal{E} \\
&c_i(X^\star) \leq 0 && \text{for } i \in \mathcal{I} \\
&\lambda_i^\star \geq 0 && \text{for } i \in \mathcal{I} \\
&\lambda_i^\star c_i(X^\star) = 0 && \text{for } i \in \mathcal{E} \cup \mathcal{I}
\end{aligned} \tag{2.3}$$

The optimal solution $(X^\star, \lambda^\star)$ is parametrized by the disturbance d. We seek to find the disturbance value for which a constraint switches from active to inactive - let us call this value d_{active}. Here, we take advantage of the fact that for any constraint c_i, either the constraint value itself or its corresponding Lagrange multiplier λ_i (or both) is zero, and that the sum of the two must be monotonous at least in a small area around d_{active}. At d_{active}, we have that $c_i + \lambda_i = 0$. Thus, finding d_{active} is equivalent to solving the equation

$$s_i(d) = c_i(d) + \lambda_i(d) = 0 \tag{2.4}$$

for d. Since the optimal solution $X^\star(d)$ is the result of an iterative process, one can not use an analytic method to solve for $s_i = 0$, thus an interpolation method is the simplest option. When using MATLAB, this will typically be the **fzero.m** solver. When using this solver, one needs to give two initial points between which the solver should search for the solution. The sign of $c_i + \lambda_i$ must be different at the two initial points in order for the solver to work.

2.3.2 Significance of Lagrange multipliers

Knowing the active constraint regions allows us to design a control structure based on the expected disturbances. However, even though we may find an optimal control structure for each region, we may be interested in simplifying it, for example by using the same control structure in several regions even if it is not optimal. If using a control structure different from the optimal one, we may end up having to back off from a constraint which is optimally active. We may also have to back off from active constraints due to dynamic reasons (for example, controller overshoot); see Figure 2.3. This gives rise to a loss, and in a small region the magnitude of the loss ($|\Delta J|$) relates to the Lagrange multiplier as follows (Nocedal and Wright, 1999):

$$|\Delta J| = \lambda_i |\Delta c_i| \tag{2.5}$$

where $|\Delta c_i|$ is the distance from the active constraint c_i (corresponding to "back-off" in Figure 2.3) and λ_i is the corresponding Lagrange multiplier. What this means, is that if we back off from the active constraint by a small margin Δc_i, we will have a loss which is locally proportional to the corresponding Lagrange multiplier. Thus, the Lagrange multiplier tells us how hard we get punished by backing off from a constraint. Obviously, we get punished harder if we back off from a constraint when we are far from a region where it is inactive, than if we back off from the same constraint at a point where it becomes active. In economics, $|\Delta J|$ is called a *shadow price* (Kanbur, 2008), in optimal control theory we have the related concept of *costate equations* (Naidu, 2003).

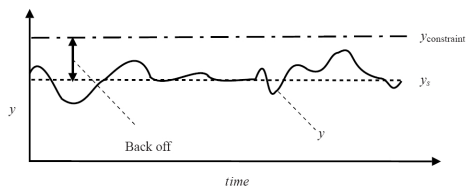

Figure 2.3: Back off from constraint due to imperfect control (illustration taken from Aske (2009))

2.4 Method for finding active constraint regions as function of disturbances

In this section, we consider the two-dimensional case (with two disturbances) unless otherwise stated. We start this section by defining the terms *constraint curve* and *region*:

Definition 1. *Constraint curve: The constraint curve corresponding to a constraint c, is the line separating the regions where c is optimally active from the regions where c is optimally inactive.* [1]

Definition 2. *Region: In this chapter, a region refers to a part of the disturbance space, bounded by constraint curves, and described by which constraints are active within that region.*

With the definitions in mind, we can make some general points about how the constraint curves and regions will behave:

- constraint curves may cross each other, so one constraint curve may span the border between more than two regions. Where two constraint curves cross each other, four regions will meet in a point.
- When one constraint curve crosses another, it will generally change slope. This is because the nature of the optimization problem will change when the set of active constraints changes.
- When there are N constraints, which all may be either active or inactive, there may be as many as 2^N *active constraint sets*. In simple cases, where constraint curves do not cross each other more than once, this means we also have a maximum of 2^N regions (as illustrated by Figure 2.4(a), where we have two constraints and four regions). In more complex cases, where two constraint curves may cross each other more than once, we may have more than 2^N regions. In that case, some regions will share the same active set. However, the number of regions is usually smaller than 2^N, since some constraint combinations may not occur, for example because they are physically impossible. For example, we often have both maximum and minimum constraints on the same variable - these will obviously never be active at the same time.

[1] In some cases, a constraint curve will be straight, and can be referred to as a constraint line. In an N-dimensional disturbance space, we will instead have (N-1)-dimensional constraint surfaces.

- In the one-dimensional case (i.e. one disturbance), each region corresponds to a line segment on the disturbance axis (x-axis). This is illustrated in Figure 2.4(b). Here, the y-axis is used to plot the optimal value of the constraint functions as functions of a single disturbance.

We now want to outline a method for identifying active constraint regions without having to optimize at a large number of points across the whole disturbance space. As an illustrative example, let us consider a hypothetical problem with two constraints:

$$[c_1\ c_2] < [c_{1,max}\ c_{2,max}] \tag{2.6}$$

We have two disturbances, d_1 and d_2. Both c_1 and c_2 are continuous functions of the disturbances, and we have four regions:

1. Both constraints are inactive
2. (only c_1 is active)
3. (only c_2 is active)
4. (both constraints are active)

The regions are shown in Figure 2.4(a): Constraint c_1 is active ($c_1 = c_{1,max}$) above the blue constraint line, and c_2 is active ($c_2 = c_{2,max}$) to the right of the red constraint line. We also show the one-dimensional case where $d_1 = 0.5$ and d_2 is on the x axis (Figure 2.4(b)). Using this example as an illustration, we now outline a method for finding active constraint regions. First it is reasonable to make the following assumptions:

1. In a two-dimensional plot with (d_1, d_2) along the axes, two neighboring regions will only differ by one active constraint, except when two constraint curves cross each other (in Figure 2.4(a) this happens in the point $(0.6, 0.5)$). For the opposite to be true, two constraint curves would have to follow each other exactly (at least along a segment).
2. We assume that the same set of active constraints does not appear in two separate regions of the disturbance space (thus, two constraint curves will not cross each other twice).
3. We assume that there will always be a maximum feed rate ("bottleneck") above which we can not satisfy all constraints.

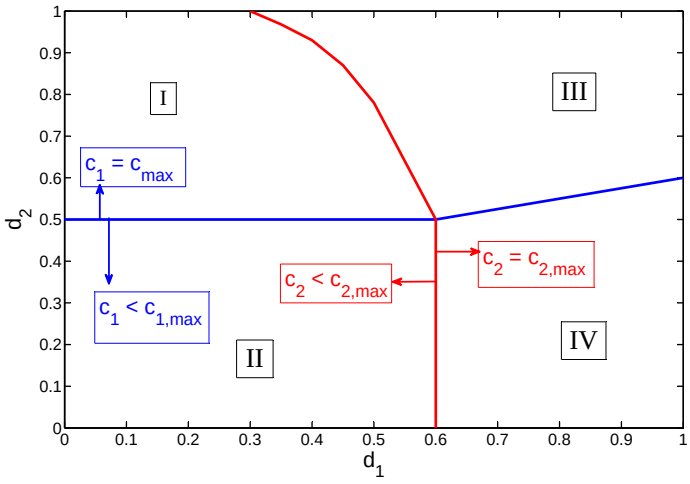

(a) Two-dimensional case (two disturbances)

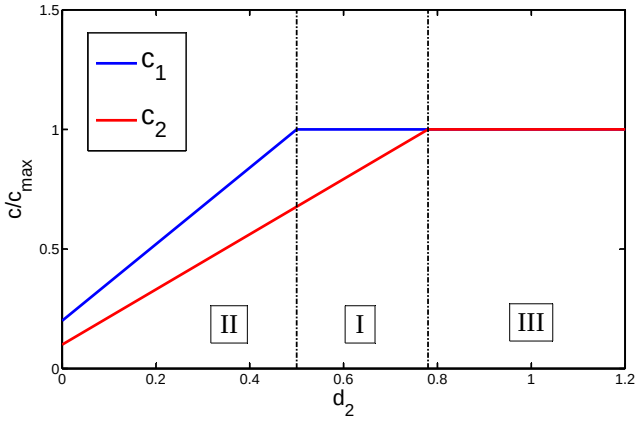

(b) One-dimensional (one single disturbance)

Figure 2.4: Example figure illustrating how constraint curves divide the disturbance space into regions, and how the regions translate to line segments in the one-dimensional case

The generality of the assumptions is discussed later in the chapter.

Based on the above definitions, considerations and assumptions, we suggest using the following procedure to find active constraint regions:

1. Using knowledge about the process model and the optimization problem, find out if any constraints will be active (or inactive) for *all* values of the disturbances, thus reducing the number of possible regions by a factor of 2 for each constraint which is always active.

2. Also use the same insight to predict whether some region borders (part of constraint curves) will be independent of one of the disturbances. In a 2D graph, these borders will correspond to vertical or horizontal lines. In the example (Figure 2.4(a)), the constraint curve separating regions I and III from regions II and IV is horizontal (independent of d_1). The line segment that separates regions II and IV is vertical (notice that this segment is only a part of a constraint curve!)

3. Locate the region borders that are found to be vertical or horizontal, by solving for the disturbance value at which the corresponding constraint changes between inactive and active. In Figure 2.4(a), this corresponds to finding the value of d_2 for which c_1 becomes active.

4. Likewise, find the value of d_1 for which we go from region II to region IV (that is, for which c_2 becomes active, with d_2 lower than the value we found in the previous step), thus locating vertical part of the constraint curve for c_2.

5. Find at least one more point along the line separating regions I and III. This means we need to do find a value of (d_1, d_2) which makes constraint c_2 switch from active to inactive. By fixing d_2 at a higher value than the one we found in step 3, and solving for the value of d_1 which makes $s_1 = 0$, we find a point on this line.

6. In the same manner, find at least one more point along the line separating regions III and IV (with d_1 fixed at a value *higher* than found in step 4).

7. If we are confident the two last region borders are straight lines, or satisfied with it as an approximation, we do not need more points. However, the true borders will often be curved (as the border between regions I and III in Figure 2.4(a)), and if we want to describe them more accurately, we need to find more pairs (d_1, d_2).

When choosing starting points for each interpolation search, one may be taken at a spot where the active constraints are already known (for example the nominal optimum). The other may be taken close to the feasibility limits, which can be found by carrying out a few sample optimizations.

The interpolation itself has been carried out using the **fzero** solver in MATLAB, which uses a combination of bisection, secant, and inverse quadratic interpolation. We have used this approach successfully in a case study which we will go through in the following sections.

2.5 Description of the example process

In this chapter, we consider the simple reactor-separator-recycle process shown in Figure 2.5:

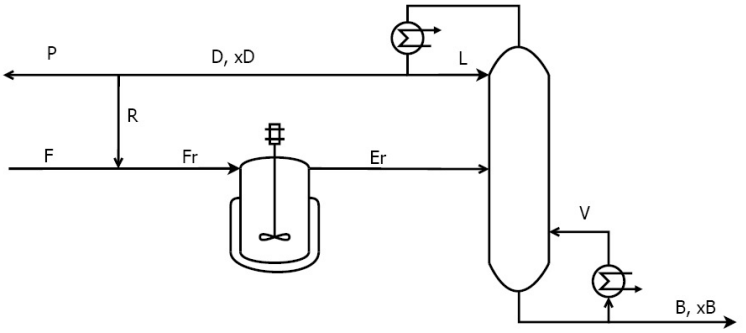

Figure 2.5: Flow sheet of the reactor-separator-recycle system

Fresh feed of A (F) is mixed with recycled distillate from the column. The mixture (F_r) goes to the reactor, which is a continuously stirred tank reactor (CSTR) with two reactions (Equation 2.7. The first yields B, which is the desired product, and the second yields C which is an undesired by-product. A real-life example of such a process could for example be a hydrocarbon isomerization process, where cracking occurs as a side reaction (this is quite common in hydrocarbon refining processes).

$$\begin{aligned} A &\rightarrow \quad B \\ A &\rightarrow \quad 2C \end{aligned} \tag{2.7}$$

In general, the steady state mass balance of a CSTR with one feed

Table 2.1: Reaction kinetics parameters

Reaction	A ($[s^{-1}]$)	E_a (J/mol)
1	$1 \cdot 10^5$	$6 \cdot 10^4$
2	$5 \cdot 10^6$	$8 \cdot 10^4$

stream and one product stream can be written as follows:

$$0 = \frac{dn_r}{dt} = F_r \cdot x_{F,r} + M_r \cdot \nu \cdot r - E_r \cdot x_r \, [mol/s] \tag{2.8}$$

where $n_r \, [mol]$ is the reactor holdup vector, $F_r \, [mol/s]$ is the flow rate entering the reactor, x_{FR} the reactor feed composition, $E_r \, [mol/s]$ is the reactor exit flow rate, ν is a matrix of stoichiometric coefficients, $r = [r_1 \;\; r_2]^T \, [s^{-1}]$ is a vector of reaction rates and x_r is the composition inside the reactor, expressed in mole fractions (in a CSTR, the exit stream is assumed to have the same composition as the reactor contents). $M_r \, [mol]$ is the total reactor holdup.

We will, for later use, define the reactant conversion X for the reactant and the product yield Y_i for each product i.

$$X = \frac{\dot{n}_{reactant,in} - \dot{n}_{reactant,out}}{\dot{n}_{reactant,in}} \cdot 100\% \tag{2.9}$$

$$Y_i = \frac{\dot{n}_{i,out} - \dot{n}_{i,in}}{\dot{n}_{reactant,in}} \cdot 100\% \tag{2.10}$$

where $\dot{n}$ indicates molar flowrate of a given component.

The reaction model uses first-order kinetics; the reaction rate of reaction i is given by

$$r_i = k_i x_A \tag{2.11}$$

where x_a is the mole fraction of A in the reactor and

$$k_i = A_i e^{-\frac{E_{a,i}}{RT}} \tag{2.12}$$

where $E_{a,i}$ is the activation energy of reaction i (in J/mol), T is the temperature in K and R is the gas constant ($8.3145 \; \frac{J}{mol \cdot K}$). Kinetic data are shown in Table 2.1. In this example, reaction 1 has a lower rate constant ($A_1 < A_2$), but also a lower activation energy, thus it is the favored reaction at lower temperatures.

The reactor product E_r is separated in a column. The distillate D is rich in byproduct (C) and unreacted A, whereas the bottom product B is

Table 2.2: Distillation column parameters

α_{AC}	0.70
α_{BC}	0.60
Number of stages	30
Feed stage location	15
Feed liquid fraction	1
V_{max}	30 mol/s

rich in the desired product B. For the distillation column, we have used a simple column model using the following assumptions: Constant relative volatilities, constant molar overflow, constant pressure over the entire column, equilibrium at every stage and negligible vapor holdups. Francis' weir equation is used to calculate liquid flow rates. The column data are shown in Table 2.2. The column model is based on the "Column A" model described in Skogestad and Morari (1988).

A fraction of the distillate is recycled (R), the remaining distillate leaves the system as a purge stream (P).

2.6 Defining optimal operation of the reactor-separator-recycle process

2.6.1 Steady-state operational economy objective

The objective J should cover all economical aspects that are influenced by the steady state operation. In general, these include cost of raw materials, energy and utilities (like cooling water), and the value of products. The cost of a product stream may be positive (if the product is sold, or processed to valuable products later on) or negative (if it is waste which must be disposed of). We may generalize to write

$$J = \sum p_{F,i} F_{F,i} + \sum p_{U,j} F_{U,j} + \sum p_{P,k} F_{P,k} \tag{2.13}$$

where $F_{F,i}$, $F_{U,j}$ and $F_{P,k}$ are the flow rates of feeds, utility streams and product streams, respectively - all in mol/s, except for energy usage which is in $[\$/kJ]$. $p_{F,i}$, $p_{U,j}$ and $p_{P,k}$ are the prices of the respective streams). In this example, we use the following objective function:

$$J = p_F F + p_V V - p_B B - p_P P \tag{2.14}$$

Table 2.3: Prices used in optimization (p_V is the nominal value)

Feed	p_F	1 \$/mol
Product	p_B	2 \$/mol
Purge	p_P	0.5 \$/mol
Energy	p_V	variable

where F, V, B and P refer to Figure 2.5, and the prices are given in Table 2.3. (The value given for p_V is listed as variable, it is used as a disturbance later on)

2.6.2 Degrees of freedom

For example by using the method outlined by de Araújo et al. (2007), we find that the process shown in Figure 2.5 has got six steady-state degrees of freedom. We may also find this number by examining the model, finding that it has 104 variables and 98 independent equations. When using the method from de Araújo et al. (2007), we relate the six degrees of freedom to:

1. Feed flow rate F
2. Recycle/purge split P/D
3. Reactor holdup M_r
4. Reactor temperature T_r (since the CSTR has a cooling jacket as shown in Figure 2.5, we may adjust this)
5. Column reboiler duty Q_R
6. Column condenser duty Q_C

However, in simulation, we may specify *any* six variables as long as the resulting 98-by-98 system is not structurally or numerically singular (as mentioned in Section 2.2). When initializing the process model, the following set of specifications was used:

- Reactor temperature T_r
- Feed flow rate F
- Mole fraction of component B in product stream B, $x_{B,B}$

Table 2.4: Constraint values used in optimization

$x_{B,B,min}$	0.90
$T_{r,max}$	$390\,K$
$M_{r,max}$	$11000\,mol$
V_{max}	$30\,mol/s$
P_{max}	$5\,mol/s$
R_{min}	$0\,mol/s$
P_{min}	$0\,mol/s$
B_{min}	$0\,mol/s$

- Reactor holdup M_r
- Column reflux L
- Purge/distillate ratio P/D

2.6.3 Constraints

When optimizing a chemical process plant, we will encounter the following types of constraints:

- There are always capacity constraints; maximum levels in tanks and liquid-phase reactors, maximum available amount of utilities, and maximum feed and product rates.
- There will usually be requirements on product quality, often in terms of maximum content of impurities.
- In addition, there are typically constraints on pressures (due to limits in piping strength) and temperatures (for example to limit catalyst degradation).

In this work, we have included maximum limits on reactor temperature T_r, reactor holdup M_r and column boilup V as well as a minimum limit on the fraction of component B in stream B. In addition we require that all flow rates are ≥ 0, and that the purge flowrate is smaller than $5\,mol/s$. See Table 2.4.

2.6.4 Disturbances

In a chemical process, there are many possible disturbances. The most important ones are usually related to feed conditions (flow rate, composition and pressure), as these often depend on the operation of an upstream process. In addition, the prices of feeds, products and utilities are often changing on a daily basis.

We may also have changes in process parameters. For example, in a catalytic process the catalyst activity may degrade, so that the value of A in the expression for the reaction rate constant k decreases. Deposits inside piping may increase pressure drop, and decrease heat transfer. Finally, downstream processes may demand changes in product flow rates and compositions.

In this work, we consider two disturbances:

- Feed flow rate F (nominal value: $1.1 mol/s$). This is the flow rate which is most likely to be given by another process unit.
- Energy cost p_V in the column (nominal value: $0.01\$/mol$) (either of the four price parameters could be used - what is really important is the energy price in relation to the difference in value between feed and products).

Since the feed flow rate is used as a disturbance, we have only got *five* degrees of freedom in the optimization problem, compared to six degrees of freedom for initialization.

2.6.5 Feed rate as disturbance or as a degree of freedom

Above we have stated that the feed flow rate is a disturbance in operation. This is typically the case when we consider a part of a bigger plant, and we just have to process the feed that we get. If the considered unit is a stand-alone unit, however, the feed rate will rather be a degree of freedom. An exception to this is if we are bound, by a contract, to process a given amount of feed anyway.

When the feed rate is a disturbance, the goal is to process this feed at a minimum cost, while satisfying the process constraints c. At some point, the feed cannot be increased anymore without breaking the given constraints - this is when the process reaches its true bottleneck.

When the feed rate is a degree of freedom, however, we may have an *economic* bottleneck as well. At a given feed rate, we may not be able to produce any more of the valuable product, and thus it will not be optimal

to increase the feed rate. Below this economical bottleneck, the active constraint regions will be the same. When the feed rate is considered a degree of freedom, one can see the maximum available feed rate $F_{\max}$ as a disturbance. Later in this chapter, we address this economic bottleneck.

2.7 Results

2.7.1 Initialization

In order to have a feasible starting point for subsequent optimization, we specified six variables as described above, and used **fmincon** to solve the model equations. To do this, the model equations and specifications were included as equality constraints in the optimization problem (corresponding to $f(x, u, d)$ in Equation 2.2), and a dummy objective function with a constant value was used. This approach is used with success in Lid (2007). An alternative approach could be to use an equation-solving method minimizing the sum-of-squares of the residuals of the equalities. Table 2.5 shows the values used for initialization, plus the resulting values of other chosen variables (reactor holdups $n_{r,i}$, conversion X_A and yield Y_i as well as product and distillate flow rates and compositions). Notice that the specification on $x_{B,B}$ was set slightly above the minimum value, this was to give an initial solution with a little margin to the most important constraint - on the other hand, the reactor holdup was initialized at its maximum value. [2]

2.7.2 Active constraint regions

According to the method outlined in Section 2.4, we start by checking if any constraints will be active for all (F, p_V). Indeed there are two, namely the constraints on product purity $x_{B,B}$ and reactor holdup M_r. The first one follows from the "Avoid Product Giveaway rule", which states that *when the product prices are constant, the minimum purity constraint in the valuable product stream is always active.* The latter is also easy to explain: Reducing the holdup leads to a lower single-pass conversion, yielding more A in the column feed, without improving selectivity in favour of the desired product. Thus the column feed will contain more A and less B, leading to a higher boilup rate. Thus, keeping the holdup at maximum saves energy.

[2] The reason for having $T_r = 355\,K$ despite the maximum is shown as $T_{r,max} = 390\,K$ in Table 2.4 is that we increased the maximum value in order to make the region where the constraint on T_r was inactive, more visible. Originally $T_{r,max}$ was $355\,K$, but this made the region very small.

Table 2.5: Initial data for the reactor-separator-recycle system, used as starting point in optimization.

Variable	Value
F	$1.1\,mol/s$
$x_{B,B}$	0.901
T_r	$355\,K$
M_r	$11000\,mol$
L	$25\,mol/s$
P/D	0.2
R	$1.512\,mol/s$
$n_{r,A}$	$5064\,mol$
$n_{r,B}$	$4159\,mol$
$n_{r,C}$	$1777\,mol$
X_A	$67.33\,\%$
Y_1	$61.82\,\%$
Y_1	$5.51\,\%$
B	$0.7649\,mol/s$
$x_{A,B}$	0.099
$x_{B,B}$	0.901
$x_{C,B}$	0.000
D	$1.8901\,mol/s$
$x_{A,D}$	0.607
$x_{B,D}$	0.167
$x_{C,D}$	0.227

We can also assume that one constraint will never be active - namely, $P \geq 0$. This is because as long as C is produced, we need to provide a way out of the system for it. Since C is the most volatile component, we will always have some of it in the distillate, thus we must purge some of the distillate to avoid accumulation of C within the system.

This means we have to find when the following variables are at their constraint values: T_r, R, V, D and B. Using **fmincon.m** for optimization and **fzero.m** for interpolation, we come up with the regions shown in Figure 2.6. Each region is referred to by a number, Table 2.6 lists which variables are at their constraint value in each respective region. The constraint curves that define the regions are as follows:

- Red constraint curve: $T_{r,max}$ becomes active.

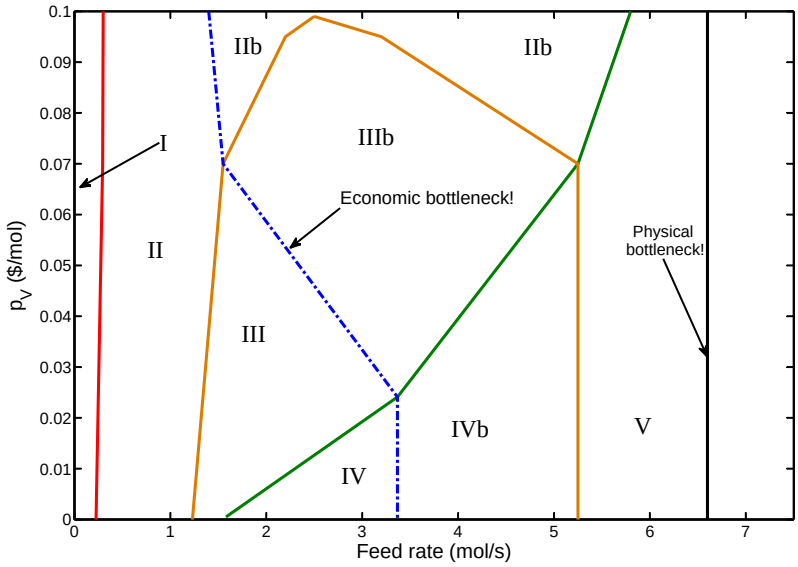

Figure 2.6: Active constraint regions for the reactor-separator-recycle system, for F up to $6\,mol/s$ and p_V up to $0.10\,\$/mol$

- Orange constraint curve: R_{min} becomes active. (It is active *below* this curve).
- Green constraint curve: V_{max} becomes active.
- The dashed blue line could be seen as a "quasi"-constraint curve - it indicates where it is not economically optimal to increase F any more, so it shows the *economic bottleneck* of the process.

In Section 2.8.1, we explain further the shape of the regions. In Table 2.7, we show the optimal value of selected model variables at four points in the disturbance space. Variables that are at a constraint are shown in **bold**.

Table 2.6: Constrained variables in each region in Figure 2.6

Region number	Constrained variables
I	$x_{B,B}$, M_r, R
II	$x_{B,B}$, M_r, R, T_r, (F)
IIb	$x_{B,B}$, M_r, R, T_r
III	$x_{B,B}$, M_r, T_r, (F)
IIIb	$x_{B,B}$, M_r, T_r
IV	$x_{B,B}$, M_r, T_r, V, (F)
IVb	$x_{B,B}$, M_r, T_r, V
V	$x_{B,B}$, M_r, T_r, V, R

Table 2.7: Optimal values of selected variables for different values of F and p_V. Numbers in **bold** indicate active constraints

Region(s)	I	II	IV	IIIb
$F\,[mol/s]$	0.1	1.0	3.0	3.0
$p_V\,[\$/mol]$	0.02	0.02	0.01	0.07
$F_r\,[mol/s]$	0.1000	1.0006	5.4219	3.3829
$E_r\,[mol/s]$	0.1024	1.0871	5.6584	3.6079
$T_r\,[K]$	328.8	**390.0**	**390.0**	**390.0**
$x_{A,r}$	0.2356	0.0815	0.2229	0.2121
$x_{B,r}$	0.7168	0.7589	0.4604	0.6225
$x_{C,r}$	0.0476	0.1596	0.3167	0.1654
$Y_1\,[\%]$	73.43	82.50	61.11	68.44
$Y_2\,[\%]$	2.44	8.64	6.30	7.17
$B\,[mol/s]$	0.0781	0.9108	2.3696	2.0511
$x_{A,B}$	0.1000	0.0900	0.0996	0.0996
$x_{B,B}$	**0.9000**	**0.9000**	**0.9000**	**0.9000**
$x_{C,B}$	0.0000	0.0100	0.0004	0.0004
$D\,[mol/s]$	0.0243	0.1762	3.2888	1.5569
$x_{A,D}$	0.6707	0.0375	0.3117	0.3603
$x_{B,D}$	0.1290	0.0300	0.1436	0.2569
$x_{C,D}$	0.2003	0.9325	0.5447	0.3828
$L\,[mol/s]$	1.6231	2.1365	26.7112	14.0009
$V\,[mol/s]$	1.6475	2.3128	**30.0000**	15.5578
P/D	1.0000	1.0000	0.2636	0.7541
$R\,[mol/s]$	**0.0000**	**0.0000**	2.4219	0.3829
$J\,[\$/s])$	-0.035	-0.863	-1.873	-1.378

2.8 Discussion

2.8.1 Shape of active constraint regions

In the following, we will explain the presence of each active constraint region, at least for those that are not obvious.

- The dashed blue line in 2.6 indicates where it is no longer optimal to increase the feed rate. That is, if F was a degree of freedom and F_{max} was specified instead, the blue line shows where the constraint $F < F_{max}$ would no longer be active. We illustrate this further with Figure 2.7(a), where the value of the objective function J at the optimal solution is given as a function of F at three different energy prices.

- We notice that the right part of the orange constraint curve in Figure 2.6, separating regions IVb and V, is vertical. This is easily explained; V_{max} is active here, and once the optimal value of V reaches V_{max}, the next region boundary must be independent of p_V, thus it is vertical. The same applies to the other constraint curves in the right part of Figure 2.6.

- We also see that for very low F, where no capacity constraints are active, we have a region (region 1 in Figure 2.6) where the maximum reactor temperature ($T_{r,max}$) is not an active constraint. This is because when the overall conversion is very high (as it is at low flow rates), we benefit from increasing the reaction *selectivity* in favor of the desired reaction (by lowering the temperature). This compensates for the lower overall conversion which also results from lower temperature. (As mentioned in the process description, reaction 1 has a lower activation energy, and thus will be favored by low temperatures.)

- R_{min} is active ($R = 0$) at low F: If F is sufficiently low, the reactor exit stream contains very little unreacted A. Thus there is no benefit from recycling, as we would only be recycling by-product C. If the value of the purge stream was zero, however, we would recycle as long as there is any A in the distillate at all.

- R_{min} is active at high F: As F increases, the reactor conversion goes down (Figure 2.8(a)) and the product stream will contain more unreacted A. This must be compensated by increasing V or decreasing L in the column. If $V = V_{max}$, we cannot increase it further and our only option is to reduce L, meaning the distillate flow rate increases and the bottoms flow rate decreases (see Figure 2.8(b). In this situation,

we have nothing to earn from recycling more, so the entire increase in distillate flow rate goes into the purge stream P, leading to a higher purge ratio P/D. For higher p_V, we may find the same even when $V < V_{max}$, because an increase in V costs more than it gives. We discuss this further below.

The physical bottleneck indicated in black in Figure 2.6 is reached when the optimal value of the purge flow rate P reaches its maximum value. The full set of active constraints at the physical quasi-bottleneck is:

$$\begin{aligned} x_{B,B} &= x_{B,B,min} \\ M_r &= M_{r,max} \\ T_r &= T_{r,max} \\ V &= V_{max} \\ P &= P_{max} \\ R &= 0 \end{aligned}$$

At this point, the plant cannot process any more feed without breaking the purity constraint on the product.

2.8.2 More on the effect of recycling

As mentioned above, we found that for low and high F it was optimal to purge all the distillate from the column, rather than recycling some of it. In Figure 2.9(a), we show how the optimal value of R (the recycle flow rate) varies with F, and Figure 2.9(b) shows the same for vapor boilup in the column. As we can see, at the lowest p_V the maximum recycle flow rate is reached just as V reaches V_{max}. However, for the two higher p_V values, the maximum recycle flow rate is reached *before* V reaches V_{max}. To understand this, consider the following: Let the fresh feed F be given, and start at a p_V value where V_{max} is inactive. Now consider that we reduce the purge fraction, thereby recycling more. This means production of B goes up, but column boilup V must increase accordingly. When the energy price becomes sufficiently high, the increased column boilup costs *more* than we earn from the increased bottoms product flow rate. In other words, we *lose* money by recycling more. If p_V is sufficiently high, it will be optimal to have $R = 0$ for *all* F - in Figure 2.6 we see that this happens at $p_V \approx 0.1\,\$/mol$.

It could be argued that when we operate in the region where the purge stream is rich in the reactant (A), it would be more economic to simply

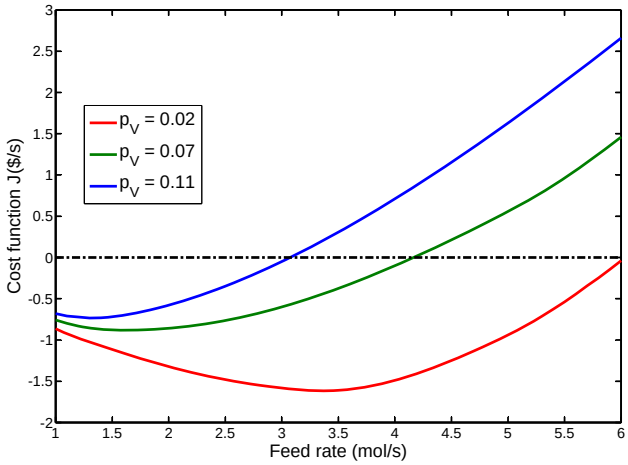

(a) Objective function J

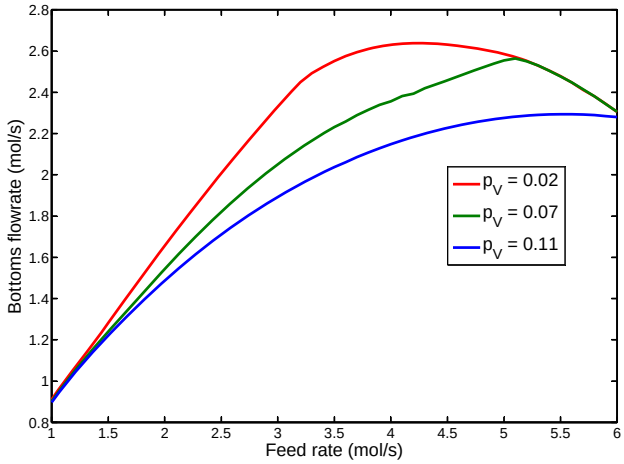

(b) Column bottoms flow rate B

Figure 2.7: Optimal objective function value J and column bottom product flowrate B as function of feed flow rate F at three values of p_V

bypass the plant, since we are not processing additional A to products anyway.

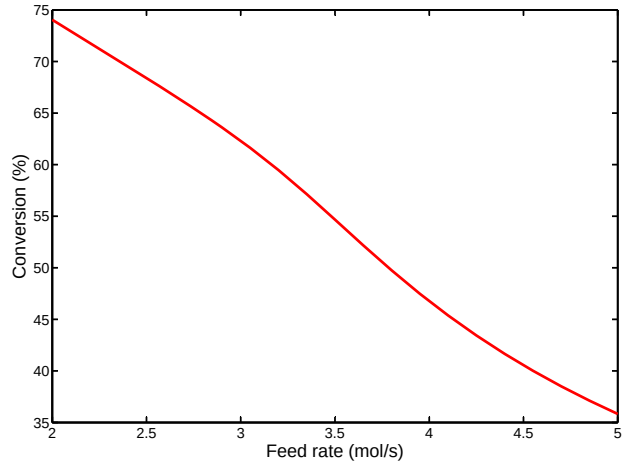

(a) Conversion as function of F

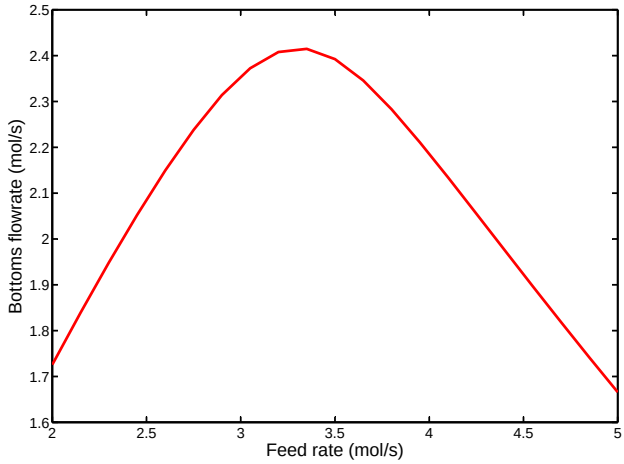

(b) Bottoms flowrate as function of F

Figure 2.8: Reactor conversion X and bottoms flow rate B as functions of F when M_r, $x_{B,B}$, T_r, V and P/D are fixed.

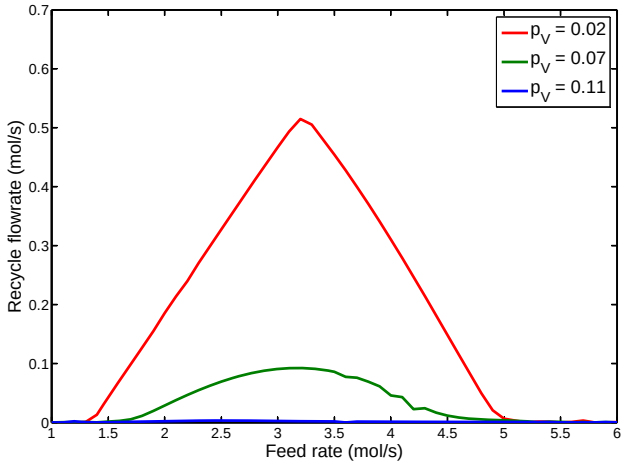

(a) Optimal value of recycle flow rate R as function of F

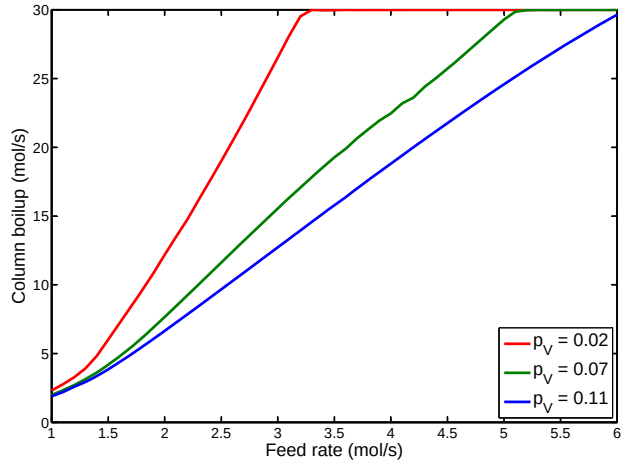

(b) Optimal value of boilup flow rate V as function of F

Figure 2.9: Selected variables as function of feed flowrate F for three different values of p_V

2.8.3 Efficiency and applicability of method

All optimizations were carried out without using analytical Jacobians, so the optimization solver would typically need 50-100 iterations to converge

to a solution. However, each iteration was quick since calculation of the objective and constraint function values was easy (as they involve no further equation solving). An interpolation search would typically require about 10 function evaluations (optimizations). If one should find the active constraint regions by just mapping the active constraints at a number of points evenly distributed over the disturbance space, it would be necessary to carry out many more optimizations - even if one kept the assumption that every region boundary was straight.

The assumptions stated earlier in the chapter are only to a certain extent *necessary* for the method. They help simplify the thinking involved, though. We can treat one constraint curve at a time, the regions will be found this way. This is simpler than starting with completely defining one region, and then trying to explore each neighboring region (if this is at all possible for highly nonlinear cases). If any single constraint function behaves highly nonlinear in parts of the disturbance space, it may be difficult to apply the method at all.

As stated in the introduction, part of the purpose of the chapter is to explore just how much can be done using process insight and how much must be found out by calculations. Our experience from this work is that when one has less *a priori* knowledge of the effect of disturbances on the process, the amount of time spent on calculations increases, but not necessarily drastically. For example, if one does not know whether a constraint line segment will be vertical/horizontal or not, one must find just one more point more than if one knows this. (That is, as long as one is satisfied with a straight line as an approximation for the true constraint curve).

The fact that the minimum constraint on R is active for both high and low F, but not for intermediate, gave rise to an additional challenge. For **fzero.m** to work, it requires two end points where the function for which we seek a zero, has different signs. Since the constraint was active both at high and low F, choosing values near 0 and F_{max} would yield two end points where the function value was positive. Thus we had to carry out a few extra optimizations at intermediate F to find a point where the optimal $R \neq 0$. In general, however, finding initial points for interpolation was easy. Generally it worked well to use the nominal point, combined with a point near the borders of the feasible region.

2.8.4 Comparison with Jagtap et.al.

Jagtap et al. (2010) study a process where two reactants A and B react according to the following reaction scheme:

$$\begin{aligned} A + B &\rightarrow C \\ B + C &\rightarrow D \end{aligned} \tag{2.15}$$

with C being the desired product and D being an unwanted byproduct. Instead of a purge stream, they use *two* distillation columns, and the desired product C is taken out in the distillate stream of the second column (however, the bottoms stream of that column may be seen as a replacement for a purge stream as this stream takes care of most of the by-product D). They use the "avoid product giveaway" rule to fix *three* specifications, all are directly related to exit stream compositions in the distillation columns. However, they use more indirect specifications, namely the ratio of B to C in the bottom stream from the first column, and the *loss* of C and D in the bottom and distillate streams, respectively, in column 2. These seem to be chosen more for the sake of easy steady-state convergence of the process model.

Like in this work, they find that when fresh feed is a degree of freedom, there is a feed rate at which the plant profit reaches a maximum, and any further increase in feed rate leads to a *decrease* in profit. This is because the increased feed rate does not lead to a sufficiently large increase in the amount of valuable product. An increased feed flow rate means a lower conversion percentage, so one gets more of the impurities in the reactor product. Then more needs to be recycled, and the increase in production rate is not high enough to "pay" for the increase in feed consumption rate.

A notable difference is that the region where the reactor temperature constraint is inactive, is much larger, and another constraint becomes active before it (V_{max} in the first column). This is probably because the reaction parameters are such that the temperature has a much stronger influence on reaction selectivity.

2.9 Conclusions

In this chapter, we have outlined a method for finding active constraint regions for a chemical process. We have applied the method to a simple reactor-distillation-recycle process, with feed flow rate and energy cost as disturbances.

For the example process, we find 5 distinct active constraint regions. There is a maximum feed flow rate, the physical bottleneck, above which we cannot operate without breaking constraints. If the feed flow rate is a

degree of freedom, rather than a disturbance, then the active constraints regions are identical, but in addition we find an economic bottleneck that occurs at lower feed flow rates. Above this economic bottleneck, increasing the feed rate leads to an economic loss.

References

Aske, E., 2009. Design of plantwide control systems with focus on maximizing throughput. Ph.D. thesis, NTNU.

Biegler, L. T., 2010. Nonlinear Programming: Concepts, Algorithms and Applications to Chemical Processes. SIAM.

de Araújo, A., Govatsmark, M., Skogestad, S., 2007. Application of plantwide control to the HDA process. I–steady-state optimization and self-optimizing control. Control engineering practice 15 (10), 1222–1237.

Gilliland, E., Gould, L., Boyle, T., 1964. Dynamic effects of material recycle. Prepr. JACC, Stanford, CA, 140–146.

Jagtap, R., Kaistha, N., Skogestad, S., 2010. Plantwide Control to Economic Optimum of a Recycle Process with Side Reaction, submitted to Industrial & Engineering Chemistry Research.Manuscript ID: ie-2010-024358.R2.

Kanbur, R., 2008. shadow pricing. In: Durlauf, S. N., Blume, L. E. (Eds.), The New Palgrave Dictionary of Economics. Palgrave Macmillan, Basingstoke.

Kiss, A., Bildea, C., Dimian, A., Iedema, P., 2004. State multiplicity in multi-reaction reactor-separator-recycle systems. In: Barbosa-Pvoa, A., Matos, H. (Eds.), European Symposium on Computer-Aided Process Engineering-14, 37th European Symposium of the Working Party on Computer-Aided Process Engineering. Vol. 18 of Computer Aided Chemical Engineering. Elsevier, pp. 223 – 228.

Larsson, T., Govatsmark, M., Skogestad, S., Yu, C., 2003. Control structure selection for reactor, separator, and recycle processes. Industrial & Engineering Chemistry Research 42 (6), 1225–1234.

Lid, T., 2007. Data reconciliation and optimal operation. Ph.D. thesis, NTNU.

Luyben, M., Fluodas, C., 1994. Analyzing the interaction of design and control–2. reactor-separator-recycle system. Computers & Chemical Engineering 18 (10), 971 – 993.

Luyben, W. L., 1993. Dynamics and control of recycle systems. 1. simple open-loop and closed-loop systems. Industrial & Engineering Chemistry Research 32 (3), 466–475.

Maarleveld, A., Rijnsdorp, J., 1970. Constraint control on distillation columns. Automatica 6 (1), 51 – 58.

Naidu, D., 2003. Optimal control systems. CRC.

Nocedal, J., Wright, S., 1999. Numerical optimization. Springer verlag.

Skogestad, S., 2000. Plantwide control: The search for the self-optimizing control structure. Journal of process control 10 (5), 487.

Skogestad, S., Morari, M., 1988. Understanding the dynamic behavior of distillation columns. Industrial & Engineering Chemistry Research 27 (10), 1848–1862.

Wu, K.-L., Yu, C.-C., 1996. Reactor/separator processes with recycle–1. candidate control structure for operability. Computers & Chemical Engineering 20 (11), 1291 – 1316.

Wua, K., Yu, C., Luyben, W., Skogestad, S., 2001. Reactor/separator processes with recycles–2. design for composition control. Computers & Chemical Engineering 27 (3), 401–421.

Chapter 3

Active constraint regions for optimal operation of distillation columns

Submitted to *Industrial & Engineering Chemistry Research*

When designing the control structure of distillation columns, with optimal operation in mind, it is important to know how the active set of constraints changes with disturbances. This issue has received little attention in the literature. This chapter applies a procedure presented in the previous chapter, to find how the active constraints for distillation columns change with variations in energy cost and feed flow rate.

The production of the most valuable product is maximized by keeping its purity on the minimum allowed, that is, by keeping the valuable product on spec. This is the "avoid product give-away" rule. In this chapter, we discuss the assumptions under which this rule is valid for the overall optimization of the plant. We find that it generally holds when product prices are constant, i.e. independent of purity.

This chapter includes three case studies; a single distillation column with constant product prices, a single column where the price of the most valuable product is dependent on purity, and two distillation columns in series. In all three case studies there is a bottleneck, corresponding to a feed flow rate above which the column(s) can not operate without breaking constraints.

3.1 Introduction

The literature on control of distillation processes is vast, some examples include Luyben (1979) (general), Waller et al. (1988) (sensitivity to disturbances), Skogestad and Morari (1987) (selection of control structure) and Nagy et al. (2007) (advanced control). The surveys by McAvoy and Wang (1986) and Skogestad (1993), covering the 1980s, illustrate just how widely the area has been researched. However, few papers deal with optimal operation. Maarleveld and Rijnsdorp (1970) and Gordon (1986) discuss active constraints, but apart from these two papers, this issue has received little attention. This is strange considering that optimal control of any process plant is completely dependent on which process constraints are active at the operating point.

Also when designing ordinary feedback control schemes, knowing the active constraint regions is important. For example, when seeking a *self-optimizing control structure* (Skogestad, 2000), one needs to know which variables are constrained and which are not. The active constraints are always selected as controlled variables to be used for feedback, in the case of output constraints, or simply set to be constant, in the case of input constraints. Also, a control structure which works fine for one set of active constraints may be infeasible for another. In some cases, it may be necessary to switch to another control structure, whereas in other cases one control structure may be optimal in one region and near-optimal in neighboring regions.

It is easy to understand how active constraints can influence on the choice of control structure; if a variable is optimally at its constraint value, it cannot be used to control another variable without accepting economic loss. This is because when we want to use the constrained variable for control, we can not keep it at its optimal value at all times. How the optimal states of the model vary with disturbances, is often formulated as a so-called *multi-parametric programming* problem (Pistikopoulos et al. (2007), Tøndel et al. (2003), Kvasnica et al. (2004)). One seeks to find a solution which itself is parameterized by the disturbances. The problem can be linear, quadratic or some other nonlinear type of problem - in chemical engineering applications like distillation, the latter is almost always the case.

In Chapter 2, we outlined a procedure for sketching the active constraint regions for chemical processes using few optimizations, and applied it on a "toy example". In this chapter we seek to use this method on distillation columns. The chapter is structured as follows:

First we discuss optimal operation of distillation columns. Next, the

case studies are described and the main results are given. We then give a short summary of the method from Chapter 2 , discuss the efficiency of the method, and go more in detail about optimal operation of distillation columns. We finally discuss the *avoid product giveaway* rule, including a simple counterexample to one of the assumptions it rests on. The following case studies are included:

- Case study Ia: A single distillation column, constant product prices.
- Case study Ib: A single distillation column where the distillate price is proportional to purity x_D.
- Case study II: Two distillation columns in sequence, again with constant product prices.

In all three case studies we use of a simple distillation model with 40 equilibrium stages with the feed entering at the middle stage. The model uses the following assumptions: Constant relative volatilities, constant molar overflow, constant pressure over the entire column, equilibrium at every stage and negligible vapour holdups. This is the "Column A" model used in Skogestad and Morari (1988)), but the product purity specifications are more lax (95% for one product versus 99% for both products for column A). The relative volatility is 1.5 for cases Ia and Ib with a single column (as for "column A"), but for case II with two columns it is 1.33 for the A/B split in the first column, and 1.5 for the B/C split in the second column.

In the discussion, we give some more insight into the behaviour of objective and constraint functions for the optimization problem in case study Ia.

3.2 Optimal operation of distillation columns

3.2.1 Form of the optimization problem

The optimization problem we are dealing with, is a nonlinear problem on the form

$$\begin{aligned} \min_{u} \quad & J(x,u,d) \\ \text{subject to} \quad & f(x,u,d) = 0 \\ & c(x,u,d) \leq 0 \end{aligned} \tag{3.1}$$

where J is the economical objective, $f(x,u,d)$ the process model equations and $c(x,u,d)$ the process constraints. x are the internal variables

(states) in the process model, u are the variables we may manipulate (inputs) and d are the disturbances. In Chapter 2 we have elaborated more on various formulations, how the optimality conditions can be related to the suggested method for finding active constraint regions, and the significance of the Lagrange multipliers at the optimal solution. In short, the latter can be summarized as follows: *At the optimal solution, the magnitude of the Lagrange multiplier λ tells us how much we lose by backing off from an active constraint.*

To define the problem, we need to formulate a cost function which captures the plant economy we are interested in. This cost function is to be minimized with respect to the available degrees of freedom u (while satisfying given constraints c) for the expected range of process disturbances d.

3.2.2 Plant economics and objective function

In distillation, the cost is related to the feed streams, as well as heating and cooling (and possibly other utilities, like pumping). The profit comes from selling the products. To optimize operation on a short time scale, say within a few hours, there is no need to include fixed costs such as capital cost, manpower and maintenance. The operational objective (cost) to be minimized can be written as

$$J = \sum_{i=1}^{n_f} p_{f,i} F_{f,i} + \sum_{j=1}^{n_U} p_{U,j} F_{U,j} + \sum_{k=1}^{n_P} p_{P,k} F_{P,k} \tag{3.2}$$

Here, n_f, n_U and n_P are the number of feed streams, utility streams and product streams, respectively. Correspondingly, p stands for the price of each stream in ($/mol) and F the feed flowrate (in mol/s).

For a single distillation column with one feed stream and two products, no side streams and no heat integration, we may simplify the cost function to the following:

$$J_1 = p_F F + p_L L + p_V V - p_D D - p_B B \tag{3.3}$$

where F, L, V, B and D are the flow rates of feed, reflux, boilup, bottoms and distillate, respectively; see Figure 3.1. The objective function can in most cases be simplified further. For a given feed, an energy balance for the column gives that the reboiler heat duty and condenser heat duty, and also the internal liquid and vapor flows inside the column, are nearly proportional.

Proof: The energy balance is:

$$Q_B + Q_C + F \cdot h_F = D \cdot h_D + B \cdot h_B \tag{3.4}$$

where Q_C is negative. For a given feed (Fh_F), and approximately constant product composition (Dh_D and Bh_B approximately constant), we have $dQ_D = -dQ_B$, so the change in reboiler duty and condenser duty are the same. It is therefore reasonable to combine the terms to give a new and simpler objective function

$$J_2 = p_F F + p_V V - p_D D - p_B B \tag{3.5}$$

where p_V in Equation 3.5 is approximately equal to $p_L + p_V$ in Equation 3.3. This is the form of objective function we will use in the case studies included in this chapter. Provided that we satisfy the product specifications, the prices are usually constant (independent of process states). However, in some cases they may depend on product quality, for example, if we pay or get paid only for the valuable component in a stream, in which case the price can be written

$$p' = px \tag{3.6}$$

where x is the mole fraction of the component we get paid for, and p is the price for the pure component. In this chapter, we include one case study where we only get paid for the light component in the distillate, i.e. $p'_D = p_D x_D$ where x_D is the mole fraction of light component.

3.2.3 Degrees of freedom

As explained in Skogestad et al. (1990), when we assume a given feed and given pressure, a distillation column has got two steady-state degrees of freedom. Dynamically, there are four remaining manipulated variables, but there are two levels that need to be controlled dynamically, but which have no steady-state effect. The two degrees of freedom can, for example, be selected as two flow rates,

$$u = [L\ V], \tag{3.7}$$

but any pair of two independent specifications can be used. For example, we may control (i.e. specify) the concentration of the key impurity in each product stream, or two tray temperatures. For optimization, we should choose as degrees of freedom the variables that make the problem easiest to solve numerically.

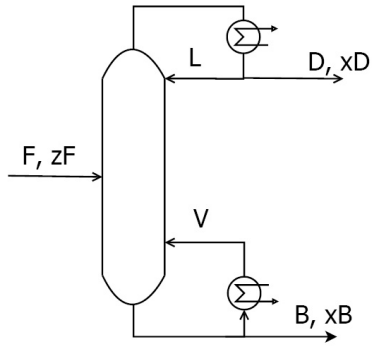

Figure 3.1: Conventional distillation column with one feed and two products

3.2.4 Constraints

The constraints ($c(x, u, d) \leq 0$) will typically consist of product purity requirements and restrictions on operating conditions. Typically, there will be maximum and minimum limits on internal flows (in a column, defined by the weeping and flooding points Kister (1990)). In addition, there may be restrictions on column pressure, since column pressure has a big influence on condensation and evaporation temperatures. The product purity constraints are usually expressed in terms of the mole fraction of the main component in each stream:

- Distillate specification: $x_D \geq x_{D,min}$ where x_D is the mole fraction of light key component in D.
- Bottoms specification: $x_B \geq x_{B,min}$ where x_B is the mole fraction of heavy key component in B.

For a two-component mixture, this is unproblematic, but for a multicomponent mixture this constraint formulation may cause problems, as there may be more than one composition that satisfies the constraint (except for the lightest and heaviest components). Thus, one may get a more robust problem specification by instead giving the following specifications (Luyben, 1992):

- Distillate specification: $x_D \leq x_{D,max}$ where x_D is the mole fraction of heavy key impurity in D.

- Bottoms specification: $x_B \leq x_{B,max}$ where x_B is the mole fraction of light key impurity in B.

Regarding the capacity constraints, there may be many just in one column: Maximum available reboiler heating or condenser cooling, flooding and weeping points, and possibly maximum flows of product streams due to a potential downstream bottleneck. In this paper, we simplify and assume that it is sufficient to specify a maximum vapour boilup V;

$$V \leq V_{max} \tag{3.8}$$

In the case study with two columns, we use different values of V_{max} for the two columns.

3.2.5 Disturbances

The disturbances (d) are the variables that influence on either the process or the economical objective, but which we cannot influence. For a distillation column, or a chemical process unit in general, the feed conditions (flow rate, temperature, pressure and composition) are important disturbances. The constraint values (including purity specifications and flow limits) are also generally important disturbances. Finally, prices of feeds, products and energy will be subject to change, and should also be considered disturbances. In the case studies included here, we consider only the feed flow rate (F) and energy cost (p_V) as disturbances.

The main reason for not including other disturbances, for example, in feed composition, feed enthalpy or product purity specifications, is that it is difficult to show the constraints regions graphically when there are more than two disturbances. We believe that the two selected disturbances in feed rate and relative energy price are very relevant in most applications. In practice, one should focus on the disturbances that are expected to be important for future operation, as a complete map of all disturbances will be very time consuming.

3.3 Case studies

3.3.1 Case Study Ia: One distillation column, constant product price

For the first case study, we consider a single distillation column with 41 stages and feed entering at stage 21, separating a feed mixture of equal

Table 3.1: Data used for case studies Ia and Ib

Variable	Value
α_{AB}	1.5
z_F	0.5
F	variable (1-1.6 mol/s)
p_F	1 \$/mol
p_B	1 \$/mol
p_D	2 \$/mol
p_V	variable (0.01-0.02 \$/mol)
$x_{B,min}$	0.990
$x_{D,min}$	0.950
V_{max}	4.008 mol/s

fractions of A and B, with relative volatility $\alpha_{AB} = 1.5$. The optimization problem may be formulated as follows:

$$\begin{aligned} \min_{u} \quad & J(u,d) = p_F F + p_V V - p_B B - p_D D \\ \text{subject to:} \quad & x_B \geq x_{B,min} \\ & x_D \geq x_{D,min} \\ & V \leq V_{max} \end{aligned} \tag{3.9}$$

where $u = [L\ V]$ and $d = [F\ p_V]$. The model equations (component mass balances for each stage and equilibrium calculations) are solved explicitly and are thus not shown in Equation 3.9. The constraints on x_B and x_D refer to the mole fractions of the main component in each stream (component B in the bottoms stream (B) and component A in the distillate stream (D), respectively). The p values refer to the prices of each respective stream. The prices and other data used in this case study are shown in Table 3.1.

The case study uses the feed rate F and the energy price p_V as disturbances, and our goal is to establish the regions where the constraints on x_B, x_D and V are active, while using as few optimizations as possible. The feed rate F varies from 1.1 to 1.6 mol/s. The prices for the feed (F) and bottoms product (B) are both set at a reference price of 1 \$/mol, whereas the valuable distillate product (D) is 2 \$/mol.

In our case study, the relative energy price p_V/p_F varies between 0.01 and 0.02, and as we argue in the following, this is a reasonable relative price range. For hydrocarbon feed mixtures, the energy can be generated by burning some of the feed, and since the heat of combustion is about 100

times larger than the heat of vaporization for hydrocarbons, we expect for hydrocarbons that p_V/p_F should be about 0.01 (or less, if cheaper energy sources are available). However, in general, for other feed mixtures, the relative energy price can vary greatly, from 0 and up to a value similar to the feed and products (about 1). Also note that energy prices can vary greatly from one day to the next, depending on external conditions and prices. For cryogenic applications, where cooling rather than heating is costly, the relative energy price p_V/p_F may exceed 0.02 or more, even for hydrocarbon mixtures. The reason is that cryogenic cooling requires electricity as the energy source.

Let us now generate the active constraint regions as a function of the two selected disturbances (F, p_V). To start, we use our knowledge about the nature of the process model and the optimization problem to state the following:

1. With $N_C = 3$ inequality constraints, there may be at most $2^{N_C} = 8$ sets of active constraints, possibly including infeasible regions where there are more active constraints than degrees of freedom. Here we have two degrees of freedom (u), so the region with three active constraints will be infeasible. As we will conclude later, there are only three regions in this case.

2. The constraint on x_D will be active for all values of (F, p_V). This is because separating this stream to a higher purity will require that we reduce the flowrate D, or increase the internal streams L and V. Since we do not get paid for the increased purity, this is not profitable. In other words, we should seek to *avoid product giveaway* (Gordon (1986), Skogestad (2007)). This rule is discussed in more detail later.

3. At low energy cost p_V, the constraint on x_B will be inactive, meaning that we should overpurify the bottom product. This is because we get a better price for the distillate, and by overpurifying the bottom product we move component A from bottoms to distillate. This is profitable when energy is cheap.

4. As p_V increases, the optimal value of x_B decreases, and at $p_V = p_{V,1}$ it reaches $x_{B,min}$. Since the column stage efficiency is assumed constant at 100% (rather than dependent of flow), the value of $p_{V,1}$ is independent of F.

5. **Bottleneck**: There exists a maximum feed rate F_{max}, above which we cannot achieve feasible operation, i.e. satisfy all three constraints.

This can be seen from a simple degree of freedom consideration: Assume we keep both purities at their constraint values by adjusting L and V. As we increase F, all other flows, including L and V will increase proportionally. Eventually, we reach $V = V_{max}$, where a further increase in F will force us to break one of the purity constraints.

6. From the above, we can conclude that we will have three feasible regions: (I): x_D active, (II): x_D and V_{max} active, and (III): x_D and x_B active. Regions I and III will be separated by a straight line (as explained above). The same goes for the border between the infeasible region (IV) and the others. See Figure 3.2.

7. The border between regions I and II intersects with the border between regions I and III exactly at F_{max}. The border between regions I and II is the only one for which we cannot say *a priori* whether it will be straight or not.

Using the method described in Chapter 2, we obtain the following numerical values, which are sufficient for sketching the active constraint regions (shown in Figure 3.2):

- The maximum feed rate is $F_{max} = 1.435\, mol/s$.
- For all $F < F_{max}$, $x_B = x_{B,min}$ is active when $p_V > 0.0144\$/mol$.
- At $p_V = 0.01$, $V = V_{max}$ is active for $F > 1.233\, mol/s$.

Notice that the line between regions I and II is shown as being straight. This is because it is based on only two data points - in reality it is slightly curved. The constraint lines in Figure 3.2 are as follows:

- Red: V_{max} becomes active.
- Blue: x_B becomes active.

The vertical parts of these two constraint lines indicate $F = F_{max}$. Table 3.2 lists optimal data at selected points in the disturbance space.

In Figure 3.3 we show how the Lagrange multipliers λ for the active constraints behave at $p_V = 0.01$. As expected, the λ corresponding to x_D is always positive. The λ corresponding to V_{max} becomes nonzero at $F = 1.233\, mol/s$. Notice that it increases very slowly up to $F = 1.37$ - this means that up to $F = 1.37$, this constraint does not influence strongly on the plant objective.

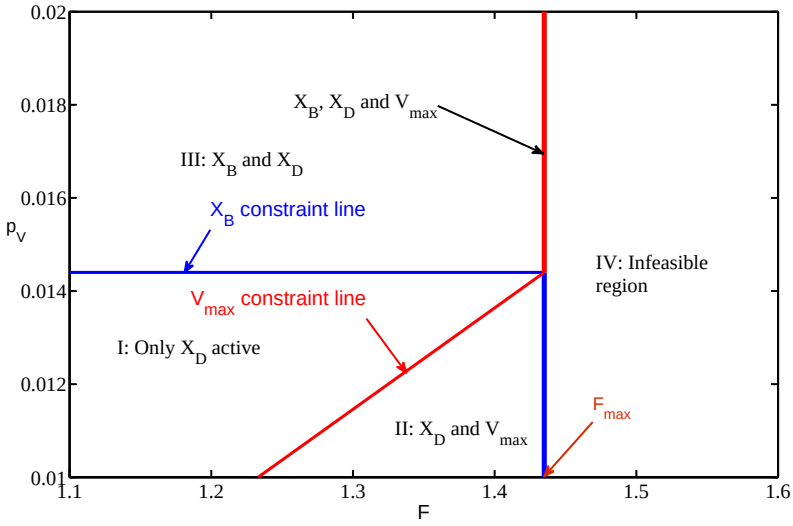

Figure 3.2: Active constraint regions for single column with fixed prices (case Ia)

Table 3.2: Single column (case Ia): Values of key variables at selected disturbances (F, p_V) (numbers in **bold** indicate active constraints)

Region(s)	I	II	III
F [mol/s]	1.2	1.4	1.3
p_V [\$/mol]	0.01	0.01	0.015
L [mol/s]	2.827	3.276	2.949
V [mol/s]	3.454	**4.008**	3.627
D [mol/s]	0.627	0.731	0.678
B [mol/s]	0.573	0.669	0.622
x_D	**0.950**	**0.950**	**0.950**
x_B	0.992	0.992	**0.990**
J [\$/s]	-0.536	-0.625	-0.566

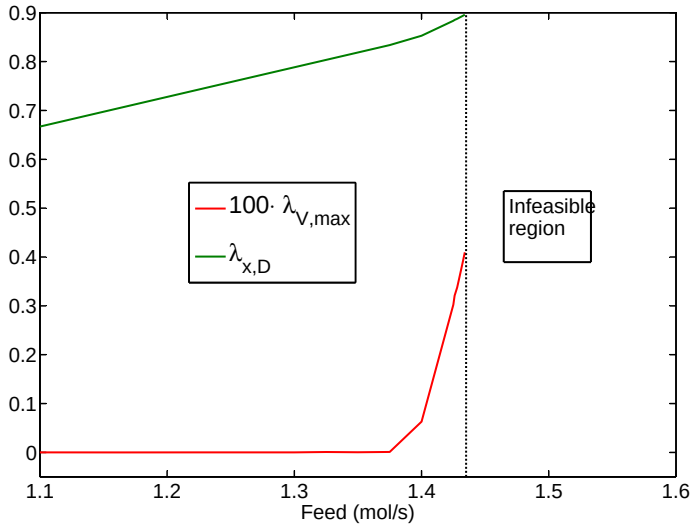

Figure 3.3: Single column (case Ia): Lagrange multipliers for active constraints at $p_V = 0.01$

3.3.2 Case Study Ib: One distillation column, variable product price

In the second study, the constraints are the same, but the objective function is altered to make the price of the distillate stream proportional to its purity, that is, one gets paid for the valuable component only:

$$J(u,d) = p_F F + p_V V - p_B B - p'_D D \tag{3.10}$$

where

$$p'_D = p_D x_D \tag{3.11}$$

p_D and the other prices are the same as in case study Ia (Table 3.1). The consequence of the varying price p'_D is that we now may have additional regions where the constraint on x_D is *inactive*. The reason for this is: When energy is cheap enough, we may overpurify the distillate D without giving away anything (as we get paid for the extra component A in the distillate D). Since component B in the distillate is now worthless, it is profitable to send it to the bottom instead. As the energy cost p_V increases, the purity

constraints become active. Just as for the first case, we can deduce some things about the active constraint regions *a priori*, before carrying out any optimizations:

1. As above, theoretically there may be at most 7 regions (since the region with three active constraints is infeasible). As we will show, only five of these regions are present.

2. The lines separating the different regions where only purity constraints are active, will be horizontal. In the following, the p_V values corresponding to these lines will be referred to as $p_{V,1}$ and $p_{V,2}$.

3. We will have a region where no constraints are active and one where $V < V_{max}$ is the only active constraint.

4. We will have a region where *one* purity constraint is active and $V = V_{max}$. The border between this region and the previous one will be vertical. This can be explained as follows: When V is fixed at V_{max}, p_V has no influence on the optimal solution - the F value for which the next constraint becomes active is independent of p_V and thus the line is vertical. This F value will be referred to as F_1.

5. As for the previous case, we have a value of F for which all constraints are active, and for any higher F value we cannot satisfy all constraints. This value will be referred to as F_{max}.

6. The two regions with two active constraints will meet in a point on the line $F = F_{max}$, just like regions II and III in Figure 3.2.

7. As $p_V \to 0$, the value of F at which $V_{optimal} = V_{max}$ will also approach 0. This is because when the energy utility is free, and there is a benefit from extra purity, we want to maximize both purity and flow rate of the distillate stream. This means we can use the point $F = 0$, $p_V = 0$ when constructing the diagram.

This means if we take the assumption that the regions with $V = V_{max}$ are also separated by straight lines from the regions where $V < V_{max}$, we are left with the task of finding just a few values for F (F_1 and F_{max}) and p_V ($p_{V,1}$ and $p_{V,2}$). The actual values are shown in Table 3.3, and the resulting active constraint regions are shown in Figure 3.4. Table 3.4 gives optimal data at selected points in the disturbance space (one point inside each region). In Figure 3.4, we have three constraint lines:

Table 3.3: Single column (case Ib): Values for F and p_V needed to draw Figure 3.4

Variable	Value
F_1	1.23
F_{max}	1.44
$p_{V,1}$	0.014
$p_{V,2}$	0.106

Table 3.4: Single column (case Ib): Values of key variables at selected (F, p_V) (numbers in **bold** indicate active constraints)

Region(s)	I	II	III	IV	V
F [mol/s]	0.7	1.2	1.3	1.0	1.0
p_V [$/mol]	0.013	0.010	0.010	0.05	0.12
L [mol/s]	2.048	3.408	3.355	2.443	2.268
V [mol/s]	2.423	**4.008**	**4.008**	2.951	2.790
D [mol/s]	0.375	0.600	0.653	0.508	0.521
B [mol/s]	0.375	0.600	0.647	0.492	0.479
x_D	0.9905	0.9918	0.9853	0.9755	**0.9500**
x_B	0.9901	0.9914	**0.9900**	**0.9900**	**0.9900**
J [$/s]	-0.3411	-0.5558	-0.6004	-0.3605	-0.1969

- The *red* constraint line indicates where x_B becomes active.
- The *blue* constraint line indicates where V_{max} becomes active.
- The *green* constraint line indicates where x_D becomes active.
- At $F = F_{max}$, the blue and green constraint lines are vertical, and they intersect in the point $(F_{max}, p_{V,2})$.

It is also worth noticing that the value of p_V for which x_D becomes active (p_{V_2}) is quite high. This is because the number of stages in the column (column A (Skogestad and Morari, 1988)) was designed to obtain 99 % purity in both ends. This makes overpurifying cheap in terms of energy.

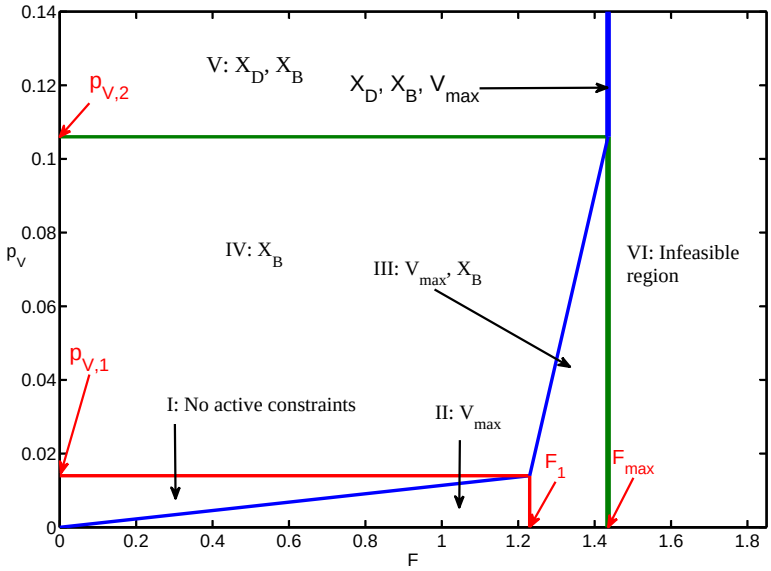

Figure 3.4: Single column (case Ib): Active constraint regions with purity-dependent distillate price ($p'_D = p_D x_D$)

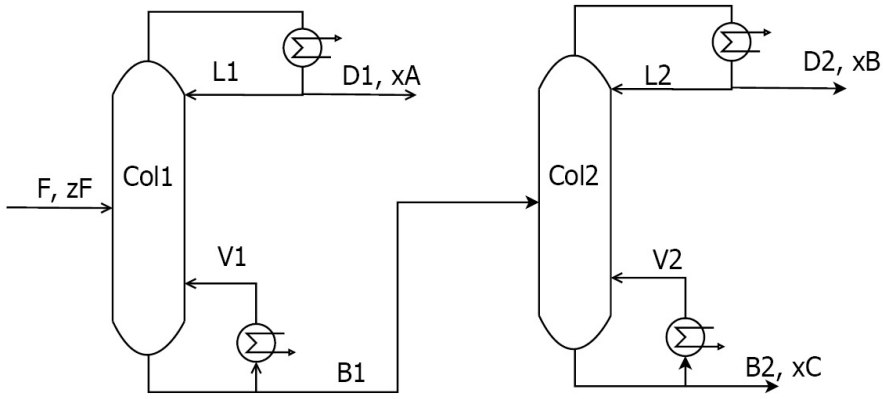

Figure 3.5: Two distillation columns in sequence

3.3.3 Case study II: Two distillation columns in sequence

In the third and final case study, we consider two distillation columns in series, both with the same number of stages (41) and feed entering at stage 21. The feed now contains three components, A, B and C, where A is the most volatile and C the least volatile, and B is the most valuable product. The two columns with stream names are shown in Figure 3.5. The relevant parameters are summarized in Table 3.5. For simplicity we will refer to x_{A,D_1}, x_{B,D_2} and x_{C,B_2} simply as x_A, x_B and x_C, respectively.

The objective function is again formulated as a function of (u, d),

$$J(u,d) = p_F F + p_V(V_1 + V_2) - p_A D_1 - p_B D_2 - p_C B_2 \tag{3.12}$$

with $u = [L_1\ V_1\ L_2\ V_2]$ [1] and $d = [F\ p_V]$.

The constraints are defined as follows;

$$\begin{aligned} x_A &\geq x_{A,min} \\ x_B &\geq x_{B,min} \\ x_C &\geq x_{C,min} \\ V_1 &\leq V_{1,max} \\ V_2 &\leq V_{2,max} \end{aligned} \tag{3.13}$$

Just as for the case of one column, we can deduce some things about the active constraints regions before carrying out optimization:

- There can be at most $2^5 = 32$ regions, of which 31 will be feasible (we have four independent inputs, so we cannot satisfy all five constraints). We will show that the actual number of regions in this case study is 8.
- There exists a value F_{max} above which we cannot satisfy all constraints.
- D_2 is the most valuable product stream, so the constraint on x_B will remain active for all disturbances d. This reduces the maximum number of regions to 16 (of which 15 are feasible).
- As for *both* one-column cases, the lines separating the regions with only purity constraints active will be horizontal. The p_V values corresponding to these lines will be referred to as $p_{V,1}$ (the lower value) and $p_{V,2}$.

[1] This choice of u is not unique, and in the optimization we actually use the four product compositions as degrees of freedom

Table 3.5: Data for two columns (case II)

Variable	Value
α_{AB}	1.333
α_{BC}	1.5
zF	[0.4 0.2 0.4]
$V_{1,max}$	4.008 mol/s
$V_{2,max}$	2.405 mol/s
$x_{A,min}$	0.9500
$x_{B,min}$	0.9500
$x_{C,min}$	0.9500
p_F	$1\,\$/mol$
p_A	$1\,\$/mol$
p_B	$2\,\$/mol$
p_C	$1\,\$/mol$
p_V	variable

- Above $p_{V,2}$, there will be a region where all three purity constraints are active while both capacity constraints are inactive. The F value for which the first capacity constraint becomes active will be independent of p_V, meaning the region in question will be bordered to the right by a *vertical* line at an F we shall refer to as F_1.

- For low p_V, we will have a region where the constraint on x_B will be active along with the constraints on V_1 and V_2. At some value of F, one of the remaining purity constraints will become active. This F value is independent of p_V, because the term $p_V(V_1 + V_2)$ in the objective function is constant in this region, meaning this region will also be bordered by a vertical line to the right. This F value is referred to as F_2.

- At $p_{V,1}$, one of the capacity constraints (V_1 or V_2) will become active at some $F < F_{max}$. We refer to this value as F_3.

To sketch the active constraint regions, we need to find $p_{V,1}$, $p_{V,2}$, F_1, F_2 and F_{max}. These are summarized in Table 3.6. For all the region borders that are neither vertical nor horizontal, we also need an additional data point in addition to their intersection with one of the already established lines. By applying the same method as above, we come up with the regions shown in Figure 3.6. The constraint lines are given different colors:

Table 3.6: Two columns (case II): Values for F and p_V needed to draw Figure 3.4

F_1	1.442 mol/s
F_2	1.469 mol/s
F_3	1.458 mol/s
F_{max}	1.489 mol/s
$p_{V,1}$	0.0382 \$/mol
$p_{V,2}$	0.1441 \$/mol

Table 3.7: Two columns (case II): Active constraints in each region

Region number	Constrained variable(s)
I	x_B
II	x_A, x_B
III	x_B, V_1
IV	x_A, x_B, x_C
V	x_A, x_B, V_1
VI	x_B, V_1, V_2
VII	x_A, x_B, x_C, V_1
VIII	x_A, x_B, V_1, V_2
IX	x_A, x_B, x_C, V_1, V_2

- Along the *red* line, x_A becomes active.
- Along the *orange* line, V_1 becomes active.
- Along the *blue* line, V_2 becomes active.
- Along the *green* line, x_C becomes active.
- The black line indicates F_{max}, which is reached when x_C once again becomes active.

In the following discussion, we will refer to the various regions in Figure 3.6 as indicated in Table 3.7. Note that region IX, with five active constraints, corresponds to the vertical black line in Figure 3.6.

When we examine Figure 3.6, we notice two things that may at first seem surprising.

- The line separating regions II and V (part of the *orange* constraint line) has a negative slope. Thus we have that the optimal value of V_1

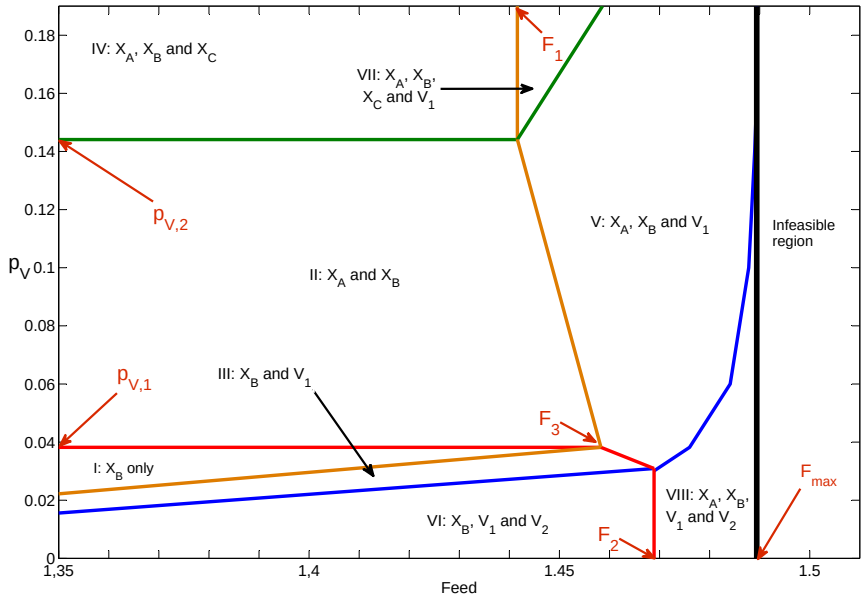

Figure 3.6: Two columns (case II): Active constraint regions

increases with increasing p_V, which seems counter-intuitive. However, this is compensated by a decrease in V_2 - the sum $V_1 + V_2$ is actually decreasing, which is what we would expect.

- The next interesting feature about Figure 3.6 is that the border between regions V and VII (part of the *green* constraint line) is *not* horizontal. Across this border, the constraint on x_C switches between active and inactive. The reason for this one not being horizontal, is the following: When starting with only the three purity constraints active, an increase in F leads to a proportional increase in all streams, until the first capacity constraint becomes active (in this case, this means V_1). Now, since V_1 is not allowed to increase further, any extra A fed to the system must either go to stream D_1, meaning the constraint on x_A is no longer active, or more A goes through to the second column where it enters the distillate stream D_2. Thus we need to put more C into stream B_2, thus making the constraint on x_C, inactive. Thus, one of two purity constraints *must* become inactive at this point. Of course, it will become active again once we reach F_{max}.

- The black line indicating F_{max} could be seen as part of the constraint line for x_C. However, the two are not connected - this is why we choose to show them in different colors.

- The line separating regions II and V (part of the *orange* constraint line) has a negative slope. Thus we have that the optimal value of V_1 *increases* with increasing p_V, which seems counter-intuitive. However, this is compensated by a decrease in V_2 - the sum $V_1 + V_2$ is actually decreasing, which is what we would expect.

- The next interesting feature about Figure 3.6 is that the border between regions V and VII (part of the *green* constraint line) is *not* horizontal. Across this border, the constraint on x_C switches between active and inactive. The reason for this one not being horizontal, is the following: When starting with only the three purity constraints active, an increase in F leads to a proportional increase in all streams, until the first capacity constraint becomes active (in this case, this means V_1). Now, since V_1 is not allowed to increase further, any extra A fed to the system must either go to stream D_1, meaning the constraint on x_A is no longer active, or more A goes through to the second column where it enters the distillate stream D_2. Thus we need to put more C into stream B_2, thus making the constraint on x_C, inactive. Thus, one of two purity constraints *must* become inactive at this point. Of course, it will become active again once we reach F_{max}.

- The black line indicating F_{max} could be seen as part of the constraint line for x_C. However, the two are not connected - this is why we choose to show them in different colors.

It is also worth noting that the objective function J becomes positive above a fairly low value for p_V (approximately $p_V = 0.05$) for all $F \in \langle 0, F_{max} \rangle$. This means operation in this region is not economically profitable - thus we would only operate in this region if we have to. Finally, Table 3.8 shows flow rates and compositions at the optimal solution at selected points in the disturbance space (one point in each of the eight regions).

3.4 Discussion

3.4.1 Method for finding active constraint regions

In Chapter 2, we outlined a method for finding active constraint regions (illustrated with a two-dimensional example). It is based on that when a

Table 3.8: Optimal data for selected points in case study II (numbers in **bold** indicate active constraints)

Region	I	II	III	IV	V	VI	VII	VIII
F	1	1.4	1.22	1.35	1.48	1.4	1.45	1.48
p_V	0.01	0.1	0.01	0.1441	0.10	0.01	0.18	0.01
V_1	3.335	3.870	**4.008**	3.754	**4.008**	**4.008**	**4.008**	**4.008**
L_1	2.935	3.290	3.516	3.194	3.396	3.436	3.407	3.396
B_1	0.600	0.820	0.732	0.791	0.869	0.829	0.849	0.869
D_1	0.400	0.580	0.488	0.559	0.611	0.571	0.601	0.612
$x_{A,D1}$	0.982	0.962	0.980	**0.950**	**0.950**	**0.950**	**0.950**	**0.950**
$x_{B,D1}$	0.018	0.038	0.020	0.050	0.050	0.050	0.050	0.050
$x_{C,D1}$	0.000	0.000	0.000	0.000	0.000	0.000	0.000	0.000
$x_{A,B1}$	0.013	0.011	0.013	0.011	0.013	0.013	0.011	0.013
$x_{B,B1}$	0.321	0.306	0.320	0.306	0.305	0.312	0.306	0.306
$x_{C,B1}$	0.666	0.683	0.667	0.683	0.682	0.676	0.683	0.682
V_2	1.862	2.015	2.275	1.843	2.310	**2.405**	2.006	**2.405**
L_2	1.662	1.772	2.031	1.618	2.048	2.139	1.764	2.136
B_2	0.400	0.577	0.488	0.566	0.607	0.563	0.608	0.600
D_2	0.200	0.243	0.243	0.225	0.262	0.265	0.242	0.268
$x_{A,D2}$	0.038	0.038	0.038	0.038	0.042	0.039	0.039	0.041
$x_{B,D2}$	**0.950**	**0.950**	**0.950**	**0.950**	**0.950**	**0.950**	**0.950**	**0.950**
$x_{C,D2}$	0.012	0.012	0.012	0.012	0.008	0.011	0.011	0.009
$x_{A,B2}$	0.000	0.000	0.000	0.000	0.000	0.000	0.000	0.000
$x_{B,B2}$	0.007	0.035	0.007	0.050	0.027	0.011	0.050	0.018
$x_{C,B2}$	0.993	0.965	0.993	**0.950**	0.973	0.989	**0.950**	0.982
J	-0.1480	0.3452	-0.1805	0.5814	0.3699	-0.2013	0.8408	-0.2042

constraint c_i changes from active to inactive, the sum of this constraint value and its corresponding Lagrange multiplier λ_i is zero. If we define this sum as s_i we have that, when constraint i changes between active and inactive,

$$s_i(d) = c_{i,opt}(d) + \lambda_{i,opt}(d) = 0 \tag{3.14}$$

where $c_{i,opt}(d)$ is the optimal value of c_i given the disturbance d, and $\lambda_{i,opt}(d)$ is the corresponding Lagrange multiplier. For the case of two disturbances, with d_1 on the horizontal axis and d_2 on the vertical axis, the method can be summarized as follows:

1. Use process and problem knowledge to predict if we have any constraints that are either always active or always inactive, thus reducing the number of potential regions.

2. If possible, deduce which constraint will become active first when changing a disturbance value.

3. Predict whether some constraint region boundaries will be independent of one of the disturbances. This corresponds to a horizontal boundary (if it is independent of d_1) or a vertical boundary (if it is independent of d_2).

4. Locate the vertical or horizontal region boundaries, by finding the disturbance value for which $s_i = 0$ for constraint i. When locating a vertical boundary, we hold d_2 constant and find the value of d_1 which gives $s_i = 0$. For a horizontal boundary, we hold d_1 constant instead.

5. For the remaining region boundaries, on which there are no assumptions about being vertical or horizontal, find as many points as desired along each boundary. If a linear approximation is deemed sufficient, one needs just one or two new points for each new boundary (one, if one knows from the previous step where this region boundary intersects with another boundary).

We have used MATLAB's **fmincon** solver for optimization and **fzero** for interpolation to find the points where $s_i(d) = 0$, but in principle, any NLP solver could be used for optimization.

3.4.2 Numerical issues in optimization and region finding

Despite the three case studies sharing many of the same features, we found that a different optimization approach was better suited for case study II

than the one used for case studies Ia and Ib. In case studies Ia and Ib we used an algebraic equation solver to solve for $\frac{dx}{dt}(x, u.d) = 0$, whereas in case study II we used dynamic simulation to find the steady states needed to calculate $J(u, d)$ and $c(u, d)$. In addition, in case study II we did not specify L and V directly, but used these for control of compositions. This made the dynamic simulation more robust. A reason for this might be that the optimization solver would suggest negative values for V_1 and V_2 as this would obviously reduce the objective function - but this would make problems for the dynamic simulation[2].

One point which we did not address above, is that we may search directly for the points where two constraint lines intersect. An example is the point $(F_1, p_{V,1})$ in Figure 3.4. Since two constraints change at the same time in these intersection points, we could try to solve the equation set

$$\begin{aligned} c_1(d_1, d_2) + \lambda_1(d_1, d_2) &= 0 \\ c_2(d_1, d_2) + \lambda_2(d_1, d_2) &= 0 \end{aligned} \tag{3.15}$$

for (d_1, d_2). However, this demands a more sophisticated equation solver, and if this solver is not more computationally efficient, using this approach would defeat the purpose of the method, which is a reduced need of repeated optimizations.

3.4.3 More on optimal operation of a single column

In Case Study Ia, we found active constraint regions for a single distillation column where the product prices p_D and p_B were constant. To give a better understanding of how the active constraints change for differing prices, we will here show how the cost function J depends on bottom purity x_B, for three different energy prices p_V, when distillate purity x_D is fixed at $x_{D,min}$. When x_D is fixed, there is one degree of freedom left, so the remaining variables can be plotted against x_B. In Figure 3.7, we show how reflux L and boilup V vary with increasing amount of light component in the bottom stream. The maximum boilup rate (V_{max}) is also included, the thin black line indicates the highest purity we can achieve without breaking the constraint $V \leq V_{max}$ (it is located at $x_B \approx 0.9917$). All calculations are done at a feed flow rate of $F = 1.4\,mol/s$

[2]The final solution would obviously not have negative flows, but the active-set method used by **fmincon.f** allows breaching of bound constraints at intermediate iterates. An alternative could be using the interior-point algorithm, but this algorithm was much slower for this problem.

Figure 3.8 shows how the objective function J varies with x_B for three different values of p_V. In each figure 3.8(a)-3.8(c), the feasible region which lies between the constraints on V and x_B is shown in green, whereas red indicates an infeasible region where a constraint would have to be broken (V_{max} to the right, $x_{B,min}$ to the left). In Figure 3.8(a) (low energy price), we see that the objective is decreasing throughout the feasible region, meaning the optimum is at the right end of this region - i.e. at the point where $V = V_{max}$. The opposite is true for Figure 3.8(c) (high energy price), where the minimum lies at the *left* end of the green part of the curve. Here, the constraint on x_B is active. In Figure 3.8(b) (intermediate energy price), we see that the minimum lies within the green region, meaning neither V nor x_B are at their constraint values. Thus Figures 3.8(a), 3.8(b) and 3.8(c) correspond to regions II, I and III in Figure 3.2.

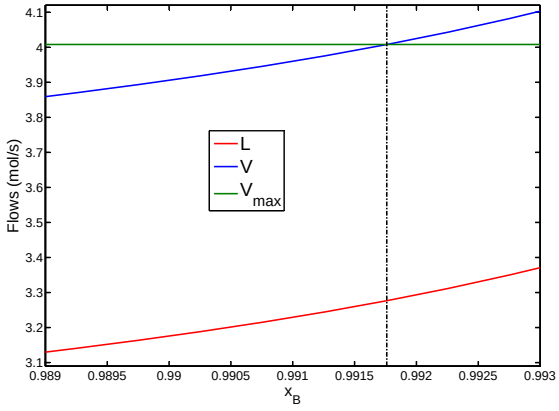

Figure 3.7: Single column (case Ia): L and V as function of x_B

3.4.4 More on the "Avoid Product Giveaway" rule

In Case Studies Ia and II, we used what we called the "Avoid Product Giveaway" rule (Gordon (1986), later used in Skogestad (2007)). The rule can be stated as follows: *The purity constraint for the most valuable product is always active.*

However, this rule relies on at least two assumptions:

- A1: *The valuable product price is constant, meaning we get paid for the impurity as well, as long as the purity specification is satisfied*

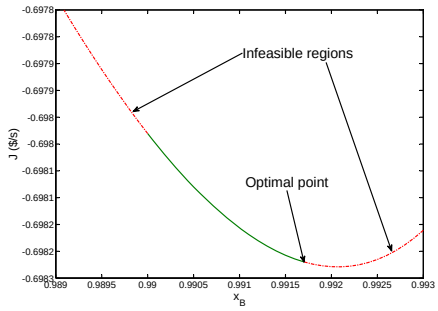

(a) $p_V = 0.010\,\$/mol$ (region II, $V = V_{max}$)

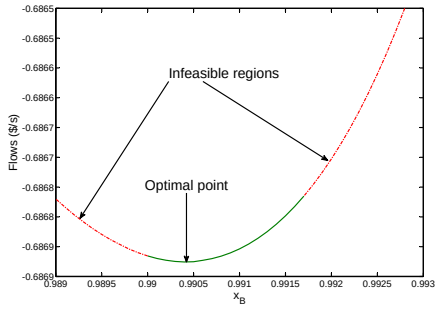

(b) $p_V = 0.0135\,\$/mol$ (region I)

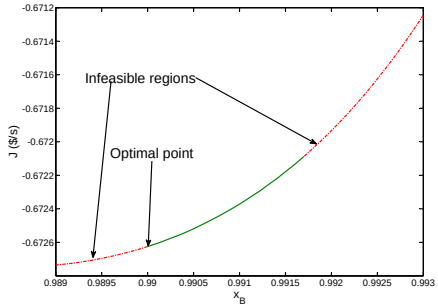

(c) $p_V = 0.018\,\$/mol$ (region III, $x_B = x_{B,min} = 0.99$)

Figure 3.8: Single column (case Ia): Cost function J as function of amount of heavy component in column bottoms for three values of p_V

(this is the case in case studies Ia and II, but not Ib). If we do not get paid for the impurity, the value of the product (in $\$/mol$ or $\$/kg$) increases when we overpurify.

- A2: *Overpurification costs extra energy.* In most cases this holds. However, in distillation, there is a rare exception when the difference in volatility between the key components is very large, so that the desired separation can be achieved in a single flash. In this case, it will take extra energy to evaporate more of the heavy component, to bring the top product on spec. Nevertheless, if energy is sufficiently cheap, it will still be optimal to keep $x_D = x_{D,min}$. Obviously, if the separation is sufficiently easy, one will not invest in a distillation column at all, so this is a hypothetical situation, although it serves as a good illustration that even a rule which intuitively may seem obvious, has exceptions.

3.4.5 Simple counterexample to the assumption "overpurification costs extra energy"

The "Avoid Product Giveaway Rule" assumes that increasing the purity of the distillate demands that we use more energy. Here we will show an example where this assumption is, in fact, incorrect.

Consider a very simple column, with two stages, as shown in Figure 3.9 assume a feed consisting of equal amounts of two components. We express the volatility of the more volatile component in terms of the K value:

$$y_B = K_B \cdot x_B \tag{3.16}$$
$$y_D = K_D \cdot x_D \tag{3.17}$$

where index D refers to the condenser (or top stage) and B to the reboiler, y is the mole fraction of the more volatile component in the vapour phase and x in the liquid phase. If we now let x_B be fixed and known, we can use the mass balance and equilibrium equations to express the boilup V as a function of y_D:

$$\begin{aligned} D =& F \cdot \frac{x_F - x_B}{y_D - x_B} \\ V =& D \cdot y_D \cdot \frac{1 - 1/K_D}{K_B \cdot x_B - y_D/K_D} \end{aligned} \tag{3.18}$$

For $K_D = K_B = 20$, $F = 1$ and $x_B = 0.1$ we then plot V as a function of y_D (Figure 3.10):

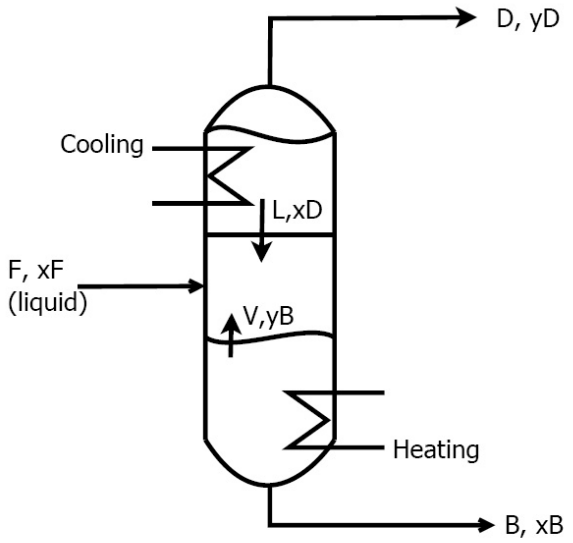

Figure 3.9: Very simple column with two equilibrium stages (including reboiler)

This shows that if the separation is sufficiently easy, increasing purity of the distillate costs *less* energy, not more. This is because if the difference in relative volatility is sufficiently high, a single flash will yield product streams at a higher purity than required. If, for example, a simple flash gives 95 % purity in the distillate and we only want 90 %, we need to boil up more of the heavy component in order to achieve this.

3.4.6 Selection of control structure

A detailed analysis of selection of controlled variables is outside the scope of this work. However, we will discuss it briefly here. Within the self-optimizing control framework, we should:

1. Control the active constraints.
2. Use the remaining unconstrained degrees of freedom to control variables whose optimal values are relatively insensitive to disturbances.

For the single column case studies, there are two degrees of freedom, so we need to find two variables to control. In case Ia, with fixed prices, regions

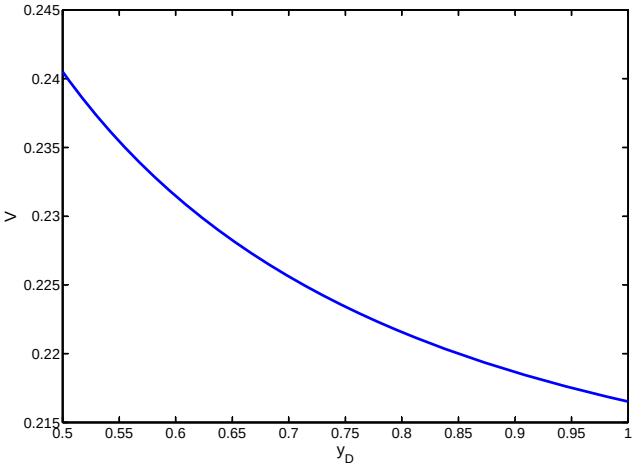

Figure 3.10: Counterexample to the assumption that "overpurification costs extra energy": V decreases with increasing y_D for hypothetical distillation case

II and III both have two active constraints, so in these regions, selection of controlled variables is straight-forward (control the active constraints). In Region I, there is one active constraint (X_D) which should be controlled. The unconstrained degree of freedom can be used to control x_B; as we see from Table 3.2, this variable is relatively constant around 0.9900.

For the two-column case study, we have a lot of room for selecting controlled variables. There are nine regions, and thus we may have to select as much as nine sets of controlled variables. However, one variable need to be controlled everywhere (the purity of the most valuable product) and some are active over large parts of the disturbance space (like the purity of stream D_1, the top product of the first column).

When the active constraints are controlled, we need to select controlled variables to be associated with the unconstrained degrees of freedom. There are four degrees of freedom. From Table 3.7 we see that that we need to find three variables in Region I, two variables in Regions II and III and one variable in Regions IV, V and VI. In Regions VII and VIII, all degrees of freedom are used to control active constraints.

The cases where only *one* unconstrained degree of freedom remains, is of particular interest. In this case, one could possibly want to control the amount of impurity A which is carried through to the second column ($x_{A,B1}$)

as variations in this concentration are likely to cause trouble for the second column. As seen from Table 3.8, the optimal value of this concentration does not vary much, which means it could be a good controlled variable in *all* regions where we have unconstrained degrees of freedom.

However, to identify the best choice of controlled variables, a more detailed analysis is needed, based on evaluation of the cost for different alternatives (Skogestad, 2000).

3.5 Conclusions

The method described in Chapter 2 has been applied to three distillation case studies. The method allowed us to find these regions using relatively few optimizations. For the cases with constant prices, we found that the purity constraint on the more valuable product was always active, as expected. For a single distillation column, we found three distinct regions (with constant prices) and five regions (with a purity-dependent distillate price). For two columns in sequence we found eight distinct regions. In all three cases, we have found the highest feed rate for which the columns can run without violating purity constraints - i.e. the physical bottleneck. We have also described the assumptions under which the "Avoid Product Giveaway Rule" is correct.

References

Gordon, L., 1986. Simple optimization for dual composition control. Hydrocarbon Process.;(United States) 65 (6).

Kister, H., 1990. Distillation operations. Mcgraw-Hill Professional.

Kvasnica, M., Grieder, P., Baotic, M., Morari, M., 2004. Multi-parametric toolbox (mpt). In: Alur, R., Pappas, G. J. (Eds.), Hybrid Systems: Computation and Control. Vol. 2993 of Lecture Notes in Computer Science. Springer Berlin / Heidelberg, pp. 121–124.

Luyben, W., 1979. Introduction and overview of distillation column control. AIChE Workshop 'Industrial Process Control', Tampa, Florida, 54–58.

Luyben, W., 1992. Practical distillation control, 1st Edition. Van Nostrand Reinhold.

Maarleveld, A., Rijnsdorp, J., 1970. Constraint control on distillation columns. Automatica 6 (1), 51 – 58.

McAvoy, T., Wang, Y., 1986. Survey of recent distillation control results. ISA Transactions 24 (1), 5.

Nagy, Z., Klein, R., Kiss, A., Findeisen, R., 2007. Advanced control of a reactive distillation column. In: Plesu, V., Agachi, P. S. (Eds.), 17th European Symposium on Computer Aided Process Engineering. Vol. 24 of Computer Aided Chemical Engineering. Elsevier, pp. 805 – 810.

Pistikopoulos, E., Georgiadis, M., Dua, V., 2007. Multi-parametric programming: theory, algorithms, and applications. Wiley-VCH Verlag GmbH.

Skogestad, S., 1993. Dynamics and control of distillation columns – a critical survey:. Control Engineering Practice 1 (3), 564 – 564.

Skogestad, S., 2000. Plantwide control: The search for the self-optimizing control structure. Journal of process control 10 (5), 487.

Skogestad, S., 2007. The do's and don'ts of distillation column control. Chemical Engineering Research and Design 85 (1), 13 – 23.

Skogestad, S., Lundström, P., Jacobsen, E., 1990. Selecting the best distillation control configuration. AIChe Journal 36 (5), 753–764.

Skogestad, S., Morari, M., 1987. Control configuration selection for distillation columns. AIChE Journal 33 (10), 1620–1635.

Skogestad, S., Morari, M., 1988. Understanding the dynamic behavior of distillation columns. Industrial & Engineering Chemistry Research 27 (10), 1848–1862.

Tøndel, P., Johansen, T. A., Bemporad, A., 2003. An algorithm for multi-parametric quadratic programming and explicit MPC solutions. Automatica 39 (3), 489 – 497.

Waller, K. V., Häggblom, K. E., Sandelin, P. M., Finnerman, D. H., 1988. Disturbance sensitivity of distillation control structures. AIChE Journal 34 (5), 853–858.

Chapter 4

Literature review: Design, simulation and optimization of natural gas liquefaction processes

4.1 Introduction

Commercial production of liquefied natural gas (LNG) commenced in the 1960s, the first regular exporting facility being opened in Algeria in 1964 (Geist, 1983). Since then, LNG has played an important role in the energy market. Currently, the size of plants is diversifying. On one hand, bigger plants than ever are being built (Pillarella et al., 2005). On the other hand, some effort is currently being put into development of floating production, storage and offloading (FPSO) units (see for example Unum (2010)), which are needed if one wants to exploit smaller gas fields located far off the coast. For such fields, building pipelines to an on-shore liquefaction or processing plant may be economically infeasible.

The majority of research papers published about LNG plants has come from the industry itself; only in the last 10-15 years has this type of plants received noticeable attention in academic circles. In this chapter we want to summarize the work that has been done on simulation and optimization, starting with the 1st LNG Exhibition and Conference held in Chicago in 1968.

We have chosen to divide the review into three sections, covering simulation, design and operation, respectively. The part covering simulation will also include references to some more general papers that are relevant. However, we want to keep within the process systems engineering scope, so production increases through installation of new equipment, or by experience-based process adjustments, are not taken into account (although this has also been the subject of several published papers).

4.1.1 Liquefaction processes

Liquefaction processes differ from each other in several ways:

- The number of cooling cycles. The simplest processes use only one refrigerant cycle, but processes using two and three refrigerant cycles are common.

- The use of single-component or mixed refrigerants. A mixed refrigerant gives better match between the heating and cooling curves, but also requires larger and more complex heat exchangers.

- The number of pressure levels. When using a single-component refrigerant, it is common to flash the refrigerant in several stages, to provide a better match between heating and cooling curves.

Combinations of the above are also used. For example, the Air Products propane-precooled mixed refrigerant (C3-MR) (Newton et al., 1986) process uses pure propane for precooling, and a hydrocarbon mixture for liquefaction. In this process, the precooling section usually has three or four pressure levels. The C3-MR process is by far the most widely used process in the LNG industry. However, other processes are also studied frequently, either because they are simpler (and thus may be more suited for case studies), or because they have been studied in cooperation with an industrial company using another process. A popular process used for academic case studies is the PRICO process (Price and Mortko, 1996), which has a single loop and uses a mixed refrigerant. Other processes mentioned in works covered by this review include the TEALARC process (TECHNIP, 1974) and the Statoil-Linde Multi-Fluid Cascade (MFC) process (Bach, 2002). Some have studied generic processes that are not used by the industry. For an overview of LNG technologies, see Barclay and Denton (2005).

4.2 Simulation of LNG processes

4.2.1 Some general remarks about simulation

Most unit operations in use in LNG processes are well-known operations which in principle are simple to simulate. However, the complex multi-stream heat exchangers that are used in liquefaction processes are not so widely studied - especially not rating. *Design* of such exchangers is more widely studied. Pacio and Dorao (2011) offer a review of various heat exchanger modelling approaches in cryogenic applications.

When developing a simulation model of a process plant, one should take into account what the model is going to be used for. It is of particular importance to choose the correct variables to specify. This selection depends on whether one is interested in design, optimization or control. For control, a causal model will be needed, meaning one must be able to calculate the *measured* variables when one knows the *manipulated* variables and the disturbances. A steady-state simulation problem can be given as, for example,

$$\begin{aligned} 0 &= f(x, u, d, p) \\ y &= g(x, u, d, p) \end{aligned} \tag{4.1}$$

where f represents mass, energy and momentum balances and constitutive equations, and g is the dependence of the measurements y on process states (x), process inputs (u), process disturbances (d) and equipment parameters (p). If f and x are of the same dimension, the system has a number of degrees of freedom equal to the number of elements in u. Now, we may specify any subset of x, u, y and p as long as the overall system can be solved. If we want a causal model, we must be able to solve it when u are specified and y is not. When doing design, one wants to calculate values for equipment parameters p. When doing rating, the values of p are fixed.

A dynamic simulation model is often written as a differential-algebraic (DAE) model:

$$\begin{aligned} \frac{dx}{dt} &= f(x, u, d, p) \\ 0 &= g(x, u, d, p) \\ y &= h(x, u, d, p) \end{aligned} \tag{4.2}$$

Here, $g(x, u, d, p)$ represents the algebraic equations. Flow relations, thermodynamic relations and control equations are usually part of g.

In the reviewed literature, commercial simulation programs have been frequently used. The most used commercial simulation program has been Aspen HYSYS®(AspenTech, 2011a), which has been succeeded by Honeywell's Unisim®Design (Honeywell, 2011). Aspen Plus®(AspenTech, 2011b) has also seen some use. All of these are flowsheet-based simulators. Some studies have also used equation-oriented modelling programs like for example gPROMS (Process Systems Enterprise, 2011). Others have hand-coded their models in FORTRAN, MATLAB or C++. Several companies use proprietary software, e.g. Statoil's SEPTIC (Strand and Sagli, 2003) and Linde's OPTISIM (Burr, 1991).

4.2.2 Literature covering simulation

In the 1980s, people in the LNG industry started to look into the use of computer models to improve operation of plants. Chatterjee et al. (1989) discuss the emerging role of computers in the industry. They point out that the lack of accurate models, especially of the main cryogenic heat exchanger (MCHE), was an issue that needed to be resolved. Owren et al. (1992) developed the simulation program CryoPro, which has seen some later use, but is little cited in the literature. Melaaen (1994) makes an effort to model coil-wound heat exchangers for dynamic simulation, including regulatory control, using first principles and a generic differential-algebraic solver written in FORTRAN. Melaaen also compares his simulation results with results made with CryoPro. Mandler (2000) discusses modelling of LNG processes for the purpose of control, and cites Melaaen's work as well as his own earlier work on the topic (Mandler and Brochu, 1991). Hammer (2004) describes development of a model of the MFC process, implemented in SEPTIC. A more recent modeling effort, focusing on the MCHE, was carried out by Hasan et al. (2007). They use a MINLP method (GAMS/BARON, Sahinidis and Tawarmalani (2005)) for optimizing the fit between their model and an actual MCHE.

Michelsen et al. (2010a) describes a dynamic model of the TEALARC process, using Simulink/MATLAB for implementation, the model is verified against a steady-state model made in HYSYS by Wahl (2007). Singh and Hovd (2007) wrote a dynamic model in gPROMS for a pilot scale LNG plant built by SINTEF (Brendeng and Neeraas, 2001). Mandler et al. (1998) discuss new control strategies for the Air Products process, using rogorous dynamic simulation to improve their understanding of process behavior.

Due to the low temperatures encountered in liquefaction, precise thermodynamic calculations are critical. Melaaen and Owren (1996) discuss how errors in thermodynamic calculations affect the optimum found using Cry-

oPro. They introduce uncertainty in the equilibrium K-values and examine how much this uncertainty influences on the optimal result.

4.3 Design and optimization

4.3.1 Types of design problems

The majority of papers related to optimization of LNG processes deal with design. Design of process plants can roughly be divided into:

- Flowsheet design, where the flowsheet configuration itself is not decided. Thus, binary (logical) decision variables are present in the problem, related to the number of process units and how they are connected. This yields a mixed-integer nonlinear optimization problem (MINLP).
- Sizing, where one has decided on a flowsheet structure and seeks to optimize process parameters p (referring to Equations 4.1 and 4.2). Here one does no longer have binary decision variables, and the problem can be formulated as a nonlinear constrained problem (NLP).

4.3.2 Optimization of design

Almost every paper we have reviewed takes a different approach to the optimization itself. Lee et al. (2002) optimize the PRICO process in the following way:

1. An initial guess is made on refrigerant composition, flow rate and pressures.
2. The refrigerant composition is optimized, seeking to minimize compressor work.
3. If the solution violates the constraints, flow rate and pressures are adjusted until constraints are satisfied.
4. The process is repeated until one can no longer retain feasibility by adjusting flow rate and pressures, and the last feasible solution is taken as the optimum.

Nogal et al. (2008) apply a Genetic Algorithm (Charbonneau, 2002) to the same process, and compare their results to Lee et al. (2002). Aspelund et al. (2010) also optimize the PRICO process, using a Tabu Search

method (Chelouah and Siarry, 2005) for optimization. Whereas Nogal et al. (2008) implement the model equations in FORTRAN, Aspelund et al. (2010) rely on HYSYS for solving the model equations, and add a penalty to the objective function whenever the HYSYS model does not converge. They use MATLAB (MathWorks, 2011) for optimization. Jensen and Skogestad (2009) use a sequential quadratic programming solver to optimize the same process. Both simulation and optimization are done in gPROMS. The objective functions used by the above mentioned studies on the PRICO process vary:

- Lee et al. (2002) and Nogal et al. (2008) both aim at minimizing power consumption for a given production rate. Their way of balancing energy cost against required heat exchanger size, is the traditional way - they specify a minimum temperature difference ΔT_{min}. As pointed out by Jensen and Skogestad (2008), the optimal solution of this problem may not be identical to the optimal solution for *operation*.

- Aspelund et al. (2010) carry out three different case studies, of which two can be seen as design studies (in that heat exchanger area is not fixed). In the first, they fix ΔT_{min} in the cryogenic heat exchanger. A higher value ΔT_{min} is added to the objective function as a penalty. In the second case study, they add together the power consumption and a cost for heat exchanger area.

- Jensen and Skogestad (2009) also use as their objective function a weighted sum of power consumption and heat exchanger area. They also study how the relative weighting between power consumption and heat exchanger area changes the optimal solution, particularly the calculated ΔT_{min}.

Other processes than PRICO have also been studied. Vaidyaraman and Maranas (2002) take a heuristic approach to synthesis of a generic mixed refrigerant cycle, seeking to minimize the average temperature difference between hot and cold composite curves for the process. Shah et al. (2007) use a genetic algorithm to carry out multi-objective optimization on a gas phase liquefaction process. They use power consumption and heat exchanger area as the two objectives. and find a Pareto-optimal front. One can see this as an alternative to the approach of Jensen and Skogestad (2009): Any given value for the weighting between power consumption and heat exchanger area should lead to an optimal solution which is a point on the Pareto-optimal front. In another paper (Shah et al., 2009), refrigerant holdup in the system is included as one of the objectives. The refrigerant holdup is

interpreted as a measure of how safe the process is (a large hydrocarbon holdup is obviously more hazardous in the case of a fire).

4.4 Optimization of operation of LNG plants

The use of computers to optimize operation of LNG plants was discussed by Chatterjee et al. (1983), and in the industry it probably got attention even earlier. However, few actual contributions have followed in the open literature. Up to the PhD thesis by Jensen (Jensen, 2008), hardly any material regarding steady-state operation of existing plants had surfaced in open literature (however, Zaim (2002) discusses *dynamic* optimization of an LNG plant). More recently, some papers have been published.

Optimization of operation is most important for control (Skogestad, 2000). Before a plant is running, it is necessary to know the optimal operating conditions and how they vary with disturbances (Jacobsen and Skogestad (2011a), Chapter 2 in this thesis), in order to design the control structure. Once the plant is running, optimization may be needed for real-time-optimization (RTO) control.

Selection of controlled variables for the TEALARC process was studied by Michelsen et al. (2010b), using the model described in Michelsen et al. (2010a). For selecting controlled variables, they use the self-optimizing control approach (Skogestad, 2000), more precisely the method proposed by Alstad et al. (2009). Others have also studied selection of controlled variables for LNG processes; Singh et al. (2008) on a pilot scale process built by SINTEF, and Jensen and Skogestad (2006) on the PRICO process. Tak et al. (2011) do a similar study, using several simplifications that Jensen and Skogestad (2006) did not use (e.g. constant compressor efficiencies instead of compressor curves). One of the case studies included in Aspelund et al. (2010) could also be seen as optimizing operation: They specify the heat exchanger area (UA) value for the main cryogenic heat exchanger, and extend the cost function J in the following way:

$$J = W_s + \log |UA_{actual} - UA_{specified}| \tag{4.3}$$

The specified UA value is the *total* UA value for the cryogenic heat exchanger. In a pure rating calculation, one would expect that one more UA value was specified (for example the UA value corresponding to the area between the natural gas stream and the cold refrigerant stream). However, they specify the outlet temperature of natural gas instead. This is justified because this temperature will always be an active constraint.

Hasan et al. (2009) seek to optimize the C3-MR process, but use a very simplistic approach with only two decision variables, namely the lowest pressure of precooling refrigerant (propane) and liquefaction refrigerant (MR). They assume the high MR pressure to be given, despite the fact that it can be seen as a degree of freedom. Alabdulkarem et al. (2011) apply a genetic algorithm to minimize power consumption in the C3-MR process. They split the process into a precooling section and a liquefaction section and optimize them separately.

Jacobsen and Skogestad (2011b) discuss optimization challenges for liquefaction processes, including testing of the reliability of heat exchanger models in Honeywell's Unisim simulation software.

The industry have published some papers related to optimization as well: Paradowski et al. (2004) seek to optimize operation of the C3-MR process using parametric studies on key process variables whereas Pillarella et al. (2005) use a proprietary optimization routine on the AP-X process, which is a modification of the C3-MR process.

4.5 Summary

Work on optimization of LNG plants has begun to gain attention in academic research, but the majority of papers still focus on design. Most papers regarding optimal operation either study very simple processes, or use very simplified models of more complex plants. In Jensen (2008) it is argued that this is due to people assuming that optimal design and optimal operation are equivalent. The thesis also points out that this is not generally true. As pointed out in Jacobsen and Skogestad (2011b), the lack of reliable steady-state models also contributes to this lack of studies on more complex processes. The most important plant vendors like Air Products and Linde rely on in-house methods for design and optimization.

References

Alabdulkarem, A., Mortazavi, A., Hwang, Y., Radermacher, R., Rogers, P., 2011. Optimization of propane pre-cooled mixed refrigerant lng plant. Applied Thermal Engineering 31 (6-7), 1091 – 1098.

Alstad, V., Skogestad, S., Hori, E., 2009. Optimal measurement combinations as controlled variables. Journal of Process Control 19 (1), 138 – 148.

Aspelund, A., Gundersen, T., Myklebust, J., Novak, M., Tomasgard, A., 2010. An optimization-simulation model for a simple LNG process. Computers & Chemical Engineering 34 (10), 1606–1617.

AspenTech, 2011a. Aspen HYSYS®. Aspen website: http://www.aspentech.com/core/aspen-hysys.aspx.

AspenTech, 2011b. Aspen HYSYS®. Aspen website: http://www.aspentech.com/core/aspen-plus.aspx.

Bach, W., 2002. Developments in the mixed fluid cascade process (MFCP) for LNG baseload plants. In: Linde Reports on science and technology. Linde, pp. 3–11.

Barclay, M., Denton, N., 2005. Selecting offshore LNG processes. LNG Journal 10, 34–36.

Brendeng, E., Neeraas, B., 2001. Method and device for small scale liquefaction of a product gas. US Patent No. US 6,751,984 B2.

Burr, P., 1991. The Design of Optimal Air Separation and Liquefaction Processes with the OPTISIM equation-oriented Simulator and its Application to on-line and offline Plant Optimization. In: AIChE Spring National Meeting, Houston, Texas, April 7-11, 1991.

Charbonneau, P., 2002. Release Notes for PIKAIA 1.2. National Center for Atmospheric Research, Technical Note 451+STR.

Chatterjee, N., Kinard, G., Geist, J., 1983. Maximizing production in propane precooled-mixed refrigerant LNG plants. In: 7th International Conference & Exhibition on Liquefied Natural Gas, Jakarta, Indonesia.

Chatterjee, N., Vinson, D., Liu, Y., 1989. The role of computers in baseload LNG plants. In: 9th International Conference & Exhibition on Liquefied Natural Gas, Nice, France.

Chelouah, R., Siarry, P., 2005. A hybrid method combining continuous tabu search and nelder-mead simplex algorithms for the global optimization of multiminima functions. European Journal of Operational Research 161 (3), 636 – 654.

Geist, J., 1983. The role of LNG in energy supply. Int. Journ. of Refrigeration 6 (5-6), 283–297.

Hammer, M., 2004. Dynamic simulation of a natural gas liquefaction plant. Ph.D. thesis, NTNU.

Hasan, M., Karimi, I., Alfadala, H., 2009. Optimizing Compressor Operations in an LNG Plant. In: Proceedings of the 1st Annual Gas Processing Symposium. pp. 179–184.

Hasan, M. F., Karimi, I. A., Alfadala, H., Grootjans, H., 2007. Modeling and simulation of main cryogenic heat exchanger in a base-load liquefied natural gas plant. In: Plesu, V., Agachi, P. S. (Eds.), 17th European Symposium on Computer Aided Process Engineering. Vol. 24 of Computer Aided Chemical Engineering. Elsevier, pp. 219 – 224.

Honeywell, 2011. Unisim®Design. Honeywell website: http://hpsweb.honeywell.com/Cultures/en-US/Products/ControlApplications/simulation/UniSimDesign/default.htm.

Jacobsen, M., Skogestad, S., 2011a. Active constraint regions for optimal operation of chemical processes. Industrial & Engineering Chemistry ResearchIn Press.

Jacobsen, M., Skogestad, S., 2011b. Optimization of LNG plants - challenges and strategies. In: Proceedings of the 21st European Symposium on Computer Aided Process Engineering. Chalkidiki, Greece, May 29-June 1, 2011. pp. 1854–1858.

Jensen, J., 2008. Optimal operation of cyclic processes - Application to LNG processes. Ph.D. thesis, NTNU.

Jensen, J., Skogestad, S., 2008. Problems with specifying ΔT_{min} in the design of processes with heat exchangers. Industrial & Engineering Chemistry Research 47 (9), 5195–5174.

Jensen, J., Skogestad, S., 2009. Single-cycle mixed-fluid LNG process part i: Optimal design. In: Proceedings of the 1st Annual Gas Processing Symposium. Elsevier, pp. 211–218.

Jensen, J. B., Skogestad, S., 2006. Optimal operation of a simple LNG process. In: Proceedings Adchem 2006, Gramado, Brazil. IFAC, pp. 241–247.

Lee, G., Smith, R., Zhu, X., 2002. Optimal synthesis of mixed-refrigerant systems for low-temperature processes. Ind. Eng. Chem. Res 41 (20), 5016–5028.

Mandler, J., 2000. Modelling for control analysis and design in complex industrial separation and liquefaction processes. Journal of Process Control 10 (2-3), 167 – 175.

Mandler, J., Brochu, P., 1991. Lng dynamic simulation. LNG Owners' Seminar IV (Air Products), Hershey, PA.

Mandler, J., Brochu, P., Fotopoulos, J., Kalra, L., 1998. New control strategies for the lng process. In: 12th International Conference & Exhibition on Liquefied Natural Gas, May 4-7, Perth, Australia.

MathWorks, 2011. Matlab optimization toolbox. The MathWorks website:. URL http://www.mathworks.com/products/optimization/

Melaaen, E., 1994. Dynamic simulation of the liquefaction section in baseload lng plants. Ph.D. thesis, NTNU.

Melaaen, I., Owren, G., 1996. How do the inaccuracies of enthalpy and vapour-liquid equilibrium calculations influence baseload lng plant design? Computers & Chemical Engineering 20 (1), 1 – 11.

Michelsen, F. A., Halvorsen, I. J., Lund, B. F., Wahl, P. E., 2010a. Modeling and simulation for control of the tealarc liquified natural gas process. Industrial & Engineering Chemistry Research 49 (16), 7389–7397.

Michelsen, F. A., Lund, B. F., Halvorsen, I. J., 2010b. Selection of optimal, controlled variables for the tealarc lng process. Industrial & Engineering Chemistry Research 49 (18), 8624–8632.

Newton, C., Kinard, G., Liu, Y., 1986. C3-MR processes for liquefaction of natural gas. In: 8th International Conference & Exhibition on Liquefied Natural Gas, Los Angeles, USA, June 15-19.

Nogal, F., Kim, J., Perry, S., Smith, R., 2008. Optimal design of mixed refrigerant cycles. Industrial & Engineering Chemistry Research 47 (22), 8724–8740.

Owren, G., Heiersted, R., Brendeng, E., Fredheim, A., 1992. The LNG plant design optimization tool CryoPro, a joint venture. In: 1992 AiChE Spring Meeting, New Orleans.

Pacio, J., Dorao, C., 2011. A review on heat exchanger thermal hydraulic models for cryogenic applications. Cryogenics 51 (7), 366 – 379.

Paradowski, H., Bamba, M., Bladanet, C., 2004. Propane precooling cycles for increased LNG train capacity. In: 14th International Conference & Exhibition on Liquefied Natural Gas, Doha, Qatar, March 21-24. pp. 107–124.

Pillarella, M., Bronfenbrenner, J., Liu, Y., Roberts, M., 2005. Large LNG trains: Developing the optimal process cycle. In: GasTech 2005, Bilbao, Spain.

Price, B., Mortko, R., 1996. PRICO - a simple, flexible proven approach to natural gas liquefaction. In: GASTECH, LNG, Natural Gas, LPG international conference, Vienna.

Process Systems Enterprise, 2011. gPROMS for Advanced Process Modelling, Simulation and Optimization. PSE website: http://www.psenterprise.com/gproms/.

Sahinidis, V., Tawarmalani, M., 2005. BARON 7.5: Global optimization of mixed-integer nonlinear programs, User's Manual. Available at http://www.gams.com/dd/docs/solvers/baron.pdf.

Shah, N., Rangaiah, G., Hoadley, A., 2007. Multi-objective optimization of the dual independent expander gas-phase refrigeration process for LNG. In: AIChE Annual Meeting, Salt Lake City, Utah, USA, Nov. 4-9.

Shah, N. M., Hoadley, A. F. A., Rangaiah, G. P., 2009. Inherent safety analysis of a propane precooled gas-phase liquified natural gas process. Industrial and Engineering Chemistry Research 48 (10), 4917–4927.

Singh, A., Hovd, M., 2007. Dynamic modeling and control structure design for a liquefied natural gas process. In: Proceedings of the 2007 American Control Conference, Marriott Marquis Hotel at Times Square, New York City, USA, July 11-13, 2007. pp. 1347–1352.

Singh, A., Hovd, M., Kariwala, V., 2008. Control variables selection for liquefied natural gas plant. Presented at the 17th IFAC World Congress, Seoul, South Korea, Jul 6-11, 2008.

Skogestad, S., 2000. Plantwide control: The search for the self-optimizing control structure. Journal of process control 10 (5), 487.

Strand, S., Sagli, J., 2003. Mpc in statoil - advantages with in-house technology. In: International Symposium on Advanced Control of Chemical Processes (ADCHEM) Hong Kong. pp. 97–103.

Tak, K., Lim, W., Choi, K., Ko, D., Moon, I., 2011. Optimization of mixed-refrigerant system in LNG liquefaction process. In: Proceedings of the 21st European Symposium on Computer Aided Process Engineering. Chalkidiki, Greece, May 29-June 1, 2011. pp. 1824–1828.

TECHNIP, 1974. Tealarc. WIPO Registration Number 411865, TECHNIP, Courbevoie, France.

Unum, A., 2010. Offshore liquefaction of natural gas. In: Proceedings of the Annual Offshore Technology Conference. Vol. 2. pp. 1132–1156, cited By (since 1996) 0.

Vaidyaraman, S., Maranas, C., 2002. Synthesis of mixed refrigerant cascade cycles. Chemical Engineering Communications 189, 1057–1078.

Wahl, P., 2007. Enabling production of remote gas: Pinocchio LNG Energy Analysis. Tech. rep., SINTEF Energy Research, Trondheim, Norway.

Zaim, A., 2002. Dynamic optimization of an lng plant, case study: Gl2z lng plant in arzew, algeria. Ph.D. thesis, RWTH Aachen.

Chapter 5

Optimization of LNG plants - challenges and strategies

Submitted to *Computers & Chemical Engineering*

Efficient and accurate optimization of natural gas liquefaction plants depends on reliable process models. In this chapter, we model the propane precooled mixed refrigerant (C3-MR) liquefaction process, and study the solution reliability of the critical parts of the model. We study the effect of shifting the equation solving between the flowsheet simulation program (Unisim®Design) and an external solver (MATLAB®). We also compare how various MATLAB solvers perform on simulation and optimization of the process model. We include a discussion on solving of heat exchanger rating problems. For the case studied here, we have found that specifying temperatures in the flowsheet simulator, and instead including the heat exchanger area specifications as equality constraints in the optimization problem, makes convergence more likely.

5.1 Introduction

Plants for production of liquefied natural gas (LNG) have been in commercial operation since the 1960s, with the first regular exporting facility opening in Algeria in 1964 (Geist, 1983). Several papers addressing optimal design of LNG plants have been published, but few that address the operation and control of existing plants. Furthermore, in the cases where operation is sought to be optimized, the approach is often debottlenecking

through installation of new equipment. Little attention has been given to optimizing process operating conditions for an existing plant, which is the focus in this work.

In this chapter we model a common liquefaction process (the Air Products C3-MR process), in a frequently used commercial modelling program (Honeywell Unisim®Design). We use this model to illustrate concerns that are present when building the model - mainly related to heat exchanger modelling and optimization. Then we formulate the optimization problem and describe the challenges that arise when optimizing the model. We use MATLAB®for optimization. The program versions used are Unisim R380 Build 14027, and MATLAB R2009a.

The chapter is structured as follows:

- In Section 5.2, we discuss optimal operation of natural gas liquefaction plants.
- Challenges in optimization are discussed in Section 5.3.
- Section 5.4 describes the propane precooled mixed refrigerant (C3-MR) process, which we have used as an example.
- Section 5.5 describes modeling of the C3-MR process, and discusses different ways of formulating heat exchanger models.
- In Section 5.6 we define the optimization problems (degrees of freedom, objectives and constraints).
- Section 5.7 summarizes the results of the reliability studies. These results are elaborated upon in Section 5.8.

Since the terms "reliability" and "accuracy" will be used frequently throughout this chapter, we shall define them here.

Definition 3. *Reliability: In the context of this work, this is taken to mean the likelihood of getting a converged process flowsheet back from the process simulation software, subject to the required solver tolerances. Reliability is referring to the solution of the process model equations only.*

Definition 4. *Accuracy: How low we can set the solver tolerances before we fail to get a solution. This refers to both solving of model equations (simulation) and to optimization.*

5.2 Optimal design and operation of LNG plants

5.2.1 Design versus operation

Optimization of a process plant can usually be formulated as a nonlinear optimization problem on the form

$$\min_u J(x,u,d) \tag{5.1a}$$
$$\text{s.t. } f(x,u,d) = 0 \tag{5.1b}$$
$$c(x,u,d) \leq 0 \tag{5.1c}$$

where x are the internal variables/states of the process model, u are the degrees of freedom (inputs, process variables that we may manipulate) and d are disturbances (variables that we can not affect, including feed and product prices). J is the objective, $f(x,u,d)$ represents the process model equations and $c(x,u,d)$ are the process constraints - typically including upper and lower bounds on the inputs u as well.

Optimization of LNG plants can refer to one of two cases (in this work, we are focusing on the second one):

1. Plant design, which deals with choosing the optimal process configuration, equipment size and other process parameters for the given circumstances. Plant debottlenecking may also be seen as a variant of plant design, where some of the equipment is given. The optimal design depends on expected feed gas conditions, economic expectations, climate at the plant location, and environmental and safety regulations. For LNG and other cryogenic processes, the climate at the plant site is of particular importance, because the temperature of the available cooling utilities influences directly on plant efficiency. This can easily be illustrated by taking a household refrigerator as an example: When the house is warm, the compressor is using more power, and when the house is cold it uses less. The same applies to any refrigeration plant, including natural gas liquefaction plants.

2. Plant operation, which deals with manipulating the operational degrees of freedom u such that the profit is maximized. Compared to the design case, this corresponds to For an LNG plant, maximizing profit often corresponds to minimizing energy and utility consumption (for a given production rate) or maximizing the production rate. This is discussed further in Section 5.6.1.

In general, the operation problem has a smaller dimension (i.e. fewer u's) than the design problem; process configuration and equipment size are free to vary in design, but are fixed during operation. Also, some constraints that are used during design are no longer relevant when we switch to operation. For example, it is very common to use the minimum ΔT in heat exchangers as a constraint during design (Jensen and Skogestad, 2008), but this should not be specified during operation.

5.2.2 Optimization using process simulators

Consider the optimization problem given above (Equation 5.1). It can be solved in different ways:

1. The optimization solver may solve the entire problem, including equality constraints. This means that the process model may be unconverged at every step - this can be seen as *infeasible-path* optimization (Biegler and Hughes, 1982).
2. The process simulator may solve $f(x, u, d) = 0$ to find x for given u and d, and return values for J and c to the optimizer. In this case, the optimizer solves a purely inequality-constrained problem.
3. The process simulator may solve some of the equations included in f and the rest can be included in the optimization problem as equality constraints.

In the first case, it is not necessary to distinguish between x and u, and the problem can instead be written as

$$\min_{u} J(z, d) \tag{5.2a}$$

$$\text{s.t. } f(z, d) = 0 \tag{5.2b}$$

$$c(z, d) \leq 0 \tag{5.2c}$$

where $z = [x\, u]$. However, in the second and third cases, the distinction between u and x becomes important. Proper selection of which variables to include in u and which to include in x can be critical in solving the optimization problem. In the third case, we also have to decide which equations f should be solved by the flowsheet simulator and which equations should be solved by the optimizer.

In the third case, which is illustrated in Figure 5.1, the optimization problem takes the form

$$\min_{u'} J'(u', d) \tag{5.3a}$$

$$\text{subject to } f'(u', d) = 0 \tag{5.3b}$$

$$c'(u', d) \leq 0 \tag{5.3c}$$

The equations $f'(u', d)$ is a subset of f, and contains the model equations that are left for the optimizer to solve. u' is defined as

$$u' = [u\ u_{\text{extra}}] \tag{5.4}$$

where u_{extra} is a subset of x. The selection of u_{extra} follows naturally from the equations that are included in f'.

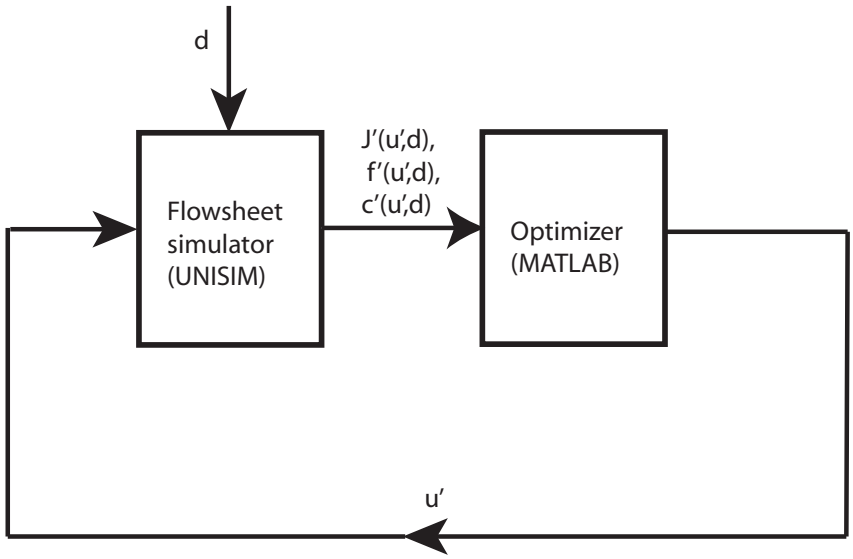

Figure 5.1: The flowsheet simulator receives u' from the optimizer and calculates J', f' and c'.

5.2.3 Earlier work on LNG optimization

The technical LNG conferences held since 1968 (GTI, 2011) have been the main arena for exchange of knowledge about LNG technology. Most papers

from these conferences focus on experiences with new process units, or on increasing plant capacity through debottlenecking. Only in the last decade has mathematical optimization of liquefaction plants received attention in the published literature. The first systematic tool in use for improving liquefaction efficiency was exergy analysis, which started to gain attention during the 1970s (Durr et al., 1998), and has since remained in use as a means of assessing efficiency losses in refrigeration processes; see also Liu et al. (1998). Pillarella et al. (2005) use an in-house sequential-quadratic programming (SQP) algorithm (Nocedal and Wright, 1999) to optimize the design of a propane precooled mixed refrigerant process, whereas Jensen and Skogestad (2006) use an SQP method and the simulation software gProms (Process Systems Enterprise, 2011) to optimize both design and operation of the simpler PRICO process (Price and Mortko, 1996). However, derivative-free methods have seen wider use than continuous methods. Shah et al. (2007) use a genetic algorithm to optimize design for gas-phase refrigeration, Aspelund et al. (2010) use a Tabu search method (Cvijovic and Klinowski, 1995) on the PRICO process. Both these works use Aspen HYSYS (AspenTech, 2011) for simulation and MATLAB for optimization. Another approach to optimization is parametric studies - simulate the model for a range of values for the key parameters to identify the optimal solution. In Paradowski et al. (2004), the C3-MR process is studied by varying refrigerant composition and compressor speed. They use an in-house process simulator. There are no studies which use a standard commercial process simulator to optimize a pure operation problem with a method that uses gradient information. In this chapter we discuss some of the challenges that may explain why.

5.3 Challenges in optimization

The most obvious challenge in optimization arises if the process simulator used for calculation of objectives and constraints is not guaranteed to converge to a solution every time it is called by the optimization routine. In these cases the model must be reformulated in such a way that it is easy to converge. In particular, this means the use of iteration loops within the process simulator should be limited if possible - unless they are guaranteed to converge, that is. When considering which equations to solve outside the process simulator, as discussed above, this is an important issue.

In sequential-modular simulators, of which Unisim is a typical example, each process unit is solved individually and information passed on to the connected units. This often requires *tearing* of the flowsheet calculation

(see e.g. Motard and Westerberg (1981)), adding equations and variables to the model. This is not an issue when using a simultaneous solver (like for example gProms).

It may often be beneficial (or even necessary) to let the convergence of these recycles be part of the optimization, rather than letting the process simulator take care of them. Thus, the process model will not be completely converged at every iteration of the optimization. This is called infeasible-path optimization (Biegler and Hughes (1982), Biegler (2010)). Whether to use this approach or not, depends on how robust the recycle solver of the process simulator is. If convergence is guaranteed every time the process model is called, there is no explicit need to use an infeasible-path method, but it may still be better in terms of computation efficiency.

If convergence cannot be guaranteed, a gradient-based method is not feasible. When using a gradient-free method, a convergence failure can for example be handled by assigning a large penalty to the objective function. Aspelund et al. (2010) use this approach.

Another challenge, especially when using a gradient-based method like SQP, is that constraints may have discontinuous gradients. A particularly difficult example is when there is a constraint on the temperature of a single-component stream which undergoes a phase change. For example, we may have a constraint $T - T_{dew}(P) \geq 5\,K$, i.e. the stream must be $5\,K$ above its dew point temperature. Now, if a process variable is changed so that the stream goes into the two-phase region, we will have $T = T_{dew}(P)$, and in a small region the gradient of this constraint is *zero* in all directions. Thus it is impossible for the solver to know in which direction it should search for a feasible point[1].

5.4 Example process: C3-MR

The Air Products C3-MR process (Figure 5.2) has been the most widely utilized process for natural gas liquefaction, since its invention in the 1970s (Chiu, 2008). The name stems from the fact it uses a propane (C3) pre-cooling cycle and a mixed refrigerant (MR) liquefaction cycle. The plant includes units for removal of water, sulfur and CO_2 and a fractionation column - for simplicity, these units are omitted in this work. Newton et al. (1986) provides an interesting discussion on different design issues related to the process. The process works as follows (referring to Figure 5.2):

[1] For a multi-component stream, in which the boiling temperature varies through the two-phase region, this is not an issue. The gradient is still discontinuous at the ends of the two-phase region, but it does not become zero.

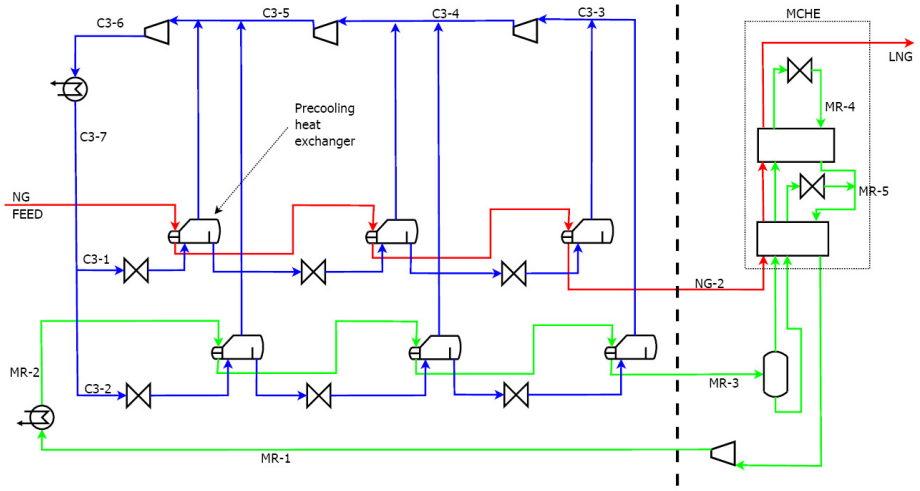

Figure 5.2: Schematic flowsheet of the C3-MR process with three precooling pressure levels. Propane (C3) flows are shown in blue, mixed refrigerant (MR) flows in green and natural gas (NG) flows in red. The dashed vertical line separates the precooling section (left) from the liquefaction section (right)

- Dry natural gas (NG FEED) and high pressure mixed refrigerant (MR-2) enter the precooling section (left end of Figure 5.2).
- They are cooled to approximately $-40°C$ by heat exchange with boiling propane (C3) in three successively colder stages.
- The precooled natural gas (NG-2) enters the main cryogenic heat exchanger (MCHE) directly, the refrigerant stream (MR-3) is first separated into a liquid stream and a vapor stream, which both enter the bottom of the MCHE. The MCHE is on the right side in Figure 5.2.
- NG and MR are both liquefied and subcooled in the MCHE. The liquid MR stream exits the exchanger in the middle, is expanded and injected back into the MCHE where it is used for cooling. The vapor MR stream, now liquefied, exits on the top, it is also expanded and sent back to the top of the MCHE.
- The subcooled NG exits at the top of the MCHE where it is expanded to storage pressure and pumped to a storage tank.

- The vaporized MR exits the MCHE at the bottom, and is recompressed to high pressure.

- The C3 in the precooling loop is first condensed with seawater, then expanded and evaporated in three stages, before it is re-compressed. The condensed C3 is split in two streams (C3-1 and C3-2). Each stream is expanded to a lower pressure and fed to the high-pressure precooling heat exchangers. Part of the C3 is evaporated and sent to the high-pressure inlet of the propane compressor, the remaining C3 (which is still liquid) is expanded further and sent to the medium-pressure precooling heat exchangers. The vapor goes to the medium-pressure inlet of the compressor, the remaining liquid is evaporated in the low-pressure precooling heat exchangers before being sent to the low-pressure inlet of the compressor.

The precooling part uses six kettle-type heat exchangers, the MCHE is a single, large spiral-wound heat exchanger. In Figure 5.2, the MCHE is represented by two multi-stream heat exchangers - the first with four streams and the second with three.

5.5 Modelling

5.5.1 Model description

The model has been made in Unisim - Figures 5.3 and 5.4 show the precooling section and liquefaction section of the Unisim model, respectively. Just like in Figure 5.2, red streams are natural gas (NG), green streams are mixed refrigerant (MR) and blue streams are propane (C3). The most important model features are described below. UA denotes the product of the area of a heat exchanger (A) and the heat transfer coefficient (U). The heat transfer coefficient is assumed to be constant throughout each heat exchanger.

- Each stage of the propane compressor is modelled as a separate compressor (in the actual process, it is *one* compressor with several inlets).

- We use simplified compressor models with constant efficiency $\eta = 80\,\%$. This basically means we keep the "design" specifications on the compressors. For optimization of an actual plant, this is not realistic. However, since compressor data are very case-specific, the simplification is acceptable for a more generic study like the one undergone

here. After all, the concern of this chapter is modelling and optimization reliability.

- The water/air coolers used for condensation of propane and cooling of mixed refrigerant are modelled as simple coolers, meaning the exit temperature of the fluid to be cooled is specified directly. This is justified by the assumption that we always use the maximum cooling available, since air/cooling water is cheap compared to compressor work.

- The six heat exchangers in the precooling section are modelled as ideal counter-current shell and tube heat exchangers, each followed by a flash tank. This is to simulate a kettle-type heat exchanger, with both a liquid outlet and a vapor outlet. For each heat exchanger, the value of UA is specified.

- The Main Cryogenic Heat Exchanger (MCHE) is modelled as two multi-stream heat exchangers - one with three hot streams and one with two hot streams. Both have one cold stream. For the multi-stream heat exchangers, specifications are made on UA between every hot stream and the cold streams. This gives a total of *five* UA specifications for the MCHE model.

- The mixed refrigerant (MR) consists of methane, ethane, propane and nitrogen. We assume that we can manipulate the composition.

- The MR compressor is modelled as a single-stage compressor whereas in the actual process, it is a three-stage compressor with internal cooling. This does not influence on the number of degrees of freedom - there is only one manipulated variable for the compressor in either case.

- The Peng-Robinson equation of state (Peng and Robinson, 1976) is used to compute the thermodynamic properties.

In the remainder of this work, we have chosen to divide the model into a pre-cooling part and a liquefaction (MCHE) part. This division is indicated in Figure 5.2.

5.5.2 Heat exchanger modeling: Design and rating

Consider the simple heat exchanger shown in Figure 5.5. It has seven variables, and it is characterized by two equations. One is the energy balance:

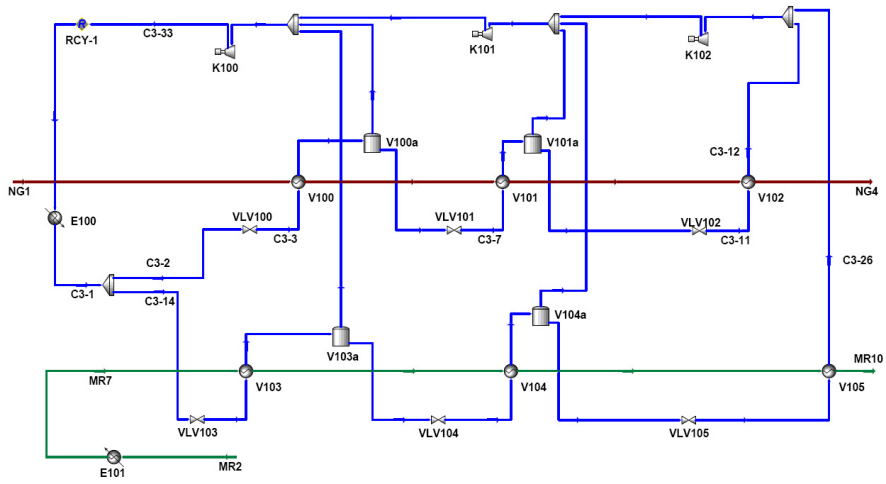

Figure 5.3: Flowsheet of the Unisim model, precooling section. NG streams are shown in *red*, C3 streams in *blue* and MR streams in *green*.

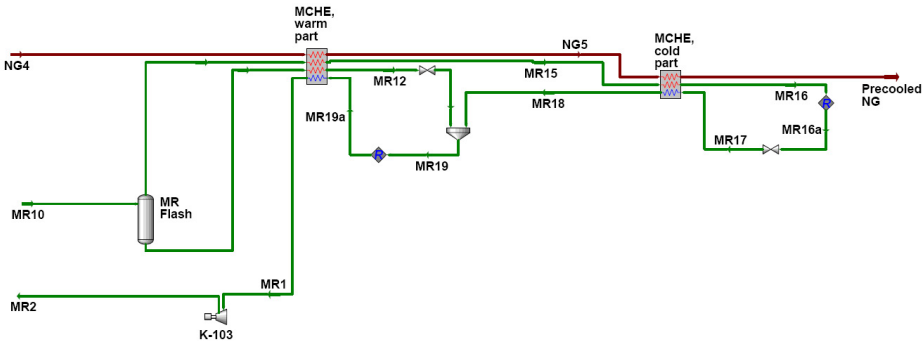

Figure 5.4: Flowsheet of the Unisim model, liquefaction section. NG streams are shown in *red* and MR streams in *green*. The blocks labeled "R" are recycle blocks, equivalent to torn streams.

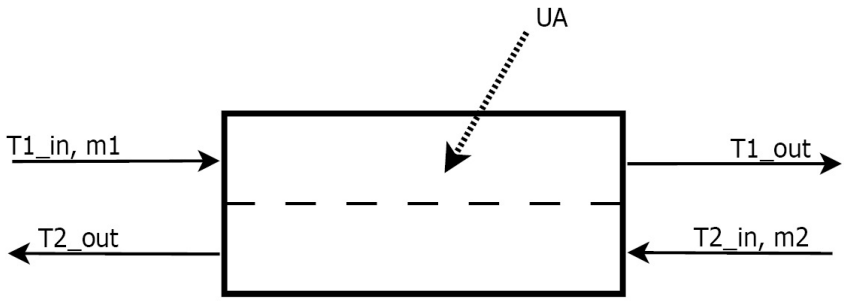

Figure 5.5: Simple counter-current heat exchanger with two streams

$$m_1 \cdot (h_{out,1} - h_{in,1}) = -m_2 \cdot (h_{out,2} - h_{in,2}) \tag{5.5}$$

The second is the expression for heat transfer, which is (if we assume constant heat transfer coefficient U):

$$m_1 \cdot (h_{out,1} - h_{in,1}) = Q = U \cdot \int \Delta T(A) dA \tag{5.6}$$

Since we have two equations and seven variables, we need to specify five variables. How difficult the heat exchanger is to calculate, depends on which variables we specify. The two following cases are common:

- *Design*: We specify the flow rates m_1 and m_2, inlet temperatures $T_{1,\text{in}}$ and $T_{2,\text{in}}$, plus one outlet temperature (or, equivalently, the minimum temperature difference (ΔT_{min})). From this, we calculate UA and the unknown outlet temperature.

- *Rating (operation)*: We know m_1, m_2, $T_{1,\text{in}}$, $T_{2,\text{in}}$ and UA, and want to calculate both outlet temperatures. In this work, we are exclusively dealing with rating problems.

If we do not know either outlet temperature, we have to solve the two equations simultaneously, or express the UA value as a function of one of the unknown temperatures and solve

$$UA(T) - UA_{\text{specified}} = 0 \tag{5.7}$$

iteratively for T.

The Unisim heat exchanger model solves the rating problem in the following way:

1. The unknown temperatures are guessed.
2. From the temperatures that are known or guessed, enthalpies at the end points are calculated.
3. For each stream, a curve of temperature as function of enthalpy is calculated, and divided into a user-defined number of intervals.
4. Using the logarithmic mean temperature difference, a UA value is calculated for each interval, and the UA values are added together to yield the total UA for the heat exchanger.
5. The calculated UA value is compared to the specified one and the error is calculated.
6. Steps 1-5 are repeated until the difference between the calculated UA the specified UA is sufficiently small.

5.5.3 Different model formulations for heat exchangers in liquefaction model

One of the main issues we address in this work, is the reliability of the multi-stream heat exchanger modules used for simulating the MCHE, which is modelled as one heat exchanger with one cold and three hot streams, and one exchanger with one cold and two hot streams. Here, we will show that the model of the MCHE can be done in three different ways, which we will refer to as *Model Formulation I, II and III*:

1. *Formulation I*: UA values are *calculated* by Unisim, by specifying temperatures. The UA specifications are added to the optimization problem as equality constraints, so Equation 5.7 is solved by MATLAB. In this formulation, there are no tear equations in the liquefaction sub-model.
2. *Formulation II*: The heat exchanger rating problem (Equation 5.7) is solved by Unisim , the tear equations (Equation 5.10) are solved by the MATLAB optimizer.
3. *Formulation III*: This is the same as Formulation II, except for that Unisim now also solves the tear equations (Equation 5.10).

Model Formulation I: As mentioned above, the MCHE model has five UA specifications, thus there are five temperatures that must be found iteratively. These are the temperatures of the streams labeled NG5, MR12, MR15, MR16 and LNG in Figure 5.4. The internal heat exchanger model uses a Newton method for the iterative solution procedure.

When doing optimization in MATLAB, this iterative solution can be included in the optimization problem by adding Equation 5.7 as equality constraints. This means that $f'(u', d)$ in Equation 5.3 will be:

$$f' = UA_i(T_i) - UA_{\text{i,specified}} = 0 \tag{5.8}$$

for $i = 1 : 5$. The five corresponding temperatures are now included in the extended input vector u':

$$u' = [u\ T_{\text{NG5}}\ T_{\text{MR15}}\ T_{\text{MR12}}\ T_{\text{MR16}}\ T_{\text{LNG}}] \tag{5.9}$$

Model Formulations II and III When we specify the five UA values in the multi-stream heat exchangers directly and let Unisim solve for the unknown temperatures, we face an additional issue. In Figure 5.4, we see that the streams labeled MR17 and MR19a are inlet streams to the MCHE (warm part) and MCHE (cold part), respectively. At the same time, the conditions of these streams depend on the conditions of the *outlet* streams labeled MR12 and MR16. Thus we have to tear those streams (indicated by the recycle blocks labeled "R" in Figure 5.4). When doing this, we have to guess the temperature of streams MR16a and MR19a, and the flowsheet is solved in the following way:

1. The inlet conditions of precooled natural gas (NG10) and mixed refrigerant are known. Together with the guessed conditions of stream MR19a, the four-stream heat exchanger is solved.

2. This gives us the conditions of streams MR1, NG5, MR12 and MR15.

3. The guessed conditions of stream MR16a allows us to calculate the conditions of stream MR17, where the pressure is specified.

4. Based on the calculated conditions of streams NG5, MR15 and MR17, the three-stream heat exchanger is solved. This gives the conditions for streams "LNG", MR16 and MR18.

5. The conditions of stream MR19 are now calculated.

6. The calculated temperatures of streams MR16 and MR19 replace the guessed temperatures in streams MR16a and MR19a, respectively.

7. The above is repeated until the residuals $T_{\text{MR16}} - T_{\text{MR16a}}$ and $T_{\text{MR19}} - T_{\text{MR19a}}$ are both smaller than the specified tolerance.

We may choose to let the Unisim recycle solver take care of the last step, or include it in the MATLAB optimization problem. In the latter case, we include the guessed values for T_{MR16a} and T_{MR19a} in u', and include Equation 5.10 below in f'.

$$f' = \begin{bmatrix} T_{\text{MR16}} - T_{\text{MR16a}} \\ T_{\text{MR19}} - T_{\text{MR19a}} \end{bmatrix} \tag{5.10}$$

In this case, the input vector u' will be

$$u' = [u \; T_{\text{MR16a}} \; T_{\text{MR19a}}] \tag{5.11}$$

This is *Model Formulation II*.

Finally, we may choose to let Unisim solve the recycles as well. In this case, there will be no equality constraints f' in the optimization problem, and $u' = u$, thus the optimizer is left to solve an inequality constrained problem. This is *Model Formulation III*.

5.5.4 Superheating: Temperature vs. enthalpy

In the optimization problem, constraints on superheating of compressor inlet streams are included. Here we will explain how the form of the superheating constraints may influence on solver reliability. It may seem obvious just to express the superheating constraints (constraints 2-4 in Section 5.6.3) as

$$\Delta T_{sup} = T - T_{dew}(p) \tag{5.12}$$

where $T_{dew}(p)$ is the dew point temperature at the current pressure. However, as the C3 streams in question are small compared to the NG and MR streams, a little change in process conditions is enough to take them from the superheated region into the two-phase region. In the entire two-phase region, ΔT_{sup} will be equal to zero, since a single-component stream evaporates at constant temperature. When the optimizer finds a zero gradient for a constraint function, it may fail to return to the feasible region. If we instead write the constraint function in terms of molar enthalpy $h(T, p)$, we avoid this problem as the enthalpy is changing monotonously throughout the two-phase region (and the gradient is never zero). Thus, we write

$$\Delta h_{sup} = h - h_{dew}(p) \tag{5.13}$$

To illustrate the difference between using Equation 5.12 and Equation 5.13, consider Figures 5.6(a) and 5.6(b). Here, we show how the superheating of C3 out of heat exchanger V102 (referring to Figure 5.3) as function of F_{C3-2}. When using Equation 5.12, we see that the superheating becomes zero and stays zero in the two-phase region. Equation 5.13, on the other hand, returns a negative value when we are in the two-phase region, and thus we avoid the problem with a zero gradient.

Later in this chapter, we will compare how these two formulations influence on optimization performance.

5.5.5 Solving - Unisim-MATLAB interaction

In this work, we use Unisim for simulation of the C3-MR process, and MATLAB for optimization. MATLAB optimization algorithms and equation solvers all require a function which accepts the decision variables as inputs, and returns the value of the objective function and constraint functions (or, in the case of equation solving, the equation residuals). In this work, we do the following:

1. The MATLAB optimization function passes a set of values for the decision variables u to the MATLAB functions which calculate J (or J') c and f'.

2. These MATLAB functions pass the values to the Unisim flowsheet and calls the solver.

3. If the Unisim simulation is successful (i.e. it calculates the values MATLAB asks for), these values are passed to MATLAB.

4. If the simulation is *not* successful, the MATLAB objective/constraint functions return a high value for J and c to the optimization solver (where "high" means a value several orders of magnitude larger than the expected value).

5.6 Description of the optimization problem

5.6.1 Optimization objectives for entire plant and for submodels

When optimizing operation of a natural gas liquefaction plant, the objective is simple: We have a single product, which is to be delivered in a given state, so the goal is to produce as much as possible, using as little energy

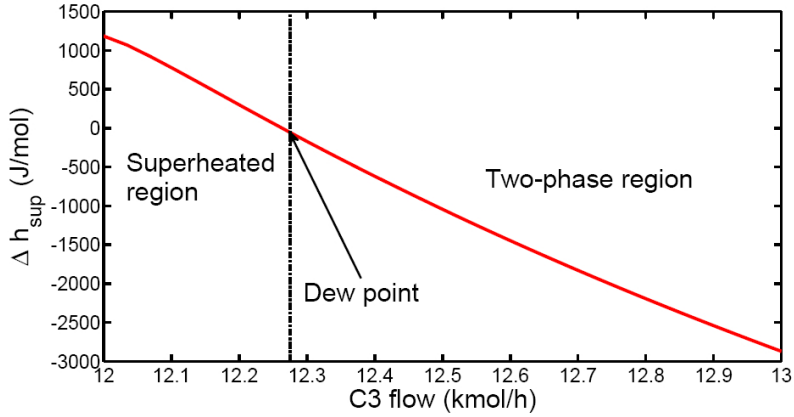

(a) Superheating expressed in enthalpy (Δh_{sup})

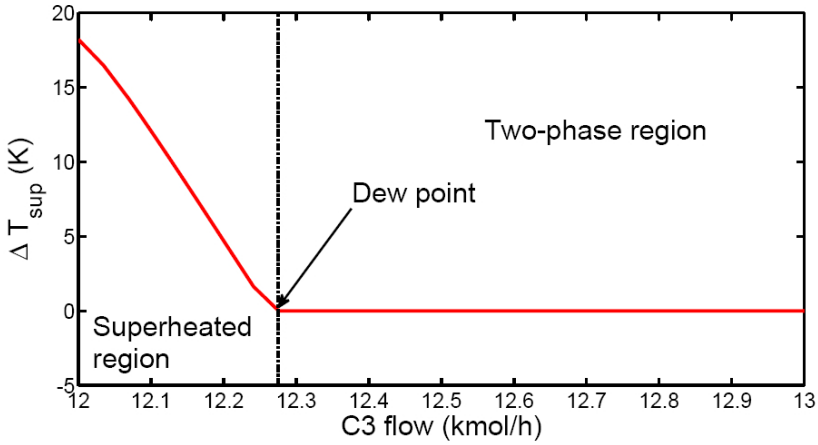

(b) Superheating expressed in temperature (ΔT_{sup})

Figure 5.6: Superheating of propane out of V102 as function of $F_{\mathrm{C3-2}}$

as possible. If we ignore utilities and pumping work (which is negligible compared to refrigerant compression), we can write the objective function to be minimized as

$$J = \Sigma W \cdot p_W - F_{\text{LNG}} \cdot p_{\text{LNG}} \tag{5.14}$$

where W is energy consumption (from compression), F_{LNG} is the production rate and p are prices. Jensen and Skogestad (2006) describes two distinct objectives called Mode I and Mode II:

- Mode I: Throughput F_{LNG} is fixed, so the cost function reduces to $J = \Sigma W$, i.e. minimize compressor work.
- Mode II When p_W is relatively low compared to p_{LNG}, we seek to maximize throughput, subject to operational constraints (maximum constraints on compressor throughput, pressures and cooling). Then the cost function can be reduced to $J = -F_{\text{LNG}}$

In this work we shall focus on Mode I ($J = \Sigma W$) This means we seek to minimize the sum of work done by all compressors, when the feed flow rate is given (thus, the feed flow rate is to be considered a disturbance). Since we are dividing the C3-MR process into a precooling section and a liquefaction section, we need to state an optimization objective for each section as well:

- For the *precooling* section, we seek to minimize the *propane* compression work, so $J = W_{\text{K100}} + W_{\text{K101}} + W_{\text{K102}}$.
- For the *liquefaction* part, we seek to minimize the *mixed refrigerant* compression work, so $J = W_{\text{K103}}$.

It needs to be emphasized that these two objective functions refer to optimal operation of each sub-model on its own. The optimal solutions found for each sub-model do not necessarily yield the optimal solution for the overall process.

5.6.2 Degrees of freedom for optimization

When the feed flowrate is considered a disturbance, rather than a degree of freedom, there are eight degrees of freedom u in the precooling section (eight variables that must be specified in the Unisim model). These must be selected so that the Unisim model can be solved (most important, we need to avoid overspecification of one unit and underspecification of another). The variables we have selected for the precooling part are:

1,2 Flow rate of the two propane streams C3-2 and C3-14.

3,4 Amount of cooling in the C3 condenser and the MR cooler, or equivalently the temperatures of streams C3-1 and MR7.

5-8 Four pressures in the propane loop (specified in the streams C3-3, C3-7, C3-11 and C3-33).

Alternative specifications could for example be temperatures rather than pressures in the propane loop. Flow rate specifications could also be expressed via a total flow rate and a split ratio, or replaced by temperature specifications.

In the liquefaction part, there are six degrees of freedom. We have selected to specify the following six variables:

1: Flow rate of stream MR10.

2-3: Pressure of streams MR10 and MR17 (high and low MR pressure).

4-6: Composition of MR (we specify molar fractions of C_2H_6, C_3H_8 and N_2).

The same considerations apply as in the precooling case, except the composition *must* be specified. The pressure specifications could again be replaced by temperature specifications. In summary, the degrees of freedom for the respective sub-plants are:

$$u_{\text{pre}} = [F_{\text{C3}-2}\ F_{\text{C3}-14}\ T_{\text{C3}-1}\ T_{\text{MR7}}\ P_{\text{C3}-3}\ P_{\text{C3}-7}\ P_{\text{C3}-11}\ P_{\text{C3}-33}] \quad (5.15)$$

$$u_{\text{liq}} = [F_{\text{MR10}}\ P_{\text{MR10}}\ P_{\text{MR17}}\ x_{\text{C2,MR}}\ x_{\text{C3,MR}}\ x_{\text{N2,MR}}] \quad (5.16)$$

5.6.3 Constraints

Precooling sub-model

When dividing the process in two parts, conditions of a stream exiting one part of the plant may be a disturbance for the other part. In addition, we may need to add constraints on certain conditions of streams leaving the section we are currently optimizing. For the precooling sub-model, the constraints are as follows:

1-2: NG and MR out of the precooling section (streams NG4 and MR10) must be colder than $-39°C$. These two constraints will be active at all times, as more cooling means more work.

3-4: C3 leaving the low-pressure evaporation stage must be at least $2.5°C$ superheated. These may also be assumed to be active.

5: C3 leaving the condenser must be liquid only: $T_{\text{C3}-33} \leq T_{\text{bubble}}(P_{\text{C3}-33})$.

Remark 1. *The lower bound on the temperature in streams NG4 and MR10 can be used as a degree of freedom for optimization of the overall plant. Changing this constraint value will shift the load between the two compressor trains.*

Remark 2. *About constraint 5: It is common to have a condenser design which makes the propane leave the condenser at the saturation point, i.e. subcooling is not possible and the constraint is always active. At steady state, the pressure of stream C3-33 will thus have to follow the temperature in the condenser. If we allow subcooling, the pressure may be higher. In this work, we make no assumptions on the condenser design, thus we allow for subcooling and constraint 5 may be inactive.*

In addition, we require that all flows must be positive and that all internal ΔT values in heat exchangers (defined as temperature on hot side minus temperature on cold side) must be positive. This is to make sure we do not find a physically infeasible solution with temperature crossovers.[2]

Liquefaction sub-model

In the liquefaction section of the plant, we have the following constraints (c):

1. $T_{\text{LNG}} \leq -157°C$ (always active).
2. $\Delta T_{sup,MR} \geq 2.5°C$ (stream MR1 to compressor K103 must be superheated).
3. All internal $\Delta T > 0$.

Depending on choice of model formulation, u will be extended as shown in Section 5.5.3, and we will thus have either 5, 2 or 0 equality constraints in addition to our inequality constraints.

[2] This is always obeyed if inlet temperatures and heat transfer area are given, but may be violated if more temperatures are specified. Notice that this is only a modelling issue. In a real heat exchanger a negative ΔT is physically impossible at steady state.

5.6.4 Disturbances

The division of the model into a precooling section and a liquefaction section means that the conditions of the streams crossing the boundary, are either degrees of freedom or disturbances for the part they are entering. In the precooling section, we have the following disturbances:

- Pressure, composition and flow rate of stream MR1a (these are degrees of freedom in the MCHE submodel).
- Conditions of the NG feed (pressure, composition and flow rate).
- Temperature of the external cooling medium, T_{amb}.

In the rest of this work, we will assume that maximum cooling is used in the propane condenser, the feed water cooler and the MR water cooler. This means we may specify the temperature of the streams "NG Feed", "C3-1" and "MR7" to the lowest possible - we will use the ambient temperature plus $5°C$. This means the temperature of these streams can be seen as a disturbance itself, just like the temperature of the feed. If we look at remaining degrees of freedom when these assumptions are made, we find that we have only *two* degrees of freedom left. We will address this further in the discussion (Section 5.8.1).

The conditions of the streams leaving the precooling section are considered as disturbances (d) for the liquefaction section. These are

- Flow rate, temperature and pressure of stream NG4
- Temperature of stream MR10 (flow rate and pressure of this stream are considered degrees of freedom).

5.7 Results

5.7.1 Reliability of Unisim model of MCHE section with different formulations

In order to be able to run optimization, we need to be able to converge the process model, to obtain values for the functions J, c and f' in Equation 5.3. Therefore, we have tested how reliable the Unisim model of the liquefaction sub-plant is with each of the different formulations described in Section 5.5.3.

The six degrees of freedom (u) given in Section 5.6.2 were varied from their minimum to their maximum values, which are shown in Table 5.1.

The results are shown in Table 5.2. The relative tolerance for solving the heat exchanger model was set to 10^{-10} in the case where temperatures were specified (Formulation I) and 10^{-5} when UA values were specified (Formulations II and III). For Formulation III, the tolerance on temperature in tear streams was set to $0.1°C$.

Table 5.1: Optimization variables u in MCHE submodel: Minimum and maximum values used in robustness study

Variable	Nominal value	Minimum	Maximum
$P_{\mathrm{h,MR}}\,[kPa]$	4340	4240	4440
$P_{\mathrm{l,MR}}\,[kPa]$	521	500	537
$F_{\mathrm{MR}}\,[kmol/h]$	102.0	101.0	103.0
$x_{\mathrm{C2,MR}}\,[\%]$	42.5	40.0	45.0
$x_{\mathrm{C3,MR}}\,[\%]$	2.0	0.0	4.0
$x_{\mathrm{N2,MR}}\,[\%]$	8.0	6.0	10.0

Table 5.2: Reliability study: Number of failed flowsheet calculations with different formulations

Model formulation	Runs	Failures
I: T specified	300	0
II: UA specified, recycles inactive	300	11
III: UA specified, recycles active	300	177

As seen from the results in Table 5.2, the only formulation in which the Unisim flowsheet converged for the whole range of flows and pressures was formulation I. In formulation II, the three-stream heat exchanger calculation failed on a number of occasions, and when using formulation III the recycle calculations failed frequently (or the heat exchanger calculations failed because of bad guesses from the recycles). Considering that a much stricter tolerance was used in Formulation I, the difference is even more apparent. It is safe to conclude that the recycle solver used by Unisim works poorly for problems with small temperature differences.

5.7.2 MATLAB solution accuracy for Model Formulations I and II

When leaving some of the model equations for the MATLAB solver of choice to solve, it is important to know whether this solver can converge the equa-

tions accurately.

1. *Solution of heat exchanger model*: As shown in the previous section, Formulation I always lets us solve the flowsheet model. However, we are left with the task of solving Equation 5.7 for the temperatures. The question is, can the MATLAB solver of choice converge this equation more accurately, or more robustly than the internal heat exchanger solver in Unisim? To check this, we have tried to solve Equation 5.7 with MATLAB to the same tolerance that was used in the Unisim heat exchanger model in the previous section. See Table 5.4.

2. *Convergence of recycles*: When testing Model Formulation III, we found that the Unisim recycle solver failed to converge in more than 50 % of the cases. To compare how different MATLAB solvers could cope in comparison, we attempted to solve Equation 5.10 using these MATLAB solvers. If the quality of the solution routines themselves is significantly different, the accuracy we can achieve will also be different. The Unisim recycle unit operation uses direct substitution for the first steps, before applying the Wegstein acceleration method (Wegstein, 1958) or the *accelerated eigenvalue method* (Orbach and Crowe, 1971) until convergence is reached. When using an external solver, e.g. a MATLAB solver, one can use a least-squares method, or a Newton method.

Since this is part of an optimization problem, we need to see whether an optimization solver (in MATLAB, the **fmincon** solver is used for this type of problems) can solve the necessary equations. However, it is also of interest to see whether other equation solvers can solve Equations 5.7 and 5.10 more reliably than Unisim can. Thus we have tested the following solvers:

- **fsolve**: The standard solver for algebraic equations in MATLAB. It seeks to find a solution where the sum of squares of the equation residuals is sufficiently close to zero.

- **fmincon**, active-set algorithm: **fmincon** is the standard solver for nonlinear optimization in MATLAB. The active-set method is the default method for problems with nonlinear constraints.

- **fmincon**, interior-point algorithm: This method makes use of slack variables. More importantly, it is programmed to always honor bound constraints, unlike the active-set method which can break bound constraints at intermediate points.

Since the **fsolve** solver attempts to minimize the sum-of-squares of equation residuals, we need to set the function tolerance equal to the *square* of the maximum error we allow for. When using the **fmincon** solver for equation solving with a constant J, the equations are supplied to the solver as *equality constraints*. Thus it is the *constraint tolerance* which is of importance. This solver uses an absolute tolerance on the *maximum constraint violation*, so here we set the tolerance equal to the maximum error we allow for. In Table 5.3 we summarize the tolerances we have used in the subsequent tests.

Table 5.3: Tolerances used for different MATLAB solvers for solving heat exchangers and recycles

Solver	Tolerance type	Max iterations	Eq. 5.7	Eq. 5.10
fsolve	TolFun	50	10^{-8}	10^{-2}
fmincon	TolCon	50	10^{-4}	10^{-1}

Table 5.4: Testing different MATLAB solvers on Equation 5.7

Solver	Runs	Failures
fsolve	150	103
fmincon, active-set	150	128
fmincon, interior-point	150	86

Table 5.5: Testing different MATLAB solvers on Equation 5.10

Solver	Runs	Failures
fsolve	150	29
fmincon, active-set	150	138
fmincon, interior-point	150	132

The results are shown in Tables 5.4 and 5.5. In all cases there is a significant number of failures, meaning we probably need to further loosen the tolerances (either on UA calculation or recycle convergence), which in turn means we will have less accurate optimization results. The number of failures when trying to solve Equation 5.10 using **fmincon** with a constant J was even higher than when we tried to use Unisim to solve the recycles. Of the approaches taken in this section, the most successful is to use model

formulation II together with the **fsolve** solver. However, even this approach failed frequently, as shown by Table 5.5 (one out of five times).

Remark 3. *:When using an optimization solver with a "dummy" objective ($J = 1$) for simulation, as done by Lid (2007), solving for the equality constraints is basically equation solving with a Newton method: The gradient of the objective function is zero for all u, and there are no inequality constraints, so we are actually left with a set of algebraic equations to solve - and the SQP algorithm is basically the Newton method applied to the KKT conditions (Nocedal and Wright, 1999).*

5.7.3 Optimization efficiency of MCHE sub-model

To test the performance of each model formulation when optimizing the MCHE sub-plant, we let each of the disturbances listed in Section 5.6.2 vary from 95 % to 105 % of their nominal values in 50 equidistant steps. We have varied the constraint and objective tolerances and recorded how this influences on how likely the optimizer was to converge to a solution. Table 5.6 shows how many optimizations succeeded for each disturbance, using Model Formulation I and varying the function and constraint tolerances for the optimization solver. We used the **fmincon** solver (active-set algorithm), using default limits on the number of iterations and function evaluations.

Table 5.6: Optimization for varying disturbances and for different tolerances: Number of successful optimizations (out of 11)

Disturbance	Tol = 10^{-3}	Tol = 10^{-4}	Tol = 10^{-5}
T_{NG}	10	7	8
F_{NG}	7	6	5
P_{NG}	10	9	8

We notice that more optimizations fail when the tolerances are loosened. This is somewhat surprising, as it should be easier to converge to a more loosely defined optimum. However, when the constraint tolerance is increased as well, we may end up further outside of the feasible region, and this may cause more frequent flowsheet convergence failures, making it more likely that the optimization fails to converge as well.

5.7.4 Optimization efficiency, precooling sub-model

To test robustness of each of the two ways of expressing the superheating constraints, we tested how often the optimizer would converge to a

function tolerance of 10^{-3} and a constraint tolerance of 10^{-1} (the latter corresponding to $0.1°C$ violation of temperature constraints, like also used for the recycles in Section 5.7.2), when starting from random initial points inside the bounds given in Table 5.7. $F_{1,\mathrm{C3}}$ and $F_{2,\mathrm{C3}}$ are the flow rates of propane to the first NG precooler (V100) and the first MR precooler (V103), respectively. Table 5.8 shows the number of failed optimizations with the two different constraint formulations. Regardless of algorithm and constraint formulation, the optimizations that started from *feasible* starting points were more likely to converge.

Remark 4. *The reason why so few optimizations were attempted using the active-set method, is that it does not honor upper and lower bounds at intermediate points, so it may try to give two pressures that give a pressure increase across a valve, or another physically infeasible set of specifications.*

Table 5.7: Optimization variables u in precooling submodel: Minimum and maximum values

Variable	Nominal value	Minimum	Maximum
$F_{1,\mathrm{C3}}\,[kmol/h]$	12.22	12.0	12.6
$F_{2,\mathrm{C3}}\,[kmol/h]$	62.1	60.5	64.0
$P_{1,\mathrm{C3}}\,[kPa]$	1100	1100	1500
$P_{2,\mathrm{C3}}\,[kPa]$	455	420	480
$P_{3,\mathrm{C3}}\,[kPa]$	225	210	250
$P_{4,\mathrm{C3}}\,[kPa]$	109.3	105	125

Table 5.8: Optimization robustness for different constraint formulations - testing for different starting points

Formulation	Algorithm	Attempts	Failures
Δh_{sup}	Interior-point	50	16
ΔT_{sup}	Interior-point	50	44
Δh_{sup}	Active-set	4	4
ΔT_{sup}	Active-set	5	4

We also want to test how robust the different formulations are to changes in disturbances. Here, we consider changes of $\pm 5\%$ in the following variables:

- Cooling utility temperature (T_{amb})(we assume that we maximize cool-

ing in condensers/coolers, so this is equivalent to changing the temperatures out of each condenser/cooler.

- NG flow rate (F_{NG}).
- MR pressure from K103 ($P_{\mathrm{h,MR}}$).

The results are shown in Table 5.9. We only used the interior-point method in this part of the study. We also used somewhat wider bounds than the ones given for flows in Table 5.7, because when changing the feed flow rate, we need to change the C3 flow rates accordingly.

Table 5.9: Optimization robustness for different constraint formulations - testing for different disturbances

Disturbance	Formulation	Attempts	Failures
T_{amb}	Δh_{sup}	11	10
T_{amb}	ΔT_{sup}	11	10
F_{NG}	Δh_{sup}	11	7
F_{NG}	ΔT_{sup}	11	10
$P_{\mathrm{h,MR}}$	Δh_{sup}	11	9
$P_{\mathrm{h,MR}}$	ΔT_{sup}	11	11

5.8 Discussion

5.8.1 Degrees of freedom in precooling section

Here we continue the discussion from Section 5.6.3. We mentioned that the temperature and superheating constraints consume four degrees of freedom, as they are assumed active at all times. From an initial number of eight degrees of freedom, we are then left with two. Furthermore, this requires that we are able to adjust the intermediate pressures (streams C3-3 and C3-7). Since in the actual process, there is only one propane compressor, it may not be possible to vary them independently. This means we would be left with *zero* degrees of freedom for optimization. However, if the goal is to optimize the C3-MR process as a whole, the constraints on temperatures in streams NG4 and MR10 may also be changed. They may be lowered until the lowest propane pressure reaches its minimum allowed value.

5.8.2 Reliability and accuracy

As seen from Table 5.2, the only formulation within Unisim which gave a result for the whole range of flows and pressures was formulation I, even though the internal tolerance of the heat exchanger was set as low as 10^{-10}. In formulation II, the three-stream heat exchanger failed frequently despite the tolerance here being much looser (10^{-5}). This large difference in reliability is caused by the fact that when temperatures are given, the internal solver of the heat exchanger operation only needs to solve the energy balance equation for the last (unknown) temperature, thus the only factor limiting solution accuracy is the underlying thermodynamic property calculations. On the other hand, when other variables are specified, the heat exchanger solver iterates on the unknown temperatures and/or flows until it meets the specifications. Basically, it does the same job as the MATLAB solver does when UA specifications are included in the optimization problem.

It is worth noticing that regardless of solver, any values for pressures, flows and composition (our decision variables for optimization) close to the upper and lower bounds were likely to cause convergence failure - especially when changing only one variable at a time. This means that when carrying out optimization, we have very limited freedom to change u, and there are strong correlations between the process variables. This indicates that there is a need to find more suitable decision variables u, so we can explore more of the state space when optimizing - this will increase the chance of finding the global optimum. Ideally we should find some variables that can be kept more or less constant, and others that may be varied more freely.

5.8.3 Optimization efficiency

Frequent flowsheet convergence failures made model formulation III unsuited for use with a gradient-dependent optimization method. A failed flowsheet calculation means that we do not get reliable gradients and Hessians, if any at all. In this work, we let the optimizer get a fixed, high value for both objective and constraint functions whenever the flowsheet calculation fails. This has assured that we always could calculate gradients. However, because of frequent flowsheet convergence failures, these gradients would be poor, and thus lead to the optimizer taking poor steps. It is obvious that this has a huge effect on optimization performance.

With formulations I and II, the flowsheet calculation rarely would fail, but progress towards a feasible solution of the optimization problem still failed frequently. In many cases, the solution found was very near to the initial point. This is surprising, since the nominal point is calculated using

a given minimum ΔT. As shown by Jensen and Skogestad (2008), this formulation will be sub-optimal when going from design to operation, thus one would expect that the solution would differ more from the initial point. Whether this is due to unreliable gradient calculations (and thus inaccurate optimization), a weakness in the optimization algorithm itself, or simply due to a very flat optimum, has not been investigated in this work.

We also found that optimization convergence was strongly dependent on the initial guesses u_0, especially when optimizing the precooling sub-model. When several constraints were not satisfied at u_0, the optimizer would frequently fail to find a feasible solution. If only one constraint was violated, the optimizer would normally converge.

5.8.4 Simpler and more robust optimization

As the above have shown, if we want to be able to optimize this and similar processes for varying disturbances, we need to overcome several issues. First of all, we must be able to converge the process model almost every time it is called by the optimization algorithm. In our case, this means we have to use temperature specifications in the liquefaction (MCHE) part of the model, and let the optimizer find the correct temperatures.

Second, it seems that the natural choices of specified variables are interacting strongly, thus it is necessary to recast the optimization problem in new decision variables. We should seek to find new variables $y = g(u)$ such that the optimal value of y is less sensitive to disturbances. Then we will be able to use the same initial values of y when optimizing over a wider range of disturbances.

Further, if it is reasonable to assume that some constraints are always active, it is possible to include them as *equality* constraints. This reduces the number of possible active constraint sets for the optimizer. Also, if a certain constraint function can be assumed to depend mainly on *one* decision variable, we may fix that variable - especially if the constraint in question is not a critical one. However, neither of these approaches are more than quick-fixes to problems that may have more fundamental causes.

Using process knowledge, we can easily identify some variables that will never change much:

- The ratio of natural gas flow rate to MR flow rate. Since the two streams are both precooled to approximately the same temperature, the ratio between them is what determines the final outlet temperature - which we want to keep constant anyway.

- The lowest pressure in the precooling loop.
- Cold end ΔT in the four-stream and three-stream sections of the MCHE, if temperature specifications are used.

An interesting parallel may be drawn between this strategy and the control strategy of self-optimizing control (Skogestad, 2000) which means "select variables to control at constant set points such that near-optimal operation is maintained when disturbances occur". The link here is that we seek to have *decision* variables whose optimal values do not change much. A major difference is that in self-optimizing control, one *depends* on being able to carry out steady-state optimization off-line, rather than seeking to simplify the optimization problem itself. We will therefore have to rely on process insight to identify the variables, or variable combinations, that are best suited to give an easier optimization problem. This will be the focus of future work.

5.9 Conclusions

We have summarized the approaches that have been taken to optimization of natural gas liquefaction plants, the methods used and some of the most common challenges. More specifically, we have examined the challenges that arise when trying to optimize a model of the C3-MR process using a commercial process simulation program (Unisim) for simulation and MATLAB for optimization. We have found the following:

- In simulation of the MCHE section of the process, the method most likely to produce a converged result is using temperature specifications in the Unisim model, and let a MATLAB equation solver find the correct temperatures for specified UA values (Model Formulation I). This removes the need for recycle operations in the Unisim model and makes flowsheet convergence robust.
- When optimizing using MATLAB's **fmincon** solver, including temperatures as optimization variables, we would generally be able to converge to a solution, but in many cases this showed to be a local minimum very near the starting point.
- When optimizing the precooling part of the process, it was necessary to write the constraints on superheating in terms of enthalpy rather than temperature, in order to avoid a zero gradient for the constraint

function. When doing this, the optimization proved to be more robust to changes in starting point. When it came to changes in disturbances, neither approach was particularly robust.

This chapter illustrates well why derivative-free methods have seen wider use in optimization of liquefaction processes.

References

Aspelund, A., Gundersen, T., Myklebust, J., Novak, M., Tomasgard, A., 2010. An optimization-simulation model for a simple LNG process. Computers & Chemical Engineering 34 (10), 1606–1617.

AspenTech, 2011. Aspen HYSYS®. Aspen website: http://www.aspentech.com/core/aspen-hysys.aspx.

Biegler, L., Hughes, R., 1982. Infeasible path optimization with sequential modular simulators. AIChE journal 28 (6), 994–1002.

Biegler, L. T., 2010. Nonlinear Programming: Concepts, Algorithms and Applications to Chemical Processes. SIAM.

Chiu, C., 2008. History of the development of LNG technology. In: AIChE Annual Meeting, Philadelphia, Pennsylvania, Nov. 16-21.

Cvijovic, D., Klinowski, J., 1995. Taboo search: An approach to the multiple minima problem. Science 267 (5198), 664–666.

Durr, C., Coyle, D., Hill, D., Ray, S., Rios, J., 1998. Improved plant design and cost reduction through engineering development. In: 12th International Conference & Exhibition on Liquefied Natural Gas, May 4-7, Perth, Australia.

Geist, J., 1983. The role of LNG in energy supply. Int. Journ. of Refrigeration 6 (5-6), 283–297.

GTI, 2011. Proceedings of the international lng conferences lng 1 - lng 16 (1968-2010). http://www.gastechnology.org/webroot/app/xn/xd.aspx?it=enweb\&xd=3TrainingConfer/LNGconferenceproceedings.xml.

Jensen, J., Skogestad, S., 2008. Problems with specifying ΔT_{min} in the design of processes with heat exchangers. Industrial & Engineering Chemistry Research 47 (9), 5195–5174.

Jensen, J. B., Skogestad, S., 2006. Optimal operation of a simple LNG process. In: Proceedings Adchem 2006, Gramado, Brazil. IFAC, pp. 241–247.

Lid, T., 2007. Data reconciliation and optimal operation. Ph.D. thesis, NTNU.

Liu, Y. N., Daugherty, T. L., Bronfenbrenner, J. C., 1998. LNG Liquefier Cycle Efficiency. In: 12th International Conference & Exhibition on Liquefied Natural Gas, May 4-7, Perth, Australia.

Motard, R. L., Westerberg, A. W., 1981. Exclusive tear sets for flowsheets. AIChE Journal 27 (5), 725–732.

Newton, C., Kinard, G., Liu, Y., 1986. C3-MR processes for liquefaction of natural gas. In: 8th International Conference & Exhibition on Liquefied Natural Gas, Los Angeles, USA, June 15-19.

Nocedal, J., Wright, S., 1999. Numerical optimization. Springer verlag.

Orbach, O., Crowe, C. M., 1971. Convergence promotion in the simulation of chemical processes with recycle-the dominant eigenvalue method. The Canadian Journal of Chemical Engineering 49 (4), 509–513.

Paradowski, H., Bamba, M., Bladanet, C., 2004. Propane precooling cycles for increased LNG train capacity. In: 14th International Conference & Exhibition on Liquefied Natural Gas, Doha, Qatar, March 21-24. pp. 107–124.

Peng, D.-Y., Robinson, D. B., 1976. A new two-constant equation of state. Industrial & Engineering Chemistry Fundamentals 15 (1), 59–64.

Pillarella, M., Bronfenbrenner, J., Liu, Y., Roberts, M., 2005. Large LNG trains: Developing the optimal process cycle. In: GasTech 2005, Bilbao, Spain.

Price, B., Mortko, R., 1996. PRICO - a simple, flexible proven approach to natural gas liquefaction. In: GASTECH, LNG, Natural Gas, LPG international conference, Vienna.

Process Systems Enterprise, 2011. gPROMS for Advanced Process Modelling, Simulation and Optimization. PSE website: http://www.psenterprise.com/gproms/.

Shah, N., Rangaiah, G., Hoadley, A., 2007. Multi-objective optimization of the dual independent expander gas-phase refrigeration process for LNG. In: AIChE Annual Meeting, Salt Lake City, Utah, USA, Nov. 4-9.

Skogestad, S., 2000. Plantwide control: The search for the self-optimizing control structure. Journal of process control 10 (5), 487.

Wegstein, J. H., 1958. Accelerating convergence of iterative processes. Commun. ACM 1, 9–13.

Chapter 6

Active constraint regions for a simple LNG process

Submitted to *Journal of Natural Gas Science and Engineering*

Optimal operation of liquefaction processes is little studied in the open literature. In particular, the issue of how optimal operation changes with disturbances has received very little attention. This chapter addresses optimal operation of a simple natural gas liquefaction process - the PRICO process. The focus is on how the active process constraints change with disturbances. It is shown that the feasible part of the disturbance space can be divided into five regions with different sets of active constraints. We also suggest control structures for the process, and find that as little as two control structures may be needed despite of the fact that there are five regions. It is suggested to use compressor speed to control the margin to surge at minimum, and to keep the turbine outlet stream at saturation at all times.

6.1 Introduction

Liquefaction of natural gas is an energy-intensive process, and efficient operation typically means great savings. One of the most important aspects in optimal operation is to control the active constraints. However, little literature exists on optimal operation, active constraints and selection of controlled variables. Papers addressing optimal operation of LNG processes include Lee et al. (2002), Pillarella et al. (2005), Jensen and Skogestad

(2006), and Nogal et al. (2008). Selection of controlled variables was addressed by Singh et al. (2008) and Michelsen et al. (2010).

In Chapters 2-3, we studied how active constraints for optimal operation varied with disturbances, for different processes. Knowledge of this is very useful when designing the control structure of a plant, because one has to control the active constraints to have optimal operation. Here, we apply the experiences from those two papers to map active constraint regions for a natural gas liquefaction process.

We have chosen to study the PRICO process (Price and Mortko, 1996), which is the one used by Jensen and Skogestad (2006). The PRICO process is chosen because it is simple, while still capturing the fundamental issues one will also find in more complex liquefaction processes.

6.2 Optimal operation of a PRICO liquefaction plant

6.2.1 Plant description

The PRICO process (Price and Mortko, 1996) (Figure 6.1) is a very simple liquefaction process. The natural gas feed stream (NG IN) enters from the left, and is liquefied and subcooled to $-157°C$ in the heat exchanger. It is then expanded (not shown here) and pumped to a storage tank. The mixed refrigerant (MR) is condensed with sea water or air (MR-1), before it is liquefied in the heat exchanger (MR-2). It is then expanded to a lower pressure, giving a lower temperature (MR-3), before it is used for cooling in the heat exchanger. It leaves the heat exchanger in a superheated state (MR-4) and is compressed back to high pressure (MR-5). The heat exchanger is typically a plate-and-fin type heat exchanger.

6.2.2 Model and simulation tools

We have used Honeywell Unisim for modelling the process. For optimization, we have used MATLAB. The two are linked through the COM interface. We have used stream data from the nominal optimum reported in Jensen and Skogestad (2006), the compressor curves are also copied from that paper. The combination of Unisim for modelling and MATLAB for optimization was also used by Aspelund et al. (2010), but they used a Tabu search algorithm (Chelouah and Siarry, 2005) whereas we use MATLAB's built-in **fmincon** solver. The stream variables we have copied are summarized in Table 6.1. Due to a slightly different heat exchanger model, and to

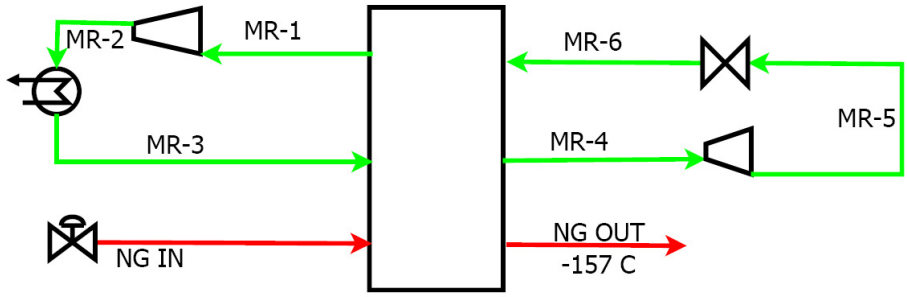

Figure 6.1: Simplified flowsheet of the PRICO process as modelled by Jensen and Skogestad (2006), not including expansion of cold natural gas

the fact that gPROMS and Unisim use different sources for the parameters used in the SRK equation of state, there are small differences in some other key variables. These are summarized in Table 6.2.

As described in Jacobsen and Skogestad (2011), the three-stream heat exchanger model has been solved by adding two temperatures to the specification vector, and adding the heat exchanger UA specifications to the optimization problem as equality constraints. In addition, we needed to tear the compressor inlet stream, because the use of compressor curves demands that the inlet conditions of the compressor are fully specified. The temperature of the torn stream is added to the decision variables, and convergence of the torn stream is included as a third equality constraint. Thus the optimization problem includes three equality constraints:

$$\begin{aligned} UA_1 &= UA_{1,specified} \\ UA_2 &= UA_{2,specified} \\ T_{MR-1,calculated} &= T_{MR-1,guessed} \end{aligned} \tag{6.1}$$

6.2.3 Optimization objective

In the PRICO process, there is one product stream and two utilities that are used (power for compression, and for pumping of cooling water). It is reasonable to ignore the cost of pumping cooling water, since this is very small compared to the power consumed by the compressor [1]. When the

[1]For the case study process, when assuming a $1°C$ temperature increase for the cooling water, a minimum ΔT of $4°C$ in the condenser, and a pressure drop of 1 bar for cooling

Table 6.1: Values of stream variables and pressure drops copied from Jensen and Skogestad (2006)

Variable	Value
Feed flow rate [kmol/h]	$1.517 \cdot 10^4$
Feed pressure [bar]	40.0
Feed temperature [°C]	30.0
Feed mole fraction CH_4	0.897
Feed mole fraction C_2H_6	0.055
Feed mole fraction C_3H_8	0.018
Feed mole fraction C_4H_{10}	0.001
Feed mole fraction N_2	0.029
MR flow rate [kmol/h]	$6.93 \cdot 10^4$
Compressor speed ω [rpm]	1000
MR Condensation temperature [°C]	30.0
Compressor inlet pressure [bar]	4.445
Hot MR temperature at HX outlet [°C]	-157.0
NG temperature at HX outlet [°C]	-157.0
Turbine outlet pressure [bar]	10.29
MR mole fraction CH_4	0.327
MR mole fraction C_2H_6	0.343
MR mole fraction C_3H_8	0.000
MR mole fraction C_4H_{10}	0.233
MR mole fraction N_2	0.097
Condenser ΔP [bar]	0.10
NG ΔP in HX [bar]	5
Hot MR ΔP in HX [bar]	4
Cold MR ΔP in HX [bar]	1
Compressor suction ΔP [bar]	0.3 (nominal)
Turbine suction ΔP [bar]	0.3

Table 6.2: Differences in key variables between this work and Jensen and Skogestad (2006)

Variable	This work	Jensen's work
W_s [MW]	119	120
Compressor outlet pressure [bar]	30.2	30.0
Compressor efficiency η	81.8	82.8
ΔT_{sup} [°C]	5.1	11.3
$\Delta T_{min,HX}$ [°C]	1.57	
UA_{NG} [kW/°C]	$9.20 \cdot 10^3$	$8.45 \cdot 10^3$
UA_{MR} [kW/°C]	$4.62 \cdot 10^4$	$5.32 \cdot 10^4$

cost of cooling water is ignored, the objective function to be minimized (with units $\$/s$) can be expressed as follows:

$$J = p_{\text{work}} \cdot W_s - p_{\text{LNG}} \cdot F_{\text{LNG}} \tag{6.2}$$

where p_{work} is the price of energy (in \$/kJ) W_s is compressor work (in kW), p_{LNG} is the difference between feed and product value (in \$/mol) and F_{LNG} is the production rate (in mol/s). Jensen and Skogestad (2006) describe two "modes" of operation, with different optimization objectives.

- Mode I: When energy is expensive, it is optimal to produce just the amount one is bound to (i.e. by contracts with customers). In this mode, the throughput of natural gas (F_{LNG}) is given, and we want to minimize W_s.
- Mode II: When energy is cheap, it is profitable to produce as much as possible. Then F_{LNG} is a degree of freedom, which we seek to maximize.

Jensen and Skogestad (2006) studied Mode II, whereas we will be focusing on Mode I, and consider F_{LNG} a disturbance.

6.2.4 Degrees of freedom and disturbances

The process has got a total of ten manipulated variables. These are:

1 Natural gas feed flow rate

water, we found a pumping power of 15 kW compared to the 120 MW consumed by the compressor.

2 Mixed refrigerant flow rate

3-5 Mixed refrigerant pressures (high, intermediate and low)

6 Cooling water flow in MR condenser

7-10 Four molar fractions in MR (since we have five components)

As stated above, we will here consider the case where the natural gas feed flow rate is a *disturbance*, i.e. it is set upstream. Like Jensen and Skogestad (2006), we will also assume that the MR composition can *not* be changed during operation. Thus, we have five degrees of freedom left before active constraints are taken into account.

The other disturbance we will consider, besides feed flow rate, is the ambient temperature (i.e. the temperature of the external coolant). The ambient temperature influences directly on the refrigerant pressure. The lower the temperature of the coolant is, the lower we may set the condensation pressure (i.e. the pressure at the compressor outlet). Like Jensen and Skogestad (2006), we finally assume that maximum cooling is used in the condenser. This means the ambient temperature sets the condensation temperature of the refrigerant directly. This assumption consumes a degree of freedom, bringing us down to four degrees of freedom for optimization.

6.2.5 Constraints

The constraints in a liquefaction process are related to the state of the product stream (temperature being the most important, usually there is also a constraint on the content of nitrogen) and to cooling and compression capacity. For a given outlet/inlet pressure ratio, a compressor will have a minimum flow rate it can handle (known as the surge flow rate) and a maximum flow rate (known as the stonewall flow rate). Jensen and Skogestad (2006) consider the surge limit, but not the stonewall limit.Instead, they consider a maximum available compressor work.

Here, we will consider the following constraints:

1. Exit temperature of natural gas leaving the heat exchanger ($T_{\mathrm{NG,out}} \leq -157°C$). *This constraint is always active.*

2. Superheating of refrigerant leaving the heat exchanger ($\Delta T_{sup} \geq 5°C$).

3. Like Jensen and Skogestad (2006), we consider compressor surge as a constraint ($\Delta M_{\mathrm{surge}} \geq 0$).

4. Maximum compressor work is 132 MW. We set it 10% higher than in Jensen and Skogestad (2006) to be able to study the effect of higher feed rates than the nominal one. Since the results from Jensen and Skogestad (2006) give the maximum processing rate, using the exactly same data would not allow us to study higher feed rates.

5. The stream leaving the turbine must be liquid only ($\Delta P_{\text{sat}} \geq 0$). In Jensen and Skogestad (2006), this constraint is handled by adding a choke valve and a liquid receiver directly after the turbine (and before the main choke valve). The first choke valve has a fixed pressure drop, and the turbine outlet pressure is indirectly given by the temperature of the refrigerant stream leaving the heat exchanger. Here, we let the turbine outlet pressure be a degree of freedom, and add this constraint.

6. Compressor speed, ω, is limited upwards to 1200 rpm (again, it is set higher than in Jensen and Skogestad (2006) to see how other constraints behave at higher than nominal feed rates).

It is clear that the first constraint will always be active, because it is never optimal to cool the natural gas more than we need to. In this work, this constraint has been implemented by simply specifying this temperature in the Unisim model (in a real process, it would have to be controlled). We are therefore left with *four* degrees of freedom for optimization.

6.2.6 Nominal optimum of the process

Since there were some discrepancies between the Unisim model used here and the gProms model used by Jensen and Skogestad (2006), a reoptimization was carried out. Compressor work (W_s) was minimized, subject to the following constraints listed in Section 6.2.5 (repeated here for convenience):

1. $T_{\text{NG,out}} = -157°\text{C}$
2. $\Delta T_{\text{sup}} \geq 5°\text{C}$
3. $\Delta M_{\text{surge}} \geq 0$ kmol/s
4. $W_s \leq 132$ MW
5. $\Delta P_{\text{sat}} \geq 0$ (no vapour at turbine outlet)
6. $\omega \leq 1200$ rpm

Table 6.3: Optimum at nominal disturbances. Variables listed in **bold** are added to the variable set to meet equality constraints

Variable	This work	Jensen's work
MR flow rate [kmol/s]	16.94	18.70
Compressor speed ω [rpm]	1143	1000
Compressor inlet pressure [kPa]	383.2	414.0
Turbine outlet pressure [kPa]	552.5	1029
Compressor inlet T [°C]	15.8	N/A
T_{MR} at HX outlet [°C]	-163.9	-157.0
T_{NG} at HX outlet [°C]	-157.0	-157.0

Table 6.4: Other key variables at nominal optimum

Variable	This work	Jensen's work
Compressor work W_s [MW]	116.4	120.0
ΔT_{sup} [°C]	19.4	11.3
$\Delta T_{min,HX}$ [°C]	0.7	N/A
Compressor efficiency η	82.1	82.8
$\Delta M_{\mathrm{surge}}$ [%]	0	0
ΔP_{sat} [kPa]	1.1	20

The **fmincon** interior-point algorithm was used. 10 initial points within the bounds were generated, and optimization carried out from each. The optimal values of the optimization variables are shown in Table 6.3.[2]

Table 6.4 summarizes the most important variables not included as decision variables.

The following points are worth discussing:

1. ΔP_{sat} is much smaller than in Jensen and Skogestad (2006). This shows that it is optimal to do as much of the expansion as possible in the turbine. This allows for a lower temperature in the cold refrigerant stream, thus giving a larger ΔT at the cold end of the exchanger, and allows us to circulate less refrigerant.

2. $\Delta M_{\mathrm{surge}}$ is zero (i.e. we operate on the surge limit). This is the same as was found by Jensen and Skogestad (2006). In our case this is to

[2]This particular solution was found in 5 of the 10 optimization runs. The other 5 runs did not converge to a feasible solution

be expected, simply because the surge limit coincides with the flow that, at any given speed, corresponds with maximum efficiency.

6.3 Results

First, one should use process insight to predict which regions must be present, and which constraints will always (or never) be active. The following can be stated even with limited *a priori* knowledge of the process:

1. The temperature of natural gas leaving the heat exchanger will always be at its maximum, as stated above.

2. For a given value of T_{amb}, a maximum throughput (feed flow rate) must exist. This maximum throughput will be low for high values of T_{amb} as the maximum work constraint becomes active.

3. As we lower P_h to exploit the lower T_{amb}, we must reduce compressor speed. This leads to a lower surge limit, which means that the surge margin constraint may become inactive at lower values of T_{amb}.

4. Theoretically, there may be as many as 26 feasible regions: Since each of the five constraints may be either active or inactive, there are $5^2 = 32$ possible combinations. However, only the combinations with three or fewer active constraints are feasible. This means we must subtract the five possible combinations of four active constraints, and the one with five active constraints.

5. Since we have only three degrees of freedom, we can only satisfy three constraints at any time. The maximum possible throughput will coincide with a point where four constraints are active.

First, the feasible region was worked out by starting at the nominal optimum, and optimizing for increasing values of T_{amb} and F until no feasible solution could be found [3]. The constraint curves corresponding to each individual constraint were then found using the interpolation method used in Chapter 2. The resulting regions are shown in Figure 6.2. Notice that the feed rate is given as $F/F_{nominal}$.

When examining Figure 6.2, we find that there are five active constraint regions. The active constraints inside each region are summarized in Table 6.5.

[3] This could also have been done by including F as a degree of freedom, and then maximize it at a sufficient number of values for T_{amb}

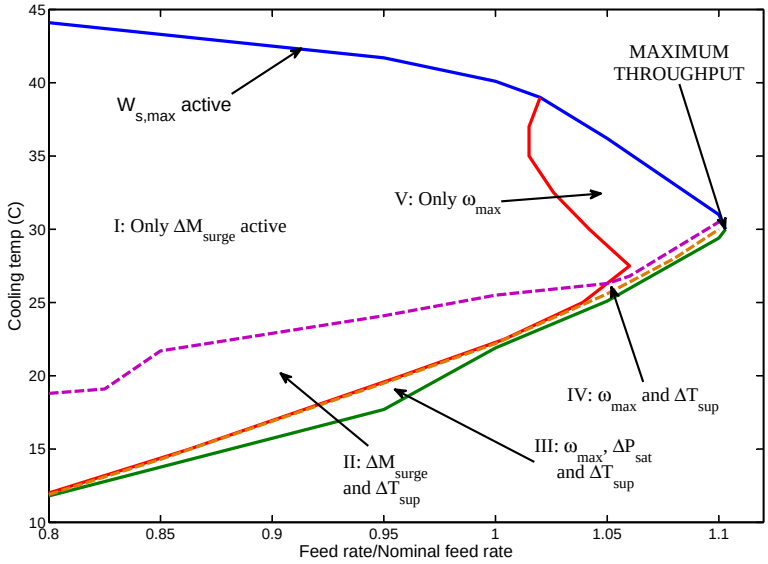

Figure 6.2: Active constraint regions for the PRICO process, as function of feed flowrate F and ambient temperature T_{amb}

Each curve in Figure 6.2 shows where a constraint switches from active to inactive:

1. The blue line, indicating the *maximum* feasible ambient temperature for a given flow rate, gives the upper boundary of the feasible region. Along this line, the maximum constraint on W_s is active.

2. The green line indicates the *minimum* feasible ambient temperature.

3. The purple dashed line indicates where the superheating constraint (ΔT_{sup}) becomes active.

4. The orange dashed line indicates where the turbine outlet saturation constraint (ΔP_{sat}) becomes active.

5. The red line shows where the maximum speed constraint becomes active (and the surge constraint becomes inactive).

Table 6.6 gives optimal values for key data at a point in each of the five regions (for region I, the nominal point from Section 6.2.6 is given). The

Table 6.5: Active constraints in each region for the PRICO process

Region number	Active constraint(s)
I	ΔM_{surge}
II	ΔM_{surge}, ΔT_{sup}
III	ω_{max}, ΔP_{sat}, ΔT_{sup}
IV	ω_{max}, ΔT_{sup}
V	ω_{max}

numbers shown in **bold** correspond to constraints that were found to be active to within the specified tolerance.

6.4 Discussion

6.4.1 Active constraint regions

Compared to the maximum possible number of regions (26), we find that we have a relatively small number of regions (5). What is of particular interest, is that the constraint curves for ΔM_{surge} and ω_{max} are identical - these two constraints switch along the curve shown in red in Figure 6.2. There is no region where both ω_{max} and ΔM_{surge} are active at the same time. This is probably because the surge limit is set to coincide with the flow giving the highest adiabatic efficiency. Consider a given temperature in Region I, where the surge constraint is active. Now assume that the feed F is increased gradually. As long as the active constraints do not change, we may change the refrigerant flow rate proportionally, and at the same time adjust the compressor speed so that we remain at the speed yielding the maximum efficiency. At some point we reach $\omega = \omega_{max}$. A further increase in F must still be followed by an increase in refrigerant flow rate, but the flow rate corresponding to compressor surge is no longer increasing. Thus, ΔM_{surge} can not remain equal to zero. Figure 6.3 shows how these two constraints switch when we go from Region I to Region V.

This also means that two neighbouring regions have the same number of constraints. This is not very common (as pointed out in Chapter 2), and usually happens when the two constraints are related to the same unit operation.

The green "minimum" curve shown in Figure 6.2 may not be a true minimum. In Region III, there are three active constraints. Along a feasibility limit there should be four; since we have three degrees of freedom,

Table 6.6: Values for key variables for various values of (F, T_{amb}). Active constraints are shown in **bold**.

Region	I	II	III	IV	V
T_{amb} [°C]	30.0	18.0	19.3	25.7	30.0
$F/F_{nominal}$	1.00	0.85	0.95	1.05	1.08
MR flow rate [kmol/s]	16.94	14.19	14.91	17.55	18.75
Comp. speed ω [rpm]	1143	1017	**1200**	**1200**	**1200**
Comp. inlet P [kPa]	383.2	323.6	322.4	380.1	408.6
Turb. outlet P [kPa]	552.5	463.5	447.7	538.2	592.7
Comp. inlet T [°C]	15.8	-2.7	-2.8	1.3	6.9
T_{MR} at HX outlet [°C]	-163.9	-167.4	-168.0	-164.4	-162.4
Comp. work W_s [MW]	116.4	86.6	98.8	116.9	127.2
Comp. efficiency η [%]	82.1	82.2	81.9	82.1	82.1
ΔT_{sup} [°C]	19.4	**5.0**	**5.0**	**5.0**	8.8
$\Delta T_{min,HX}$ [°C]	0.70	0.43	0.25	0.58	0.79
$\Delta M_{\mathrm{surge}}$ [%]	**0.00**	**0.00**	0.90	0.01	0.01
ΔP_{sat} [kPa]	1.1	1.9	**0.4**	1.2	0.9
$T_{\mathrm{NG,out}}$ [°C]	**-157.0**	**-157.0**	**-157.0**	**-157.0**	**-157.0**
Unconstrained DOF	2	1	0	1	2

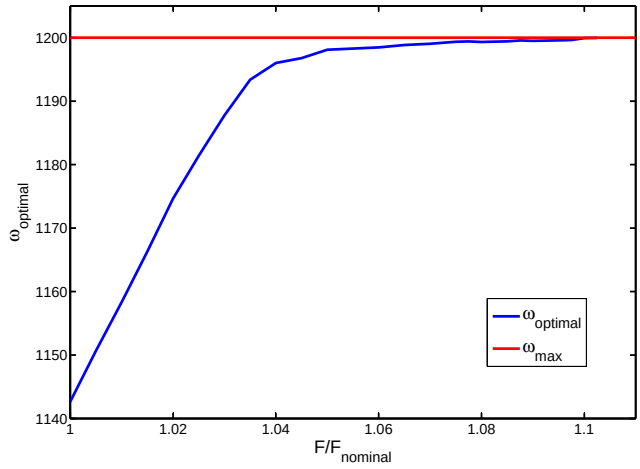

(a) Compressor speed ω (rpm)

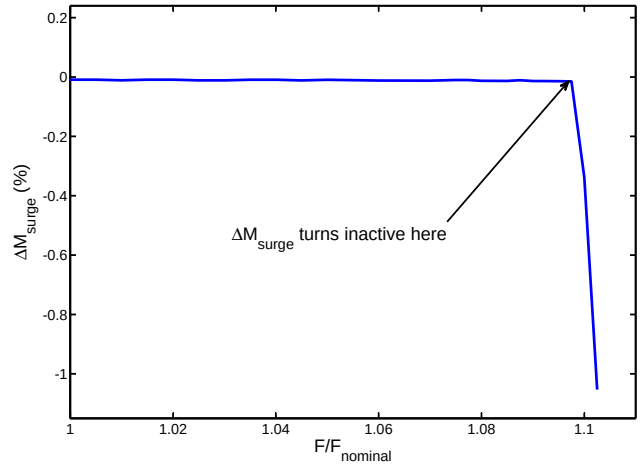

(b) ΔM_{surge} (%)

Figure 6.3: Plots of optimal compressor speed (ω) and distance to surge (ΔM_{surge}) as function of $F/F_{nominal}$ when going from Region I to Region V

we are able to meet three active constraints. However, when approaching the "minimum" curve, the minimum temperature approach in the heat

exchanger becomes so small that it falls within the constraint tolerance, making convergence difficult. What is observed, though, is that within this region compressor work will *increase* with decreasing ambient temperature. This happens because maximum compressor speed is reached, causing a drop in compressor efficiency. Figure 6.4 shows how η changes as T_{amb} is gradually reduced from its nominal value of 30°C to the minimum feasible temperature, at nominal flow rate.

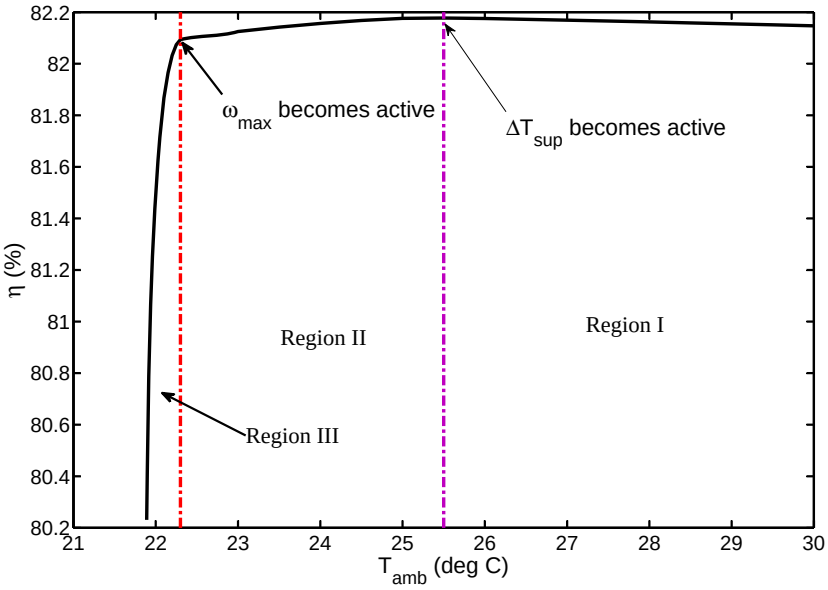

Figure 6.4: Compressor efficiency at the optimal solution, as function of ambient temperature T_{amb} for $F = F_{nominal}$

6.4.2 Issues in optimization

When finding the feasibility limits, quite many optimizations were needed, especially for the lower limit. This might have been avoided if a slightly different form of the optimzation problem had been used for this particular task. If feed rate had been included as a degree of freedom, leaving T_{amb} as the only disturbance, the feasibility limit could have been found by maximizing the feed rate, subject to the same constraints as before. The reason why this approach was not used, was that it would have required making

alternative versions of nearly all the MATLAB files used.

The **fmincon** solver used in this work, can use two different algorithms: An **active-set** method, and an **interior-point** method (Byrd et al., 2000). The former does not require that bound constraints are satisfied at every intermediate point, whereas the latter does. Because values outside of the specified bounds were likely to cause the flowsheet solver to fail to converge, the interior-point algorithm has been used for all optimizations in this chapter. A drawback with this algorithm is that due to its use of slack variables, it may give a solution where a constraint function c is negative and its corresponding Lagrange multiplier λ is positive at the same time. This may introduce some extra incertainty to the solution of the equation

$$s = c + \lambda \tag{6.3}$$

which is used to determine the constraint curves.

6.4.3 Control

For optimal operation, the active constraints should obviously be controlled at all times. In the case studied here, there are five active constraint regions, so theoretically, five different control structures are needed. However, if one control structure is optimal in one region and near-optimal in another, it may be better to use the same control structure, thus simplifying the necessary switching logic. In our case, we see that Regions III and IV are very small, and it could be argued that it is not necessary to include control structures for these, but instead use the same structure as for regions II and V, respectively.

1. In all regions, $T_{\mathrm{NG,out}}$ must be controlled.

2. In Regions I and II, $\Delta M_{\mathrm{surge}}$ should be controlled, and in the other regions, ω should be at its maximum. Thus it makes sense to use ω to control $\Delta M_{\mathrm{surge}}$ (possibly via a cascade loop).

3. ΔP_{sat} should be controlled in Region III. However, its optimal value is close to zero in the other regions as well, and it makes sense to control it in all regions.

4. ΔT_{sup} must be controlled in Regions II, III and IV. However, in regions I and V it seems like a bad choice, as its optimal value is far from the constraint value. An alternative variable to keep constant could be the active charge, as discussed below.

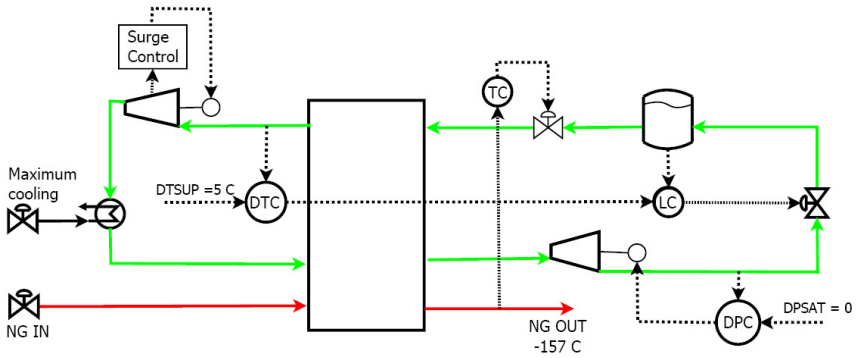

Figure 6.5: Suggested control structure for the PRICO process. TC = Temperature controller, LC = level (active charge) controller, DTC = ΔT controller and DPC = ΔP controller

.

One of the degrees of freedom in the process is related to the *active charge* of the plant (Jensen, 2008). In order to be able to use this degree of freedom, we must be able to change the active charge. This may be done if we introduce an extra valve and a liquid receiver after the turbine, like in Jensen and Skogestad (2006). If this is included, the active charge can be adjusted by changing the set point for the level in this receiver. Alternatively, the active charge itself may be used as a controlled variable.

By introducing this, we suggest the following control structure, illustrated in Figure 6.5.

1. The natural gas outlet temperature from the main heat exchanger is controlled at $-157°C$, using the choke valve between the turbine and the main heat exchanger.

2. Compressor speed ω is used to keep $\Delta M_{\text{surge}} = 0$.

3. Turbine speed is used to control $\Delta P_{\text{sat}} = 0$.

4. In Regions II, III and IV, the active charge is used to control $\Delta T_{sup} = 5°C$. In Regions I and V this controller is switched off, and the active charge controller can instead operate with a constant, default set point.

6.4.4 Applicability to other liquefaction processes

The PRICO process is a very simple process compared to many that are in use in the industry today. However, several points made in this chapter are valid for all kinds of refrigeration processes. Most notably, the fact that compressor performance sets both maximum and minimum limits to the ambient conditions the process can handle. If the assumed location of the surge limit (i.e. near the peak efficiency) is reasonable, the results found here are probably applicable to most liquefaction processes.

6.5 Conclusions

This chapter discusses active constraints for the PRICO process for liquefaction of natural gas. We find five regions with different sets of active constraints inside the feasible area. Based on these results, we propose to control the compressor surge margin and turbine saturation margin at zero in all regions. In Regions I and V we have one additional unconstrained degree of freedom, which should be used to control an additional self-optimizing variable.

References

Aspelund, A., Gundersen, T., Myklebust, J., Novak, M., Tomasgard, A., 2010. An optimization-simulation model for a simple LNG process. Computers & Chemical Engineering 34 (10), 1606–1617.

Byrd, R. H., Gilbert, J. C., Nocedal, J., 2000. A trust region method based on interior point techniques for nonlinear programming. Mathematical Programming 89, 149–185, 10.1007/PL00011391.

Chelouah, R., Siarry, P., 2005. A hybrid method combining continuous tabu search and nelder-mead simplex algorithms for the global optimization of multiminima functions. European Journal of Operational Research 161 (3), 636 – 654.

Jacobsen, M., Skogestad, S., 2011. Optimization of LNG plants - challenges and strategies. In: Proceedings of the 21st European Symposium on Computer Aided Process Engineering. Chalkidiki, Greece, May 29-June 1, 2011. pp. 1854–1858.

Jensen, J., 2008. Optimal operation of cyclic processes - Application to LNG processes. Ph.D. thesis, NTNU.

Jensen, J. B., Skogestad, S., 2006. Optimal operation of a simple LNG process. In: Proceedings Adchem 2006, Gramado, Brazil. IFAC, pp. 241–247.

Lee, G., Smith, R., Zhu, X., 2002. Optimal synthesis of mixed-refrigerant systems for low-temperature processes. Ind. Eng. Chem. Res 41 (20), 5016–5028.

Michelsen, F. A., Lund, B. F., Halvorsen, I. J., 2010. Selection of optimal, controlled variables for the tealarc lng process. Industrial & Engineering Chemistry Research 49 (18), 8624–8632.

Nogal, F., Kim, J., Perry, S., Smith, R., 2008. Optimal design of mixed refrigerant cycles. Industrial & Engineering Chemistry Research 47 (22), 8724–8740.

Pillarella, M., Bronfenbrenner, J., Liu, Y., Roberts, M., 2005. Large LNG trains: Developing the optimal process cycle. In: GasTech 2005, Bilbao, Spain.

Price, B., Mortko, R., 1996. PRICO - a simple, flexible proven approach to natural gas liquefaction. In: GASTECH, LNG, Natural Gas, LPG international conference, Vienna.

Singh, A., Hovd, M., Kariwala, V., 2008. Control variables selection for liquefied natural gas plant. Presented at the 17th IFAC World Congress, Seoul, South Korea, Jul 6-11, 2008.

Chapter 7

Conclusions

7.1 Conclusions

The points of focus of the material presented in this thesis are *finding active constraint regions for optimal process operation*, and *optimal operation of natural gas liquefaction processes*.

In Chapter 2 a simple method is introduced, and applied to a generic reactor-separator-recycle system. The main outcome of this chapter is that for a coarse sketch of the active constraint regions, the method is efficient and accurate, provided the optimization can be carried out with sufficient accuracy. Chapter 3 applies the method to more realistic distillation case studies.

Chapters 4-6 focus on natural gas liquefaction processes. The main conclusion of the literature review (Chapter 4) is that little work has been done on optimal operation of liquefaction processes, and that most papers with this focus have taken a rather simplistic approach. The main conclusions of Chapter 5 are:

- One should try to formulate the model such that one avoids objective and constraint function gradients that are zero over a range of values. A concrete example is the superheating constraint in the cold end of the precooling loop, which should be expressed in terms of enthalpy rather than temperature.

- Tear stream convergence is better included in the optimization problem, as additional equality constraints, than solved by the process model simulator. This can probably be generalized to say the following: Only calculations that are very unlikely to fail, should be inside the "black box". In other words, when the optimization algorithm

calls the process simulator, the latter should always be able to converge to a solution, and return values for objective and constraint functions.

These conclusions will be useful for future work on optimization of LNG processes, and in the author's opinion they are an important contribution from the thesis.

In Chapter 6, the experiences from the previous chapters are used to find active constraint regions for the PRICO liquefaction process, with ambient temperature and feed rate as disturbances. The process is found to have five constraint regions, but it may still be sufficient to use two control structures.

7.2 Suggestions for future work

With the work presented in this thesis, the author hopes to have opened several doors for others who want to study optimal operation of chemical processes. Since the thesis itself is quite diverse, the suggested directions for future work will have to be the same.

Chapter 2, dealing with finding active constraints for generic processes, should serve as a starting point for further discussion on active constraints for optimal operation and control. The author recognizes the need to make the approach more mathematically stringent. If methods earlier applied in multi-parametric programming could be expanded to general nonlinear cases, the issue could be dealt with in a more stringent way. In special cases, it could also be possible to predict the shape of constraint curves from analytic expressions this could be an interesting topic which would also be good for gaining insight into the processes that are studied.

As stated in the introductions to Chapter 2, the main reason why one needs to know the active constraint regions is to control the processes optimally. Thus, selection of control structures based on knowledge of active constraint regions is an obvious direction for future work. As shown in Chapter 6, one may find that a control structure which is optimal in one region is near-optimal in neighbouring regions. This can be exploited to reduce the amount of switching logic which is needed. Knowledge of the active constraint regions can be combined with methods from self-optimizing control (for example the maximum scaled gain rule). Since Chapter 3 does not go in detail about control structures for optimal operation of distillation columns, this should also be investigated further.

Chapters 4, 5 and 6, each in its own way addressing optimization of natural gas liquefaction processes, should fill a few gaps in the field, and

open some doors for subsequent work. Several pitfalls in optimization have been pointed out. With this in place, it should be possible to undertake the task of studying self-optimizing control for natural gas liquefaction plants, and subsequently to design plantwide control structures.

Chapter 5 shows that in order to optimize operation of LNG plants, one will probably need to formulate the problem in more suitable variables one should seek to find variables that are not expected to change much when disturbances hit the process. A thorough approach to this would be a considerable step forward in optimization of LNG plants.

Finally none of the case studies included in the thesis deal with disturbances in feed composition. As this disturbance is very common in the process industry, it is natural to include it in future studies.